Spring 5-7-2021

POLYANILINE AND ITS NANOCOMPOSITES FOR GREEN ENERGY PRODUCTION AND STORAGE

Wang Lin
Pittsburg State University, 1169203554@qq.com

Recommended Citation

Lin, Wang, "POLYANILINE AND ITS NANOCOMPOSITES FOR GREEN ENERGY PRODUCTION AND STORAGE" (2021). *Electronic Theses & Dissertations*. 367.
https://digitalcommons.pittstate.edu/etd/367

POLYANILINE AND ITS NANOCOMPOSITES FOR GREEN ENERGY PRODUCTION AND STORAGE

A Thesis Submitted to the Graduate School
in Partial Fulfillment of the Requirements
For the Degree of
Master of Science

Wang Lin

Pittsburg State University

Pittsburg, Kansas

May 2021

POLYANILINE AND ITS NANOCOMPOSITES FOR GREEN ENERGY PRODUCTION AND STORAGE

Wang Lin

APPROVED:

Thesis Advisor ______________________________
Dr. Ram Gupta, Department of Chemistry

Committee Member ______________________________
Dr. Khamis Siam, Department of Chemistry

Committee Member ______________________________
Dr. Charles Neef, Department of Chemistry

Committee Member ______________________________
Dr. John Franklin, Department of English and Modern languages

Acknowledgments

First of all, I would like to thank Dr. Gupta. His important meaning to me is not only reflected in his professional skills and kindness to students, but more importantly, he is like a spiritual mentor, encouraging and teaching me to realize my self-worth. He is committed to creating a relaxed atmosphere to sharpen my ability to deal with difficulties and challenges. Without his help, my study life at this stage would not be easy. I am so grateful for everything he has done for me.

Secondly, I would like to thank my parents and sisters. Without their full support, I would not have the opportunity to study abroad. I would like to thank Dr. Khamis Siam, Charles Neef, and Dr. John Franklin for being on my thesis committee. I am deeply grateful for the people and things encountered in this small town. Last but not least, I am grateful to the Department of Chemistry for the funding provided to me so that I can complete this stage of study at Pittsburg State University without any worries.

POLYANILINE AND ITS NANOCOMPOSITES FOR GREEN ENERGY PRODUCTION AND STORAGE

An Abstract of the Thesis by
Wang Lin

To address increasing energy demands, more energy storage options are needed. N-doped carbon with rich open mesoporous structures is formed by high-temperature activation using potassium hydroxide. The effect of different mass ratios of polyaniline and potassium hydroxide on the microscopic morphology of activated carbon materials was studied. In addition, composite materials of polyaniline and transition metal oxides were synthesized by in-situ polymerization. The surface morphology, pore distribution, specific surface area, and pore structure of these materials were explored by scanning electron microscopy (SEM) and Brunauer–Emmett–Teller (BET) methods.

The results show that these materials are rich in mesoporous structures. A three-electrode system was used to test the energy storage performance of these materials. In addition, the transition metal oxides and their composites with polyaniline were also tested for their performance as electrocatalysts for water splitting. When the mass ratio of PANI and KOH was 1:1, the specific surface area of the material was as high as 3259 m^2/g, which yielded good supercapacitor energy storage performance, with a specific capacitance as high as 194 F/g at a current density of 1 mA/g. In addition, the PANI: KOH (1:1) exhibited excellent rate performance shown through the charge and discharge current density being increased ten times from 3 mA/g to 30 mA/g, while still completing

84.4% charging. In addition, PANI: KOH (1:1) showed good electrochemical stability as seen up to 5000 charge-discharge cycles as the specific capacitance retention was as high as 92%. PANI/Co_2NiO_4 and Co_2NiO_4 coated electrodes exhibited good electrochemical performance, especially as a catalyst for the electrolysis of water. The hydrogen evolution reaction (HER) and oxygen evolution reaction (OER) of Co_2NiO_4 showed low overpotentials of 145 mV and 320 mV, respectively. In addition, both Co_2NiO_4 and PANI/Co_2NiO_4 showed good electrochemical stability up to 18 hours of chronoamperometry test. These results suggest that the porous carbon nanotube synthesized using PANI had good electrical double-layer capacitor characteristics and PANI/Co_2NiO_4 and Co_2NiO_4 exhibited good electrocatalytic performance for water splitting.

TABLE OF CONTENTS

LIST OF TABLES

TABLE PAGE

LIST OF FIGURES

FIGURE PAGE

CHAPTER I

INTRODUCTION

1. 1. Energy

One of the fundamental reasons for the rapid development of human society in the past few hundred years is that people have discovered how to use natural resources with efficiency. As early as hundreds of years ago, people have used wind power in many applications such as for ships, mills, and irrigation systems [1]. Especially since the beginning of the 20th century, with the development of internal combustion engine technology and the widespread use of electric power, people quickly moved from agricultural civilized society to industrial civilized society, and then to the modern information society. The main reason behind all this is that mankind has mastered the power of energy use.

Electricity can be called universal energy because it can be directly converted into heat, mechanical, chemical, and other forms of energy. Therefore, people's demand for electricity has been increasing rapidly since the beginning of industrialization. To meet the electricity demand a large number of fossil fuels such as oil, coal, and natural gas have been exploited and used in large quantities. The direct consequence of this is significant resource depletion and substantial environmental pollution [2]. As a response to the energy crisis, people have begun using environmentally friendly energy sources such as wind, solar, tidal energy, geothermal energy, and nuclear energy to reduce their dependence on energy from fossil fuels [3].

Compared with electricity, hydrogen energy is a new type of energy with great potential and environmentally friendly. As a secondary energy source with zero carbon emissions, high energy density and a wide range of sources, hydrogen energy can be regarded as the most ideal renewable resource at present. The most environmentally friendly production method of hydrogen energy is through the electrolysis of water. Electrolyzed water can generate high-purity hydrogen. Hydrogen can be converted into electricity through fuel cells and only water is generated in the process, which can be regarded as an ideal green cycle. At present, hydrogen is widely used in petrochemical and metallurgical industries. Having a high calorific value as fuel, hydrogen energy has been used in aircraft for many years [4], [5].

Unfortunately, the global distribution of these environmentally friendly energy sources is extremely uneven and the cost in the utilization process is also huge. As primary energy sources wind and solar energy cannot be directly transmitted. When the energy is converted into hydrogen energy by electrolysis of water, the energy can be easily transported in the form of hydrogen [6].

The purpose of renewable and environmentally friendly energy is to cope with the energy crisis and alleviate environmental pollution. However, the use of these energy sources requires a large amount of investment and a long payback period. Therefore, how to efficiently use environmentally friendly energy to shorten the payback period should become a greater concern.

1.2. Energy storage

The demand for energy in modern society is high. This demand is not only reflected in the use of energy but more importantly in energy storage, which allows people to use energy more efficiently and conveniently. The common form of energy storage in nature is through fossil fuels.

Batteries, electrochemical supercapacitors, and fuel cells are different electrical energy storage devices, and their performance is also very different. A battery is a simple device that can directly convert chemical energy into electrical energy. Electrochemical supercapacitors are a new type of electrical energy storage device based on carbon materials, metal compounds, and conductive polymers. A fuel cell is a device that can directly convert the chemical energy of fuel into electrical energy [7].

As a universal form of energy, electrical energy can be stored in two different ways. The first way is to store it in batteries as potentially available chemical energy. This storage method generates a potential difference between the electrodes caused by the oxidation of the electrochemically active material. The second way to store electrical energy is more direct. Positive and negative charges are stored between the two plates of the capacitor in the form of static electricity [8].

As a representative of commonly used rechargeable batteries, lithium-ion batteries are recognized for their superior performance. Therefore, comparing the characteristic parameters of lithium-ion batteries with the corresponding parameters of electrochemical capacitors can effectively help us understand advantages and disadvantages of these devices.

Table 1.1. Comparison of some characteristics of supercapacitors and batteries [9].

Characteristic	Supercapacitors	Lithium-ion batteries
Power density (W/Kg)	10-	240+
Energy density (Wh/Kg)	10,000+	3000
Charge time	Seconds	Minutes
Cell voltage	2.5 V	3.6 V
Cycle life	10^6 +	3000
Operating temperature range	-40 °C to 65 °C	0 to 45 °C
Self-discharge	50% within a month	Less than 3% within a month

Table 1.1 shows the comparison of some performance parameters of supercapacitors and chemical batteries. The conclusions that can be drawn are as follows: supercapacitors have: (1) higher power density than batteries; (2) faster charge and discharge times; (3) a million times more charge and discharge life; and (4) a relatively wide operating temperature. However, the shortcomings of supercapacitors must also be

stated which are that they have low energy density and high self-discharge rate. Both of these shortcomings have greatly affected their application in the market [9].

Since chemical batteries and supercapacitors have different characteristics their application in the market is also different. As an energy storage device with a low self-discharge rate, small size, and high capacity, batteries are widely used in various fields, such as electronics, automobiles, biomedical, etc. This means that the stability and reliability of the battery are widely recognized.

Supercapacitors are widely used in various fields. In the field of renewable energy, supercapacitors are usually used in conjunction with wind power generation equipment and solar power generation equipment. Wind energy is an instantaneous but unstable energy source. The output power of wind turbines fluctuates with changes in wind energy, thereby affecting the power quality of the grid. The voltage of the wind farm can be stabilized by adding energy storage equipment and can be adjusted in a wide range. Supercapacitors that can realize high energy storage have great application value in wind power generation. Due to their thousands of charge and discharge cycles and high current charge and discharge characteristics, supercapacitors can adapt to the high current fluctuations of wind energy.

Batteries and electrochemical supercapacitors can also be used in conjunction to take full advantage of their respective characteristics. For example, electric vehicles require huge amounts of energy at the moment of starting and electrochemical supercapacitors can deliver this needed energy perfectly. However, when the electric vehicle is running continuously the battery can provide stable and long-lasting power [10].

Like batteries and supercapacitors, fuel cells can also be regarded as electrochemical power generation devices because they can directly convert chemical energy into electrical energy. Ragone diagram (**Figure 1.1**) shows the energy and power densities of various devices. As seen, fuel cells show high energy density. Commonly used fuels for fuel cells include natural gas, methanol, ethanol, hydrogen, and other hydrogen-containing fossil fuel products. As a result, the fuel cell emits very little or no harmful gas based on the choice of fuel. Therefore, from an environmental point of view fuel cells can be regarded as the best power generation option.

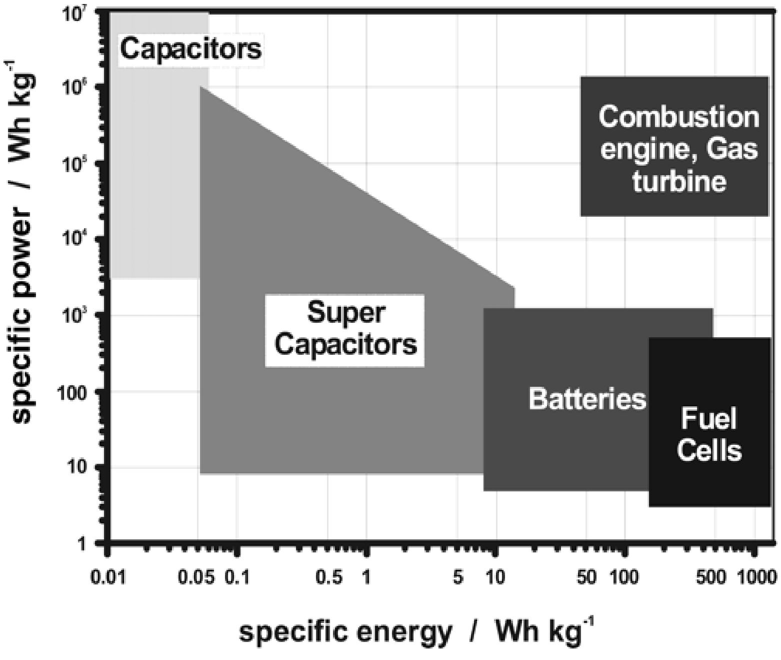

Figure 1.1. Ragone diagrams of different energy storage devices. Adapted with permission from [11]. Copyright 2004, American Chemical Society.

1.3. Supercapacitor

A supercapacitor is a relatively new type of energy storage device that has both the fast charge and discharge characteristics of a capacitor and the energy storage characteristics of a battery.

1.3.1. Classification of supercapacitors and electrode materials

Based on the difference in energy storage mechanisms, supercapacitors can be divided into the three categories: (1) electric double-layer capacitors, (2) pseudocapacitors, and (3) hybrid supercapacitors.

Electric double-layer capacitors do not involve redox reactions in the energy storage process. Its energy storage mechanism is to store energy by capturing ions in the electrolyte by the polarized electrode surface material. Carbon is the material of choice for electrodes in electric double-layer capacitors because it meets the requirements of electrochemical energy storage materials which are conductivity, electrochemical stability, and high specific surface area. The sources of carbon materials are also very extensive.

As a cheap and environmentally friendly precursor of activated carbon materials, biological wastes such as coffee residues, corn stalks, cotton stalks, and soybean stalks are used as the source of carbon materials for electric double-layer capacitors. Carbon nanospheres, carbon nanotubes, and graphene are other choices for electric double-layer capacitors [9], [10], [12].

Pseudocapacitors store energy differently from electric double-layer capacitors. Their energy storage mechanism is a rapid and reversible oxidation-reduction reactions that occur on the surface of the material. Compared to EDLCs, these redox reactions greatly increase the specific capacitance of the capacitor. However, the specific capacitance increased by the redox reaction is not conducive to the power performance of the capacitor. This is because although the redox reaction is rapid its rate cannot be compared with ion adsorption in EDLC. Pseudocapacitors also have limited EDLC character but since the conductivity of the active material is relatively weak and the specific surface area of the active material is much lower than that of the carbon material, the contribution of the electric double layer phenomenon to the specific capacitance of the capacitor is usually very limited. The most common active materials for pseudocapacitors are conductive polymers and transition metal oxides, but nitrides and sulfides of transition metals have also been extensively studied [10], [13].

Conductive polymers are a potential source of supercapacitor electrode material due to their good conductivity, perfect electrochemical reversibility, and fast doping/dedoping ability. The redox reaction of the conductive polymer is mainly due to the delocalized electrons found in the conjugated polymer backbone. Among various conductive polymers polyaniline, polypyrrole, and polythiophene have been extensively studied for use as supercapacitor materials. These research results show that supercapacitors using polymers as electrode materials have outstanding advantages. They have a high specific capacitance, which is much higher than that of carbon materials and are even comparable to metal oxides [14]. However, their shortcomings are also detrimental to widespread implementation. Random deposition during the manufacturing process leads to higher electron spin resonance, which greatly slows down the diffusion rate of ions in the electrode. Another flaw of conductive polymers for supercapacitors is their poor cyclic stability. This is due to the repeated expansion and contraction of the material caused by the doping-dedoping process during the charging and discharging process [15].

Low specific capacitance was a problem faced at the beginning of the development of supercapacitors. However, transition metal compounds with excellent pseudocapacitance characteristics provide new possibilities for researchers [16]. The common feature of the various metal oxides studied their variable valency. As a result, the supercapacitors using these electrode materials have poor cycle characteristics because their charge storage mechanism is the same as the battery charge storage mechanism [17].

The final type of supercapacitor is the hybrid supercapacitor. The concept of a hybrid supercapacitor is proposed to improve the shortcomings of the low energy density of supercapacitors. According to the calculation of the energy density of a supercapacitor, it can be shown that increasing the specific capacitance of the capacitor and/or increasing the overall voltage window of the supercapacitor can achieve a higher energy density. The common practice in the industry is to combine a carbon electrode material in an electric double-layer capacitor with a pseudo-electrode material, which can more efficiently use the potential window of the two electrodes and thereby achieve the goal of increasing the energy density of the supercapacitor [9], [10] [18].

1.3.2. Features and application of supercapacitors

The characteristics of supercapacitors are simple and clear, such as high-power density, high cycle life, and wide operating temperature range. Because batteries do not have these characteristics the application of supercapacitors in some fields has unique advantages and is favored. Supercapacitors are not only widely used in the fields of wind power and solar power generation, due to their long cycle life and high-power density [19], [20], they are also widely used in industrial fields such as with forklifts, cranes, and elevators which consume a lot of energy during the initial startup process [21]. More importantly, supercapacitors can achieve efficient energy recovery for subways and trams running at high speeds. Due to the short distance between platforms, there is frequent braking that will cause a lot of energy loss. The use of supercapacitors in conjunction with these rail transit facilities can not only provide sufficient power when starting but can also efficiently recover energy when braking. Since the supercapacitor has a wide operating temperature range it can meet some power requirements in extreme climate areas, such as transportation facilities in polar regions and other electrical equipment [9], [10].

1.4. Hydrogen energy

1.4.1. Overview of hydrogen energy

Hydrogen energy is regarded as the most ideal energy source in the 21st century due to its clean, efficient, safe, and sustainable development. As the first element in the periodic table, hydrogen is the most widely distributed element in the universe. In nature, hydrogen mainly exists in the form of compounds and the most accessible form for humans to harvest is water. At present, some of the main methods of industrial hydrogen production are cracking of methanol or ethanol, petroleum cracking, the water gas method, and the production of hydrogen by electrolysis of water [5].

Hydrogen production via electrolysis of water is the most ideal way to produce hydrogen from the perspective of environmental protection, but it is costly due to its high energy consumption during electrolysis. However, with technological breakthroughs and the use of renewable energy to generate electricity as a source of power for electrolysis, the cost of hydrogen production will decrease. This shows that the electrolysis of water to produce hydrogen has great potential and is an environmentally friendly way of producing energy [5], [22].

1.4.2. Electrocatalytic water splitting

Electrocatalytic dissociation of water is a technology that uses water as raw material and breaks it into hydrogen and oxygen through an electrolytic cell device. The electrocatalytic water splitting involves the hydrogen evolution reaction at the cathode and the oxygen evolution reaction at the anode [22]. At present, electrocatalytic dissociated water has not been widely promoted in industry due to its high energy consumption. To overcome this barrier two aspects should be considered, (1) using a low amount of electric energy to produce high-yield hydrogen and (2) improving energy conversion efficiency. Under standard conditions the theoretical voltage required for electrolysis of water is 1.23 V, but in actuality, this voltage is much higher than the theoretical value which is referred to as overpotential. The main reasons for this phenomenon are the presence of electrical resistance in the electrolyte, electrode polarization, and the migration of ions and oxygen bubbles [23], [24]. At present, it is recognized that the electrocatalysts with the best catalytic for water electrolysis are platinum, iridium, ruthenium, and other precious metals as well as their oxide materials. However, the high cost and scarcity of these materials limit their large-scale use. As a result, researchers are still investing a lot of time and energy into finding low-cost and abundant reserves with catalytic performance comparable to precious metal materials.

1.4.2.1. Electrocatalytic hydrogen evolution

The reaction path of the hydrogen evolution reaction in the electrocatalytic hydrolysis process depends on the acidity or alkalinity of the electrolyte. This pathway transfers two electrons under ideal conditions for each water molecule. The reaction mechanism of hydrogen evolution reaction for acidic and alkaline electrolytes is shown in the following table [25], [26].

Table 1.2. Reaction mechanisms for hydrogen evolution reaction in acidic and alkaline solutions.

Total reaction equation	**Reaction process**
$2H^+ + 2e^- \rightarrow H_2$ (acidic solutions)	$H^+ + e^- + * \rightarrow H*$ (Volmer) $H* + H_2O + e^- \rightarrow H_2 + OH^-$ (Heyrovsky) or $2H* \rightarrow H_2$ (Tafel)
$2H_2O + 2e^- \rightarrow H_2 + 2OH^-$ (alkaline solutions)	$H_2O + e^- \rightarrow H* + OH^-$ (Volmer) $H* + H_2O + e^- \rightarrow H_2 + OH^-$ (Heyrovsky) or $2H* \rightarrow H_2$ (Tafel)

In the process of hydrogen evolution reaction, the mechanism can be divided into two based on the rate of reaction, (1) Volmer-Heyrovsky mechanism or (2) Volmer-Tafel mechanism.

1.4.2.2. Electrocatalytic oxygen evolution

Like the hydrogen evolution reaction, the reaction mechanism of the electrocatalytic oxygen evolution reaction is also directly related to the pH of the electrolyte solution. The proposed reaction mechanisms are shown in **Table 1.3** [27], [28]. It can be seen from the reaction mechanism, the oxygen absorption reaction is a four-electron transfer process and the reaction kinetics are relatively slow, which is another reason why the over-potential hinders the efficiency of water electrolysis. The use of electrocatalysts can improve the stability and reaction kinetics of this reaction.

Table 1.3. Reaction mechanisms for oxygen evolution reaction in acidic and alkaline solutions.

Total reaction equation	Reaction process
$2H_2O \rightarrow O_2 + 4H^+ + 4e^-$ (acidic solutions)	$* + H_2O \rightarrow *OH + H^+ + e^-$ $*OH \rightarrow *O + H^+ + e^-$ $*O + H_2O \rightarrow OOH* + H^+ + e^-$ $OOH* \rightarrow *O_2 + H^+ + 4e^-$ $*O_2 \rightarrow * + O_2$
$4OH^- \rightarrow 2H_2O + O_2 + 4e^-$ (alkaline solutions)	$* + OH^- \rightarrow *OH + e^-$ $*OH + OH^- \rightarrow *O + H_2O + e^-$ $*O + *OH \rightarrow OOH* + e^-$ $OOH* + OH^- \rightarrow H_2O + *O_2 + e^-$ $*O_2 \rightarrow * + O_2$

1.4.3. Classification of electrocatalysts

1.4.3.1. Noble metal-based electrocatalysts

At present, the electrocatalysts for the hydrogen evolution reaction with good performance are Pt, Ru, Rh, Ir, and Pd [29]. It is currently recognized that the best hydrogen evolution catalyst is platinum, which has the best stability and performs well in acidic electrolytes. Scientists have done a lot of work to seek efficient and stable utilization of these electrocatalysts while reducing the cost. Zhang et al. [30] reported that the integration of Rh and NiFe-LDH can greatly improve the HER performance without sacrificing the OER performance of NiFe-LDH. Ruiz et al. [31] proposed that Ir exposed on the surface of IrO_X-Ni $(OH)_X$ surface greatly reduces the amount of noble metal used in the catalyst, and the activity and stability of the catalyst can still be comparable to IrO_X catalysts. Tsuji et al. [32] showed that the performance of the electrolyzed water catalyst prepared by the simple flame annealing method after immersing the cheap graphite electrode in the Pt and RuO_X catalyst precursor has been greatly improved. From these works, the main research direction of precious metal electrocatalysts is to further improve the performance of precious metal catalysts by adjusting the microscopic morphology. In addition, in order to reduce the cost of electrocatalysts, a single layer of precious metals is deposited on the surface of inexpensive materials, or precious metals are compounded with other metals to increase the active sites while reducing the total amount of precious metals used.

1.4.3.2. Transition metal-based electrocatalysts

Researchers have done a lot of work to find electrocatalysts that can replace noble metals. Among them, the transition metal-based catalysts have had a more eye-catching performance. However, compared with noble metal-based electrocatalysts these catalysts still have problems, such as poor stability and low activity. To improve the performance of these transition metal-based catalysts, different technical methods are used. One such method is to form hybrid nanoparticles which have good performance for electrolysis of water. Han et al. [33] proposed a hybrid nanoparticle named $FeN_{0.023}/Mo_2C/C$ that exhibited a low overpotential of 227/76 mV corresponding to the OER/HER at 10 mA/cm^2. When $FeN_{0.023}/Mo_2C/C$ was used as a two-electrode catalyst, was needed to reach 10 mA/cm^2 with only 1.55 V external voltage needed, and its stability was maintained for at least 10 hours. The composites of transition metal nanomaterials and porous carbon-based materials are effective materials to improve the conductivity of transition metal compounds. Hou et al. [34] reported MoS_2 nanosheets embedded in Co-N doped carbon nanocages which also showed good performance for both HER and OER.

1.5. The basis for the topic selection and the content to be studied in this topic

To cope with the energy crisis and alleviate environmental degradation, environmentally friendly energy sources such as wind power, solar, and tidal energy have been used more and more widely. However, the main reason why the use of these new energy sources does not dominate the entire energy market is that these new energy sources are unstable and provide intermittent power to the grid. This means that excessive reliance on these new energy sources may cause a transient energy crisis.

Supercapacitors can be used in conjunction with wind, solar, and other energy power generation devices to increase energy utilization and improve grid reliability. The current direction of supercapacitor modification is to improve the electrochemical performance of supercapacitors, such as energy density, specific capacitance, cycle stability, and rate performance so that they can be implemented in large-scale applications like wind farms.

Hydrogen energy is regarded as the cleanest energy source in the 21st century. Among the many hydrogen energy production methods, the electrolysis of water is the most ideal hydrogen production method from an environmental protection point of view.

At present, the main reason restricting the large-scale commercialization of electrolyzed water is high energy consumption for this process. This causes the cost of hydrogen production by electrolysis of water to be much higher than other hydrogen production methods, which is unacceptable in commerce.

There are two direct ways to solve this problem: one is to seek a low-cost power supply and the other is to find better catalysts to reduce energy consumption in the process of electrolysis. New energy power generation facilities are mainly distributed in places with low population density and relatively harsh natural environments. For areas where new energy power generation facilities are widely distributed, the electricity demand is usually relatively small so there is also a large amount of energy loss in the process of electricity transportation. If this electric energy can be directly used for the production of hydrogen it will not only greatly reduce the cost of electrolyzing water to produce hydrogen energy but also serve to use this electric energy with maximum efficiency.

Both electrical energy and hydrogen energy have their advantages. Compared with electrical energy, hydrogen energy is more stable and both pipeline transmission and tank storage energy losses are very low. This is a great development opportunity for the utilization of new energy. Due to the high cost of supporting and long-distance high-voltage transmission facilities, new energy power generation has been restricted to some extent. If these small-scale new energy power generation facilities with low commercial value and unstable supply of electricity generated by newer green energy sources are directly converted into hydrogen energy for on-site storage and transportation, it will help people make better use of new energy. The most direct and effective way to improve the efficiency of the conversion of electrical energy to hydrogen is to reduce the cost of the electrocatalyst and improve the performance of the electrocatalyst. Whether it is supercapacitors or electrolyzed water catalysts, their modification methods are undertaken to improve the electrochemical performance of their active materials.

In 1984, the benzoquinone polyaniline structure model was proposed by MacDiarmid and was widely accepted. Made through a simple synthesis method with good thermal stability, good electrical conductivity, and low cost, environmentally friendly polyaniline quickly attracted a lot of attention [35], [36]. Because of these properties, polyaniline was further developed and applied in many fields. Polyaniline is used as an anti-corrosion material because it can form a chemical barrier to cut off the contact between metal and oxygen [37]. Polyaniline is also used in antistatic and electromagnetic shielding materials due to its high affinity with other polymers [38]. In addition to polyaniline’s excellent electrochemical properties, it has been reported from time to time that it is used as an electrode material for supercapacitors and as a catalyst material for the electrolysis of water [39]–[47].

In this work, polyaniline was used as the basic material for the study of its electrical and catalytic properties. Different technical methods were used to explore the improvement of the electrochemical performance of polyaniline. This topic can be divided into two parts:

(1) Synthesis of polyaniline nanotubes by a chemical oxidation method was accomplished first. The synthesized nano-tubular polyaniline is used as a precursor for performing 800 ℃ pyrolysis to obtain a heteroatom-doped carbon material. In this process, polyaniline mixed with potassium hydroxide in different mass ratios was activated at high temperatures under a nitrogen atmosphere. These activated polyaniline-based carbon materials were analyzed and tested to determine their performance in supercapacitor electrode materials.

(2) Cobalt oxide, nickel oxide, and nickel cobalt oxide were synthesized by a hydrothermal method. To improve the conductive properties of these materials, in-situ polymerization was used to composite these transition metal oxides with PANI. These composite materials of polyaniline and metal oxides were used as catalysts for the electrolysis of water and supercapacitor.

CHAPTER II

EXPERIMENTAL DETAILS

2.1. Materials

The chemicals used in this work are as follows:

Table 2.1. Chemicals and reagents used in this work.

Materials	Purity (%)	Company
Aniline, $C_6H_5NH_2$	99.5	Sigma-Aldrich
Ammonium Peroxodisulfate, $H_8N_2O_8S_2$	98	Aldrich Chemical
Methanol, CH_4O	99.5	Fisher
Acetic Acid, $C_2H_4O_2$	100	Fisher
Potassium Hydroxide, KOH	98.5	Fisher
Cobaltous Nitrate Hexahydrate, $Co(NO_3)_2 \cdot 6H_2O$	99	Stern
Nickel Nitrate Hexahydrate, $Ni(NO_3)_2 \cdot 6H_2O$	99	Stern
Ethanol, C_2H_6O	100	Fisher
Polyvinylpyrrolidone, $(C_6H_9NO)_n$	99	ACROS
Urea, CH_4N_2O	98	ACROS
Perchloric acid, $HClO_4$	70 (V/V)	ACROS
Ammonium persulfate, $(NH_4)_2S_2O_8$	98	ACROS

2.2. Synthesis of carbon-based supercapacitor electrode materials

2.2.1. Polyaniline synthesis

Two solutions were made by adding 1.82 ml of aniline monomer and 5.71 g of ammonium peroxodisulfate in two 100 ml solutions containing 1 M methanol and 0.4 M acetic acid, respectively. Then the aniline solution and the oxidizer solution were placed in an ice bath at 0 °C to cool for 30 min. Then these two solutions were mixed and stirred rapidly for 30 s, left for 16 h at 0 °C. The final product was dried at 70 °C for 12 h after being filtered and washed with deionized water. Finally, the powder was ground to obtain dark green polyaniline nanotubes [48].

2.2.2. Synthesis of polyaniline-based porous carbon electrode materials

The synthesis of polyaniline-based porous carbon was performed by using 800 mg of the pre-synthesized polyaniline that was mixed with 0, 400, 800, and 1600 mg of KOH each, in four beakers containing 20 ml of DI water and then sonicated for 30 min until the polyaniline and potassium hydroxide were fully mixed. After that, the mixture was dried on a hot plate. Then, it was placed in a tube furnace and heated at 800 °C (5 °C/min) for 2 h under nitrogen flow. The carbonized polyaniline was washed with 1 M hydrochloric acid and deionized water until the pH reached 7. The product was dried in an oven at 70 °C and then ground into fine powder for later use.

2.3. Synthesis of polyaniline and transition metal oxide composites

2.3.1. Synthesis of transition metal oxides by hydrothermal method

Transition metal oxides were synthesized by hydrothermal method and the specific steps were as follows: 300 mg polyvinylpyrrolidone and 12 mM urea were dissolved in 18 ml DI water and ethanol solution with a volume ratio of 1:1. Then three solutions were prepared by adding 3 mM $Co(NO_3)_2 \cdot 6H_2O$ or 3 mM $Ni(NO_3)_2 \cdot 6H_2O$ or 2 mM $Co(NO_3)_2 \cdot 6H_2O$ and 1 mM $Ni(NO_3)_2 \cdot 6H_2O$, respectively in the solution prepared previously. These completely dissolved solutions were transferred into 3 different autoclave reactor vessels lined with Teflon. These hydrothermal reactions took place at 140 °C for 12 h. The final products were washed with DI water and collected via centrifugation. Finally, they were ground for use after being dried at 70 °C for 12 h.

2.3.2. Synthesis of polyaniline and transition metal oxide composites

The nanocomposite of polyaniline and transition metal oxide was synthesized by an in-situ composite method. In this process, first 0.35 g of cobalt oxide, or nickel oxide, or nickel-cobalt oxide were dissolved in 10 mL of ethanol and then sonicated for 15 min to completely dissolve. Then 20 ml of perchloric acid (60% by volume) and 130 ml of deionized water were added to the reactor. The reactor was then moved into an ice bath and 0.65 g ammonium persulfate was added. After being stirred for 20 min, the temperature of the mixture in the reactor also reached the freezing point at the same time, then 410 µL of aniline was added. The entire reaction took place in an ice bath under sonication for 6 h. Afterward, the dark green product was thoroughly washed with deionized water and methanol. The final product was powdered after drying at 70 °C for 12 h [49].

2.4. Material characterization

2.4.1. Specific surface area

The specific surface area and pore size distribution of the material greatly affect the performance of the material. Taking an electric double-layer capacitor as an example, its specific capacitance is directly affected by the specific surface area of its active electrode material. Besides, the performance of various types of active materials used to make catalysts and inductors are also closely related to their surface area and pore size distribution. The Brunauer–Emmett–Teller BET) test is the most widely used and highly reliable method to test material is specific surface area, pore-volume, and pore size distribution.

In this work, the surface area and pore size distribution were obtained through BET (ASAP 2020 Models, Micrometrics, Norcross, GA, USA). All the samples were first degassed for 24 h at 70 °C, then the testing was performed at liquid N_2 temperature.

2.4.2. Scanning electron microscope (SEM)

Scanning electron microscopy shows the microscopic appearance of materials. It uses the material on the surface of the sample for microscopic imaging. It is characterized by high magnification and excellent three-dimensional images without damaging and contaminating the composition and morphology of the original sample. Based on the working principle of the scanning electron microscope the sample to be tested must have good conductivity. For materials that do not have conductivity, it is usually necessary to sputter gold on the surface of the sample to make it conductive before testing.

In this project, all tested materials have good conductivity and therefore do not need to be sputtered with gold. The microstructural properties of the samples were investigated by using a Quanta 200 SEM (FEI, Hillsboro, Oregon, USA).

2.4.3. X-ray diffraction analysis (XRD)

The degree of crystallinity of the material was obtained by XRD analysis. The basic principle is to obtain information such as the composition and the structure of the internal atoms or molecules of the material by X-ray diffraction analysis of the material.

In this work, a Shimadzu X-ray diffractometer (Lenexa, Kansas, USA) was used to record the XRD patterns. $CuK_{\alpha1}$ radiation (λ = 1.5406 Å) was used as an X-ray source in the 2θ-θ mode to study the crystallinity and phase purity of the synthesized materials.

2.5. Electrochemical testing

All the electrochemical properties (supercapacitor, hydrogen evolution reaction, and oxygen evolution reaction) were studied using a Versastat 4-500 electrochemical workstation (Princeton Applied Research, Oak Ridge, TN, USA).

2.5.1. Electrode preparation

The working electrodes used for electrochemical testing were made in the same way. The specific process is as follows: 2 mg of PVDF binder was added into a vial containing 1-methyl-2-pyrrolidinone. The solution was then heated up to 70 °C for 30 min until the PVDF binder was completely dissolved. Then, 16 mg of PANI sample and 2 mg of acetylene black were added to the solution. Half of the cleaned nickel foam with dimensions of 0.6 × 1.5 cm^2 was immersed in the prepared mixture to obtain a nickel foam electrode uniformly covered by the sample. These electrodes were placed in a vacuum oven to dry for 48 h.

2.5.2. Electrolyte selection and three-electrode test system

Supercapacitor electrolytes can be divided into three categories: water-based electrolytes, organic electrolytes, and ionic liquid. Each electrolyte has its unique advantages and disadvantages. In this work, 3M KOH was used as an electrolyte.

A three-electrode system was used to test the electrochemical performance of the active material. A saturated calomel electrode, and Pt wire were used as a reference and counter electrode.

2.5.3. Cyclic voltammetry (CV)

Cyclic voltammetry was used to study the electrochemical properties of materials, using three electrode system. The main reason for adopting the three-electrode system is that it can reduce the ohmic resistance. During the cyclic voltammetry test, the potential scanning speed of the working electrode changes linearly with time, and at the same time, the currents at different potentials are recorded. During this experiment, the scan rate range was 2 - 300 mV/s. It can analyze the electrode reaction mechanism and the relevant properties of the sample from the redox peak position, peak height, and symmetry. Equation 1 is the relationship between specific capacitance and CV scan rate

$$C_{(F/g)} = \frac{A}{m \times \Delta V \times \frac{\delta v}{\delta t}} \quad \text{……} \quad (1)$$

Where: $C_{(F/g)}$ is the specific capacity (F/g), A is the area under the CV curve. m is the mass of the electrode (g), $\frac{\delta v}{\delta t}$ is scan rate (V/s), and ΔV is the potential window (V).

2.5.4. Galvanostatic charge-discharge test

Its basic working principle is to charge the electrode up to a certain voltage and then discharge while measuring the time to charge and discharge under constant current. Then study the charge/discharge performance of the electrode and calculate its actual specific capacity from those results. In this work, the current density in the range of 0.5 - 30 A/g was used to study the electrochemical performance of active materials.

Galvanostatic charge-discharge tests can determine specific capacity, rate characteristics, cycle performance, and other parameters of the electrode material. Based on the galvanostatic charge-discharge test data, the specific capacitance (Equation 2), energy density (Equation 3) and power density (Equation 4) of the electrode material can be calculated.

$$C_{sp} = \frac{i \times t}{m \Delta V} \qquad \text{(2)}$$

Where: C_{sp} is specific capacitance (F/g), i is discharge current (A), t is discharge time (s), m is mass (g), and ΔV is the potential window for discharge.

$$E = C_{sp} \times (\Delta V)^2 / 7.2 \qquad \text{(3)}$$

Where: E is energy density (Wh/Kg), C_{sp} is specific capacitance (F/g), and ΔV is the potential window for discharge.

$P = E \times 3600/t$……………………………………………………………………………………………………(4)

Where: P is power density, and t is the discharge time (s).

2.5.5. Electrochemical impedance spectra

The electrochemical impedance spectroscopy is a method that uses small amplitude AC voltage or current to obtain AC impedance data. The principle is to calculate the corresponding electrode reaction parameters based on the simulated equivalent circuit of the electrode.

2.5.6. Cycle performance test

The cycle stability test of the electrode was performed to obtain the long-term stability of the electrode material. In this work, the electrode material has undergone 5000 cycles of constant current charging and discharging tests. The cycle performance test can obtain the changing trend of the specific capacitance of the electrode material as the number of cycles. Also, the Coulombic efficiency (CE) is a parameter describing the charge efficiency of the electrode in charging and discharging

CE = Discharge capacity/ Charge capacity = discharge time/charge time……………………(6)

2.5.7. Electrocatalytic performance

In the process of electrocatalytic dissociation of water, the widely recognized evaluation indicators include overpotential, Tafel slope, and stability.

Overpotential

The overpotential is the difference between the electric potential measured in the actual experiment and the theoretical potential. A larger overpotential value means more energy consumption than ideal. Under standard conditions the theoretical voltage required for electrolysis of water is 1.23 V, for which the electrode potential of the hydrogen evolution reaction occurring at the cathode is 0 V and the potential of the anode oxygen evolution reaction being 1.23 V. In the actual measurement, this potential is usually much higher than the theoretical voltage.

Tafel slope

The Tafel slope is another indicator to measure the performance of the electrocatalyst and is obtained through the linear relationship between the steady-state current density and the overpotential. The Tafel slope is calculated by fitting the linear part of the Tafel diagram based on the overpotential being proportional to the logarithm of the absolute value of the current density. The Tafel slope is calculated by Equation 7.

$$\eta = a + b \log j \quad (7)$$

where: a is the overpotential with a current density of 1 mA/cm^2, η is the overpotential (mV), b is the Tafel slope (mV/dec), and j is the current density (A/cm^2).

Stability

Stability is one of the most important parameters for the commercial use of electrochemical catalysis. There are two main methods for measuring catalyst stability, one is the constant current or constant potential method which involves carrying out long-term catalytic reactions of the electrolysis device under a given current or voltage and analyzing the duration of non-decay. The change of the decay is used to judge the stability of the catalyst. The second method for measuring stability is through cyclic voltammetry, in which thousands of cyclic scans are performed within the voltage range required for the catalytic reaction and the changes in the polarization curve before and after the cycle are observed to determine the performance of the catalyst. During the high number of cycles, the smaller the change in the polarization curve means higher catalyst stability.

CHAPTER III

RESULTS AND DISCUSSIONS

3.1. Polyaniline-based activated carbon materials

3.1.1. Scanning electron microscope analysis

Figure 3.1 shows the morphology of PANI at different resolutions. As seen in the high-resolution image (**Figure 3.1b**), polyaniline nanotubes were successfully synthesized. In the low-resolution image (**Figure 3.1a**), the nanotubes are clumped together with a tight arrangement.

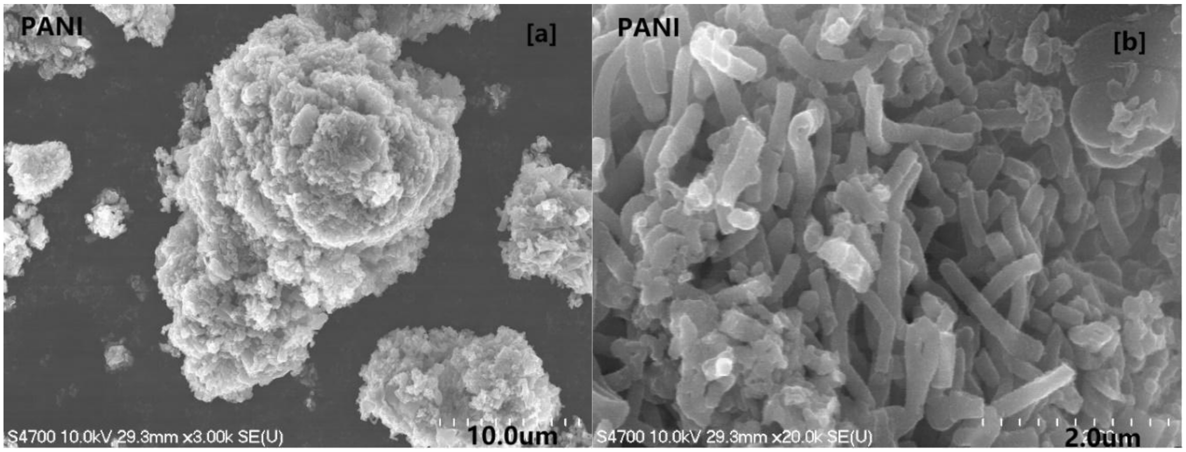

Figure 3.1. SEM images of PANI at different resolutions.

Figure. 3.2 shows the morphology of polyaniline nanotubes after being carbonized at a high temperature. The high-resolution shows that nanotubular structure of polyaniline was retained even at high temperatures.

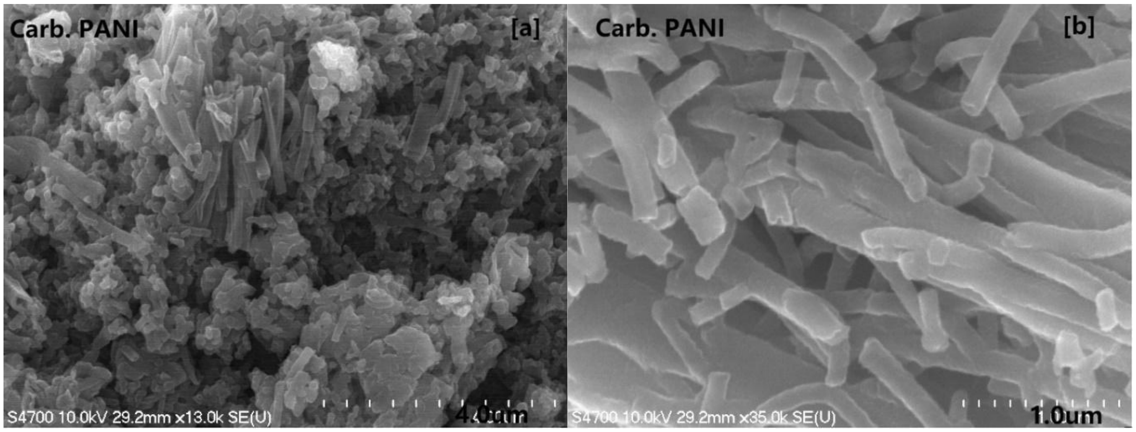

Figure 3.2. SEM images of carbonized PANI at different magnifications.

Figure 3.3 shows the high-temperature activation of the material with a mass ratio of 1:0.5 of polyaniline and potassium hydroxide. Compared with the untreated polyaniline material, the participation of potassium hydroxide changes the morphology of the material. The high-resolution image shows that the nanotubes have been eroded making it difficult to see intact nanotubes on the surface of the material. When the ratio of polyaniline to potassium hydroxide is increased to 1:1, the nanotube morphology disappears completely and is replaced by a porous carbon nanostructure.

As can be seen in **Figure. 3.4**, the overall structure of the particles is still relatively intact even though the material as a whole suffers from potassium hydroxide erosion. However, when the quantity of potassium hydroxide was increased to twice the amount of polyaniline, the overall structure of the materials was unable to maintain its shape because the potassium hydroxide consumed huge amounts of carbon.

In comparing **Figure. 3.4b** and **Figure. 3.5b**, it is seen that the microstructure of the material was further changed by the additional potassium hydroxide. Essentially, the structure of the material became porous.

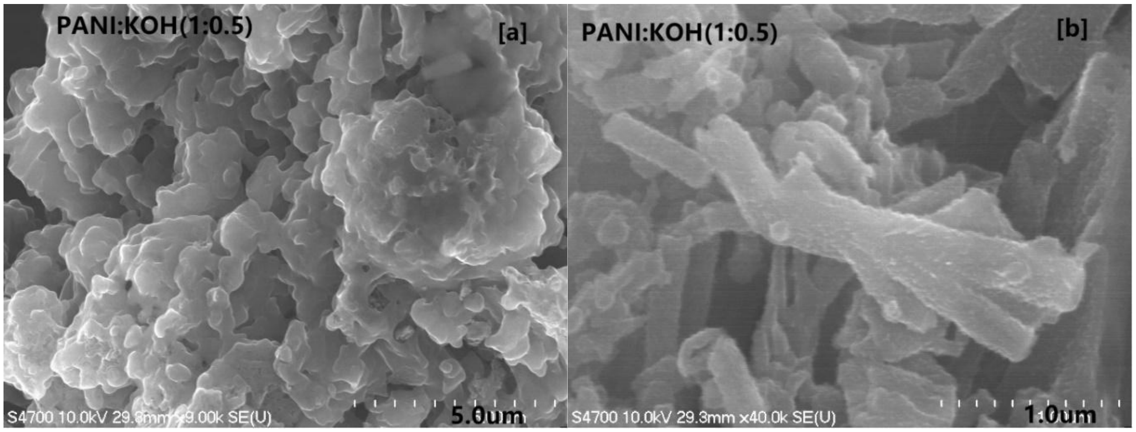

Figure 3.3. SEM images of PANI:KOH (1:0.5) at different magnifications.

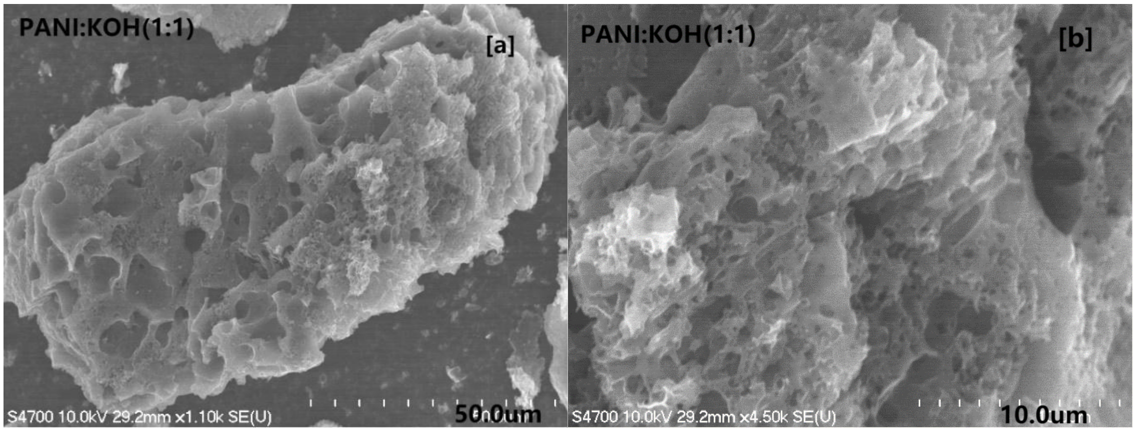

Figure 3.4. SEM images of PANI:KOH (1:1) at different magnifications.

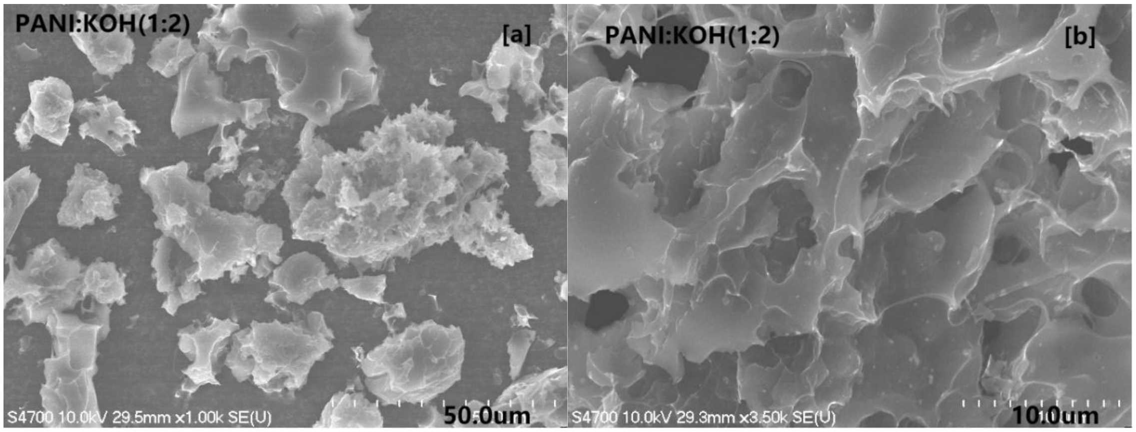

Figure 3.5. SEM images of PANI:KOH (1:2) at different magnifications.

3.1.2 BET Analysis

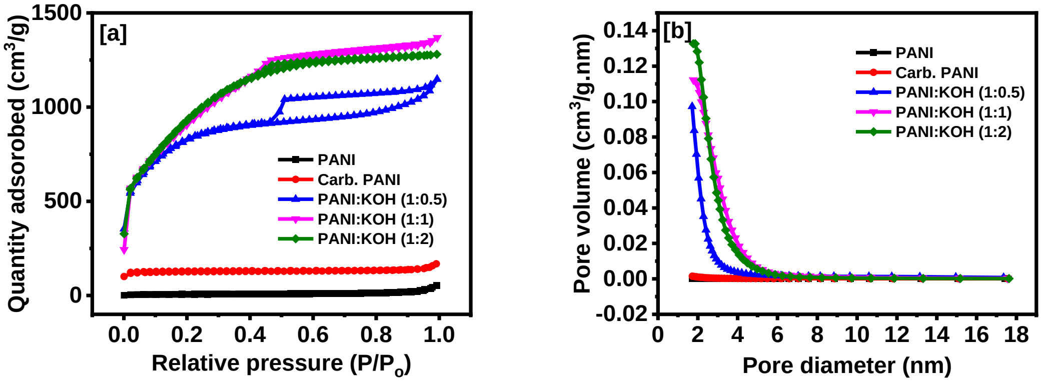

Figure 3.6. (a) Nitrogen adsorption-desorption isotherms and (b) Barrett-Joyner-Halenda (BJH) pore size distribution of all samples.

Figure 3.6.a shows the N_2 adsorption and desorption curves and, the pore size distribution curves of the materials. As shown in the adsorption and desorption curves for polyaniline and carbonized polyaniline, the adsorption amount of N_2 did not change significantly with the increase of pressure. According to IUPAC, there are six types of isotherm adsorption. The isotherm adsorption curves of PANI and carbonized PANI are the same, which is a type II isotherm adsorption curve, and there is no hysteresis loop in

the desorption process. These results indicate that there are some mesoporous structures in the PANI and carbonized PANI samples but are more abundant in carbonized PANI than in the as synthesized PANI. This result was verified by the SEM images of PANI and carbonized PANI in **Figure 3.1** and **3.2**, and that the high temperature for carbonization did not greatly change the microstructure of the material compared to the as-synthesized PANI. Compared with the isothermal adsorption and desorption curve of PANI, the microscopic pore structure of activated carbon material formed by high temperature activated polyaniline with potassium hydroxide exhibited a greater change. By adding potassium hydroxide during high-temperature activation, the isothermal adsorption and desorption curves of the active materials were compared with standard curve IV from the IUPAC isothermal adsorption data. This suggests that the increase in the amount of potassium hydroxide also showed an increase in the pore in these microporous structures. This result is consistent with the microstructural changes of activated carbon materials after activation by potassium hydroxide in SEM images. The isothermal adsorption and desorption curves of the polyaniline-activated carbon materials activated by potassium hydroxide show clear hysteresis loops. These hysteresis loops are in good agreement with the H4 type IUPAC hysteresis loops indicating that the contribution of these pore structures mainly comes from the slit pores produced by the layered structures. BET test results showed (**Table 3.1**) that the specific surface area of the active carbon material increased significantly from 21 m^2/g (PANI) to 393 m^2/g (Carb. PANI), 2776 m^2/g (PANI:KOH=1:0.5), 3259 m^2/g (PANI:KOH=1:1), and 3339 m^2/g (PANI:KOH=1:2).

It can be seen from the **Figure 3.6b** that mesoporous structures were formed in the potassium hydroxide activated carbon materials.

Table 3.1. BET surface area and BJH average pore width of all samples.

Sample	S_{BET}/m^2g^{-1}	Pore size/nm
PANI	21	5.8
Carb. PANI	393	3.8
PANI:KOH(1:0.5)	2776	2.6
PANI:KOH(1:1)	3259	2.7
PANI:KOH(1:2)	3339	2.5

3.1.3. Electrochemical measurement

A three-electrode test system was used to test the electrochemical performance of these active materials. The working electrode was made from clean nickel foam as the active material carrier, the counter electrode was a platinum wire, the reference electrode was a Hg/HgO electrode, and the electrolyte used was a 3 mol/L KOH solution.

3.1.3.1. Cyclic voltammetry

CV was performed in the potential range of -1 to 0 V in the scan range 2-3 mV/s.

The results of the cyclic voltammetry curve of PANI (**Figure 3.7**) show that the material exhibits pseudocapacitance characteristics. There are two oxidation peaks and two reduction peaks in the curve. We can see that with the change of scanning rate, the peak potential has a shift, which indicates that the reversibility of polyaniline is poor. In the process of cyclic voltammetry, the current flowing through the polyaniline material is very low, resulting in a very specific capacitance of the material.

In contrast, carbonized polyaniline exhibits electrical double-layer capacitance type characteristics (**Figure 3.8**). In the low potential scans, there were two oxidation peaks in the CV curve and the positions of the two peaks were consistent with the oxidation peaks of polyaniline, indicating that the heteroatoms in polyaniline were not lost due to carbonization at a high temperature. However, the electrical double layer capacitance of polyaniline after high-temperature carbonization has occupied the dominant position of material capacitance. The polyaniline CV curves (**Figures 3.9 - 3.11**) activated at high temperature by potassium hydroxide show nearly perfect double-layer capacitor properties. All the graphs are rectangular and have no obvious redox peak and all the graphs have the characteristic of centrosymmetry.

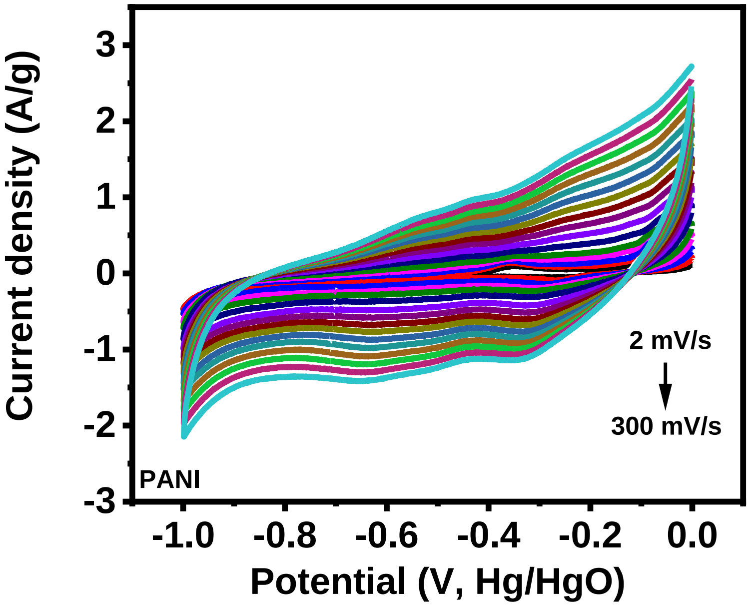

Figure 3.7. CV curves of PANI at different scan rates.

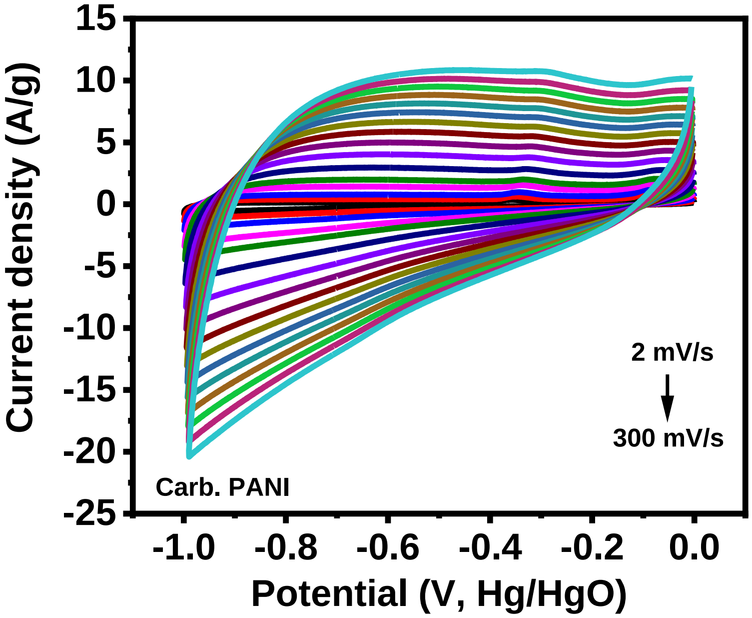

Figure 3.8. CV curves of Carbonized PANI at different scan rates.

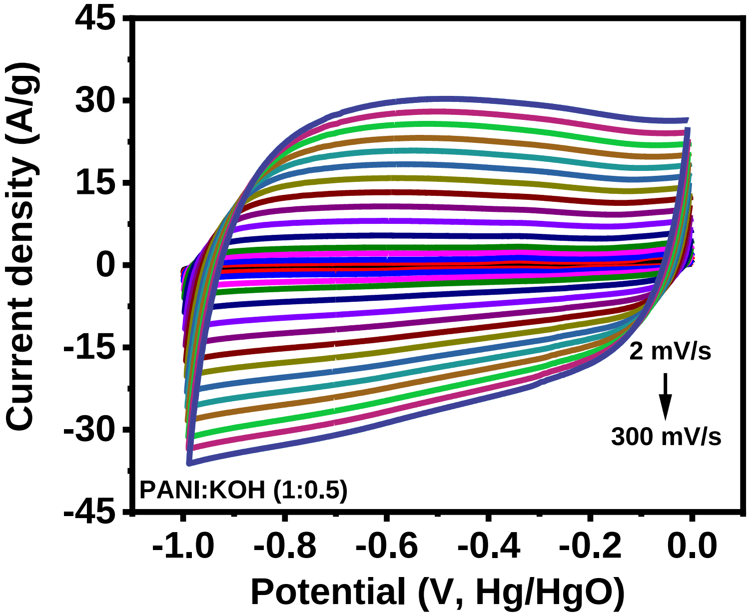

Figure 3.9. CV curves of PANI:KOH (1:0.5) at different scan rates.

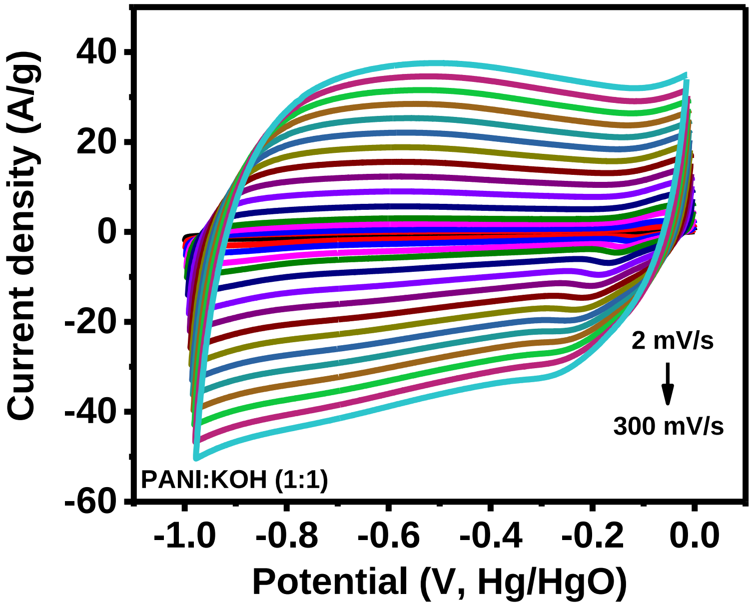

Figure 3.10. CV curves of PANI:KOH (1:1) at different scan rates.

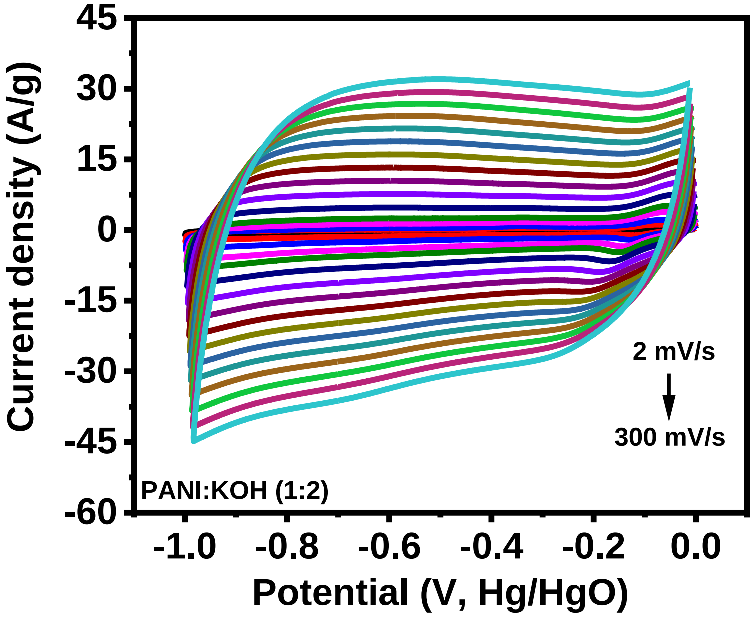

Figure 3.11. CV curves of PANI:KOH (1:2) at different scan rates.

As can be seen in **Figure 3.12**, all materials show that the specific capacitance gradually decreases with the increase in scan rate. In general, the electrochemical performance of polyaniline activated by potassium hydroxide has been significantly improved and the material has the best electrochemical performance when PANI:KOH= 1:1. The main reason is that the etching of potassium hydroxide makes it become an active carbon material with a specific surface area up to 3259 m^2/g. This also explains that the electrochemical performance of the material decreases slightly when PANI:KOH=1:2 and the increase of potassium hydroxide leads to erosion of the carbon material. When the scanning rate is 2 mV/s the specific capacitances of PANI, carbonized PANI, PANI:KOH (1:5), PANI:KOH (1:1), and PANI:KOH (1:2) are 100 F/g, 216 F/g, 3587 F/g, 550 F/g, and 359 F/g, respectively.

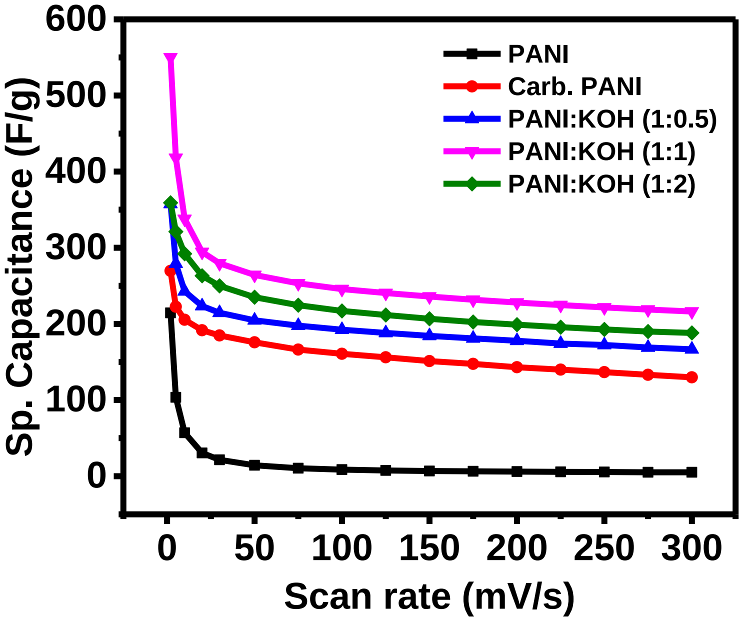

Figure 3.12. Specific capacitance versus scan rate for all the samples.

3.1.3.2. Galvanostatic charge-discharge

Galvanostatic charge-discharge was performed in the current density range from 30 A/g to 0.5 A/g and a test voltage range of -1 to 0 V. Constant current charge and discharge can help to understand the specific capacitance of the material at different current densities and the rate performance of the material.

Figure 3.13 reveals the charge-discharge curves of PANI at different current densities. When the current density is higher than 7 A/g, the charge-discharge curves cannot accurately reflect the chemical properties of PANI. It can be seen from the low current density charge-discharge curves that aniline has obvious pseudocapacitance characteristics but it has poor electrochemical performance in constant current charge-discharge tests.

The most intuitive manifestation is that under the same charge-discharge current density **Figure 3.14**, the carbonized PANI takes a longer time to complete the charge-discharge than PANI (**Figure 3.13**). This means that carbonization increases the specific capacitance of the carbon material. In addition, the charge-discharge curve of carbonized PANI is similar to a triangle, which shows good electrical double-layer capacitance characteristics, but the non-smooth curve reflects that the material still has pseudocapacitance characteristics.

According to the galvanostatic charge-discharge curves of the activated polyaniline activated carbon material activated by potassium hydroxide (**Figure 3.15 - 3.17**), the material shows a double-layer capacitance characteristic. What is more noteworthy is that the charge-discharge time of the active material is greatly improved compared with that of polyaniline and carbonized polyaniline. This means that the capacitive performance of the material has been improved.

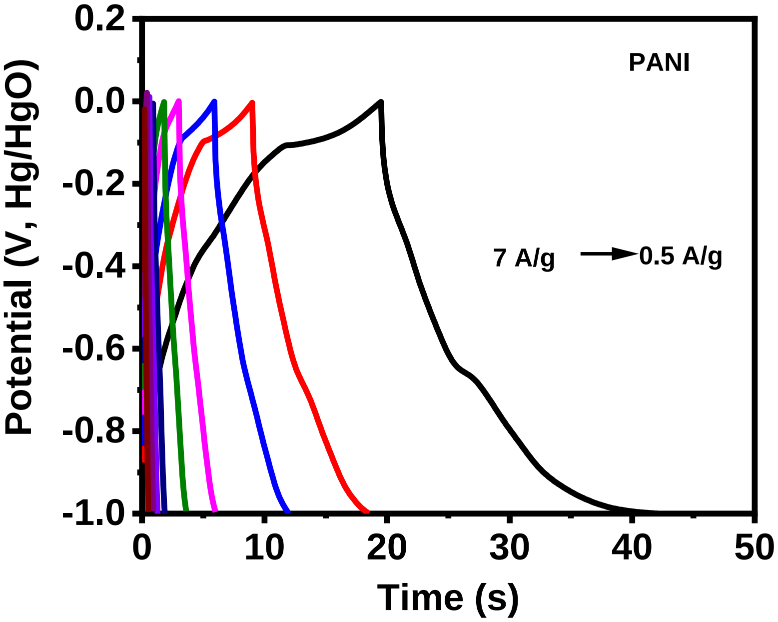

Figure 3.13. Potential versus time at different current density for PANI.

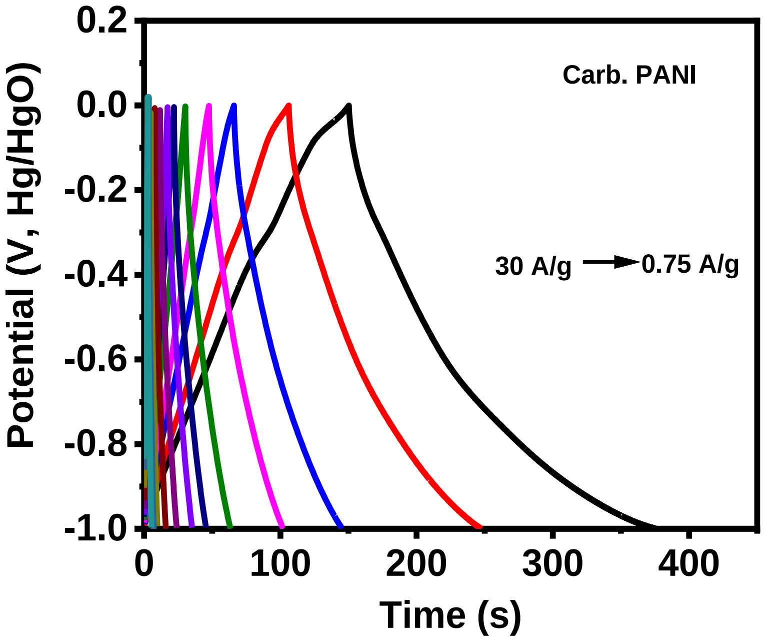

Figure 3.14. Potential versus time at different current density for carbonized PANI.

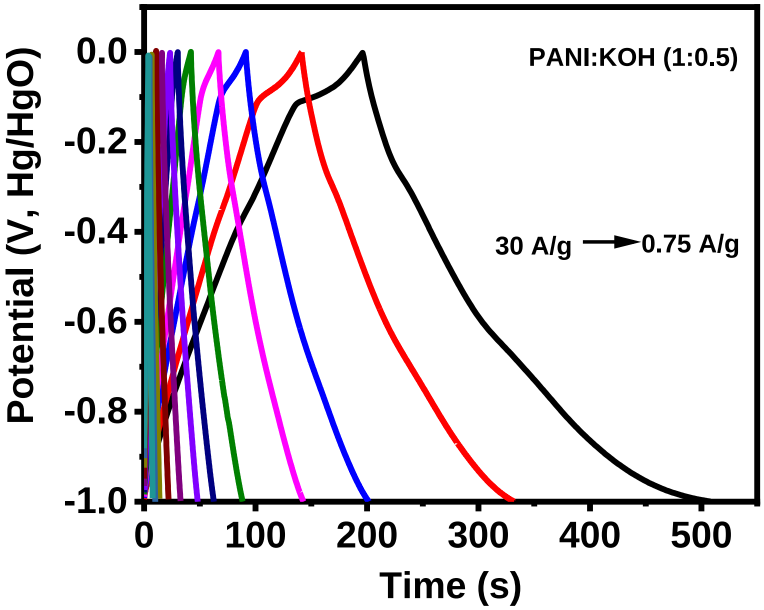

Figure 3.15. Potential versus time at different current density for PANI:KOH (1:0.5).

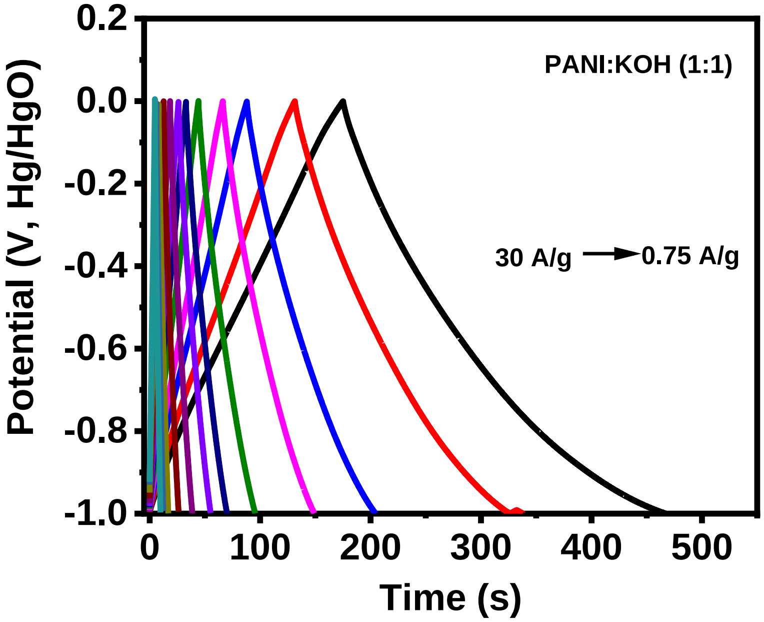

Figure 3.16. Potential versus time at different current density for PANI:KOH (1:1).

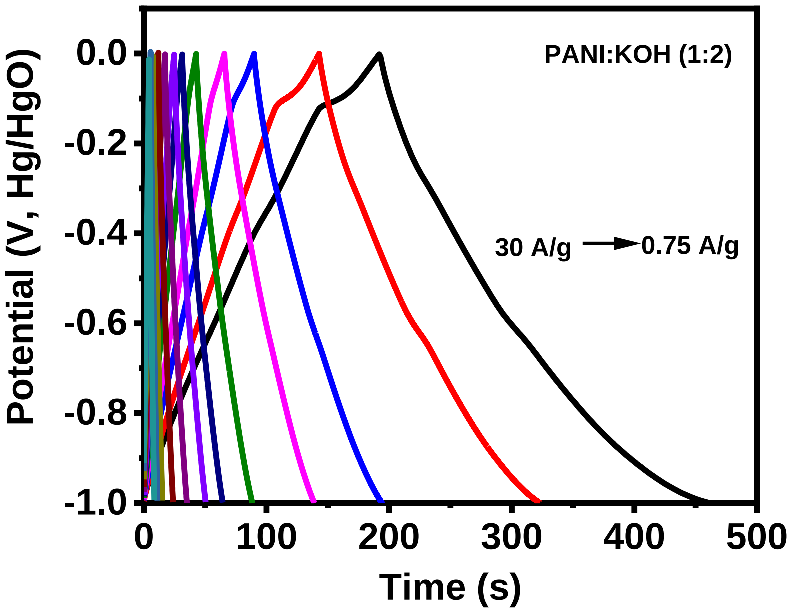

Figure 3.17. Potential versus time at different current density for PANI:KOH (1: 2).

When the charging current is 1 A/g the specific capacitances of PANI, carbonized PANI, PANI:KOH (1:0.5), PANI:KOH (1:1), and PANI:KOH (1:2) are 5.4 F/g, 97.9 F/g, 191.7 F/g, 194.3 F/g, and 181.2 F/g respectively. The results are in good agreement with those of the electrochemical properties of the materials detected by cyclic voltammetry. In addition, it can be seen from **Figure 3.18** that when the charge and discharge current density is higher than 3 A/g the specific capacitance of the materials only decreases slightly with the increase of the charge and discharge current density. From each study, the electrochemical performance of PANI:KOH (1:1) sample is better than that of the other.

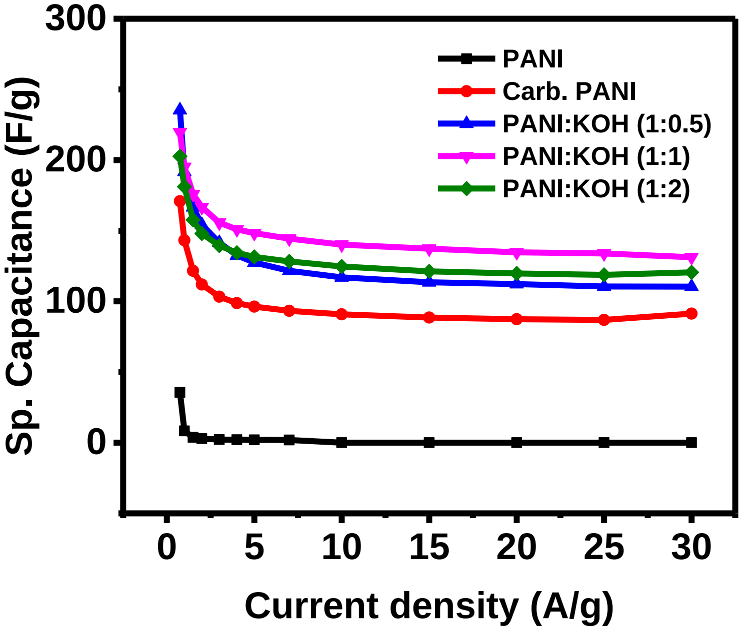

Figure 3.18. Specific capacitance versus current density for all the samples.

Figure 3.19 shows the relationship between the energy density and power density of all materials. It can be seen that all materials show similar energy density and power density changes. When the current density is low the material shows a high energy density but the power density is poor. Taking PANI:KOH (1:1) with the best electrochemical performance as an example, the energy density is 26.87 Wh/kg when the charging current density is 1 A/g and the corresponding power density is 498 W/kg. When the charge/discharge current density is 30 A/g the energy density is 15.6 Wh/kg while the power density at this time is as high as 11436 W/kg.

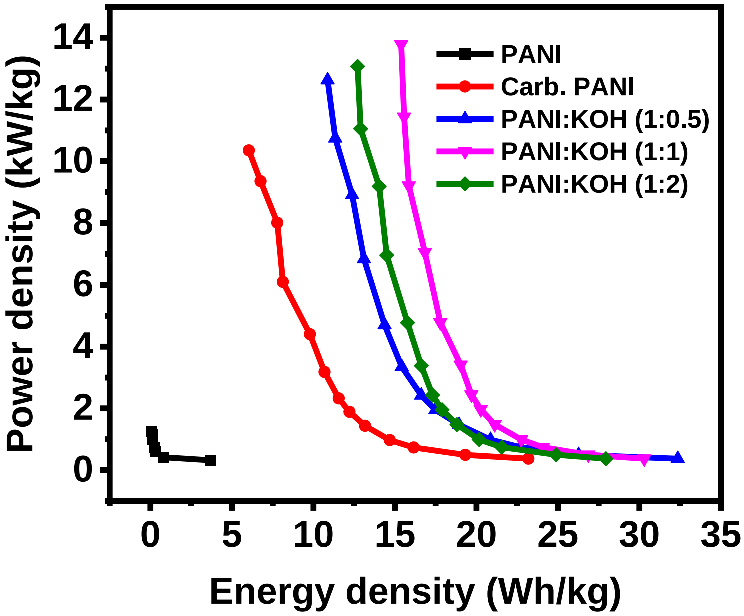

Figure 3.19. Power density versus energy density for all the samples.

Figure 3.20 shows the stability test result for PANI:KOH(1:1). As seen, the sample shows high capacitance retention (92%) even after 5000 charge-discharge cycles. In addition, coulombic efficiency was about 100%.

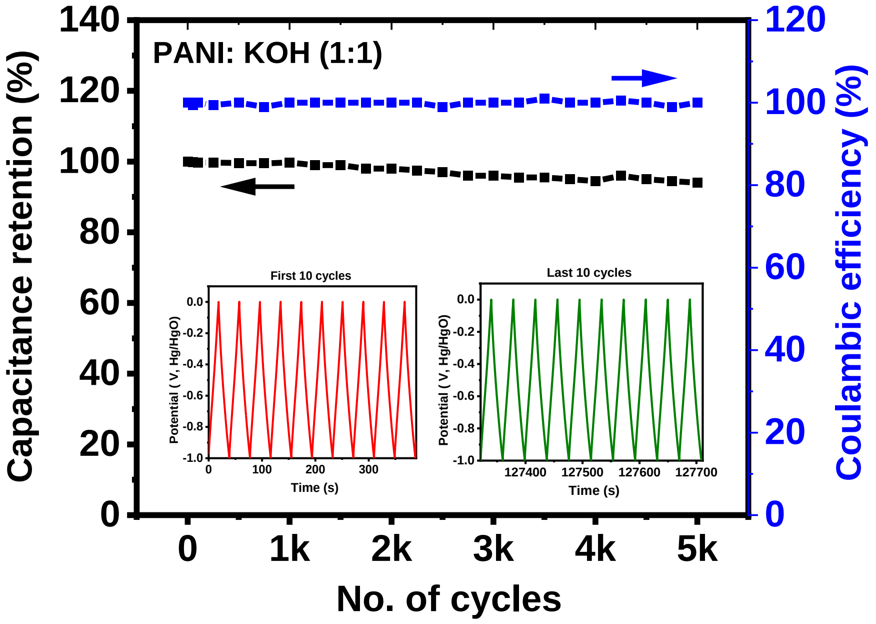

Figure 3.20. Stability curves for PANI:KOH(1:1).

3.2. Structural and electrical characterization of composite polyaniline and transition metal oxides

In this part of the work, 7 materials were studied: PANI, Co_3O_4, NiO, Co_2NiO_4, PANI/Co_3O_4, PANI/NiO, and PANI/Co_2NiO_4.

3.2.1. BET analysis

Figure 3.21 - 3.27 show the nitrogen isothermal adsorption and desorption curves of PANI, Co_3O_4, NiO, Co_2NiO_4, PANI/Co_3O_4, PANI/NiO, and PANI/Co_2NiO_4. All these materials show similar nitrogen isothermal adsorption and desorption curves. According to the IUPAC standard these curves can be classified as type II, emphasizing the non-porous structure of the material. The nitrogen adsorption and desorption curves also have hysteresis loops that can be classified as H3, indicating that these porous structures come from the accumulation of sheet materials. From **Table 3.2**, it can be seen that NiO had the highest surface area which was 52.60 cm^2/g.

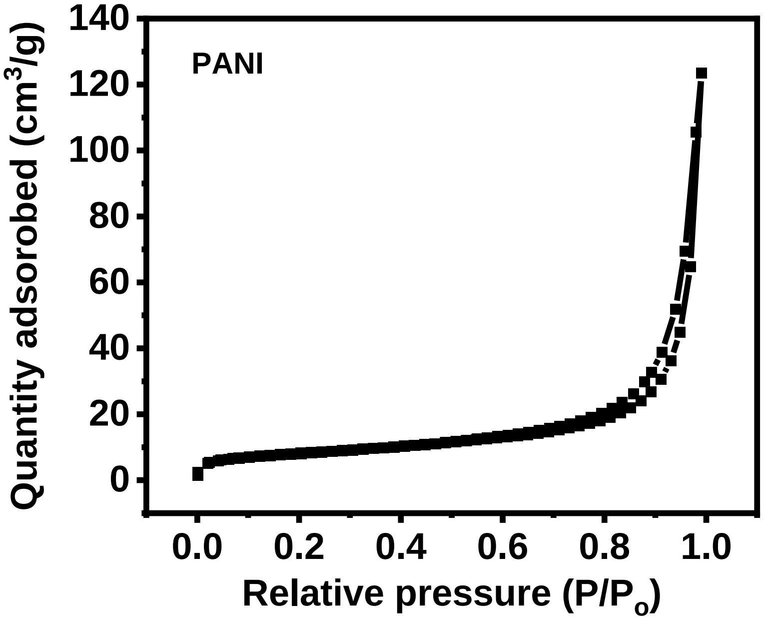

Figure 3.21. Nitrogen adsorption-desorption isotherms of PANI.

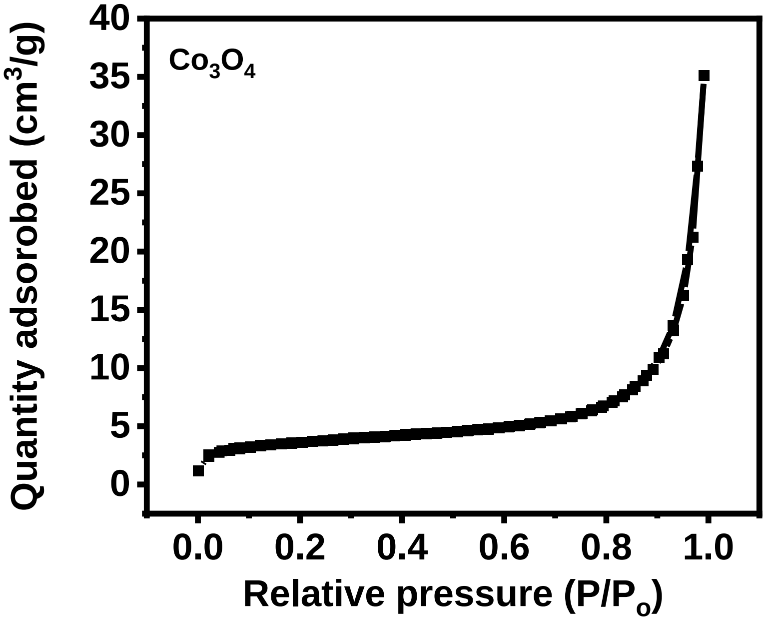

Figure 3.22. Nitrogen adsorption-desorption isotherms of Co_3O_4.

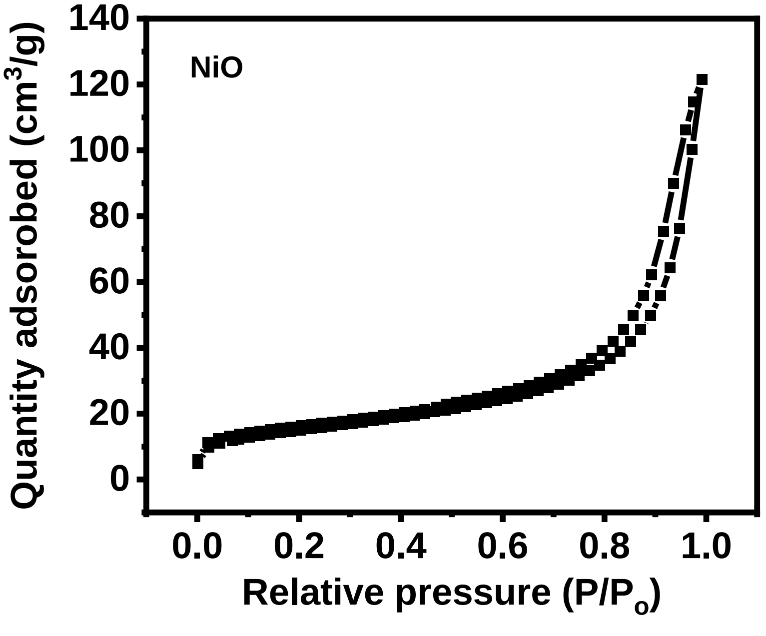

Figure 3.23. Nitrogen adsorption-desorption isotherms of NiO.

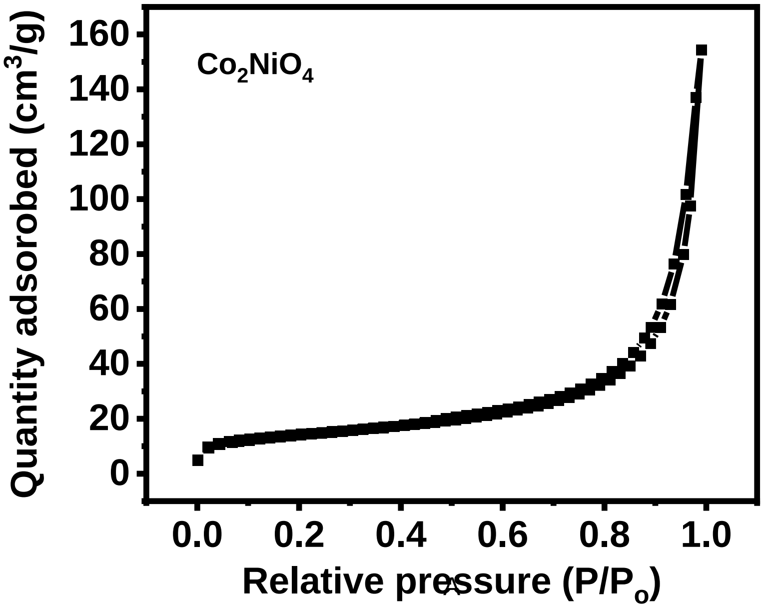

Figure 3.24. Nitrogen adsorption-desorption isotherms of Co_2NiO_4.

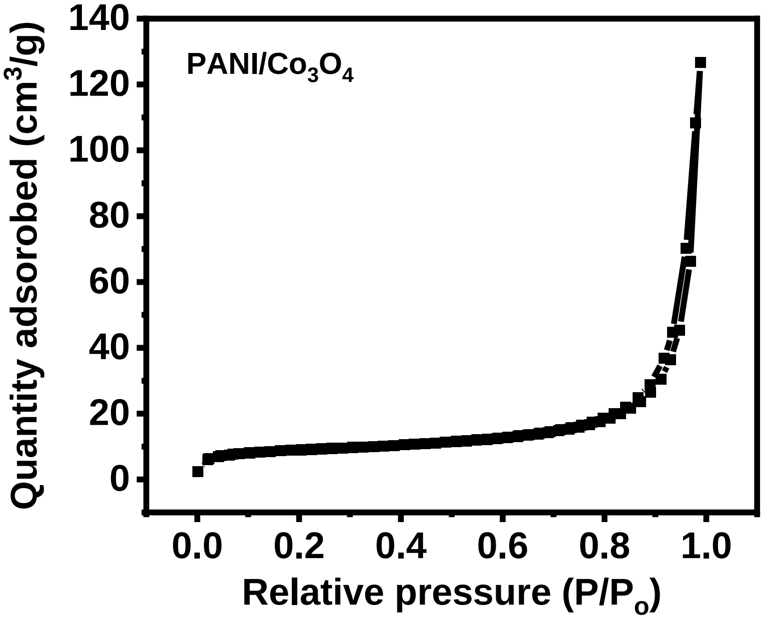

Figure 3.25. Nitrogen adsorption-desorption isotherms of PANI/Co_3O_4.

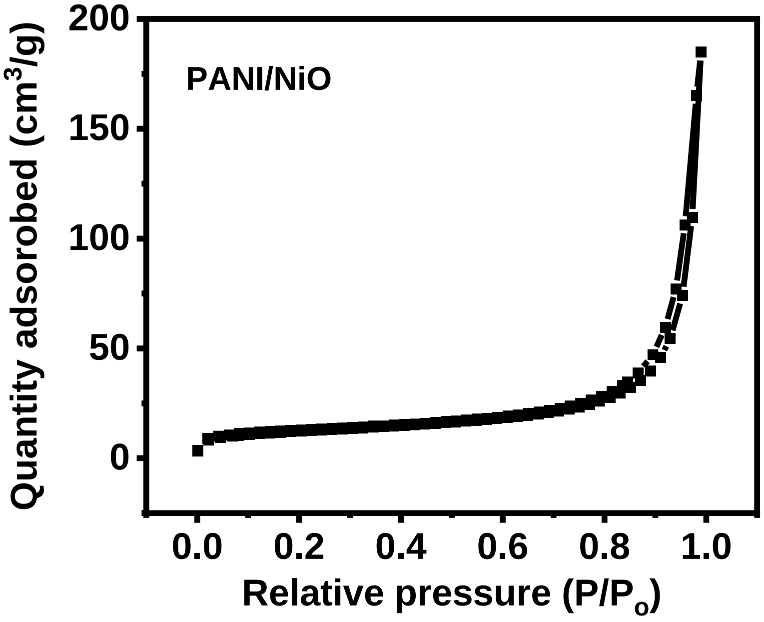

Figure 3.26. Nitrogen adsorption-desorption isotherms of PANI/NiO.

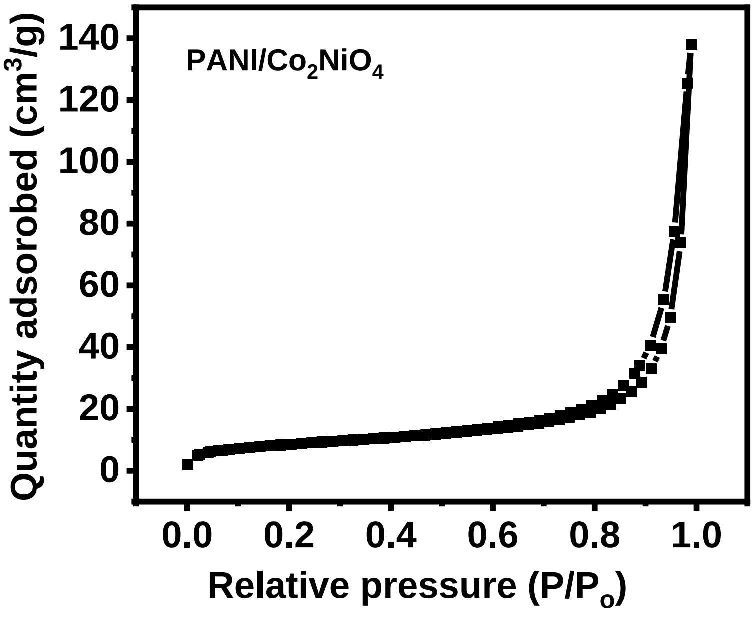

Figure 3.27. Nitrogen adsorption-desorption isotherms of PANI/Co_2NiO_4.

Table 3.2. BET surface area and BJH average pore width of all samples.

Sample	S_{BET}/m^2g^{-1}	Pore size/nm
PANI	28.6	6.6
Co_3O_4	12.2	7.2
NiO	52.6	6.4
Co_2NiO_4	48.5	6.9
PANI/Co_3O_4	30.3	7.6
PANI/NiO	42.2	7.0
PANI/Co_2NiO_4	30.2	6.7

3.2.2. XRD analysis

Figure 3.28 - 3.34 show the X-ray diffraction pattern of PANI, Co_3O_4, NiO, Co_2NiO_4, PANI/Co_3O_4, PANI/NiO, and PANI/Co_2NiO_4. Except for nickel oxide, other materials exhibited an amorphous structure. These results are not of substantial help to the exploration of the microstructure of the material.

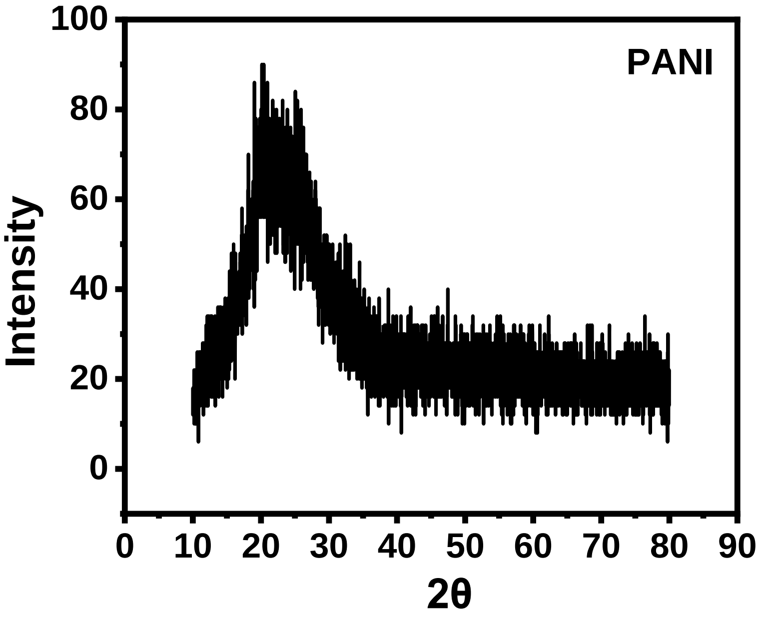

Figure 3.28. XRD patterns of PANI.

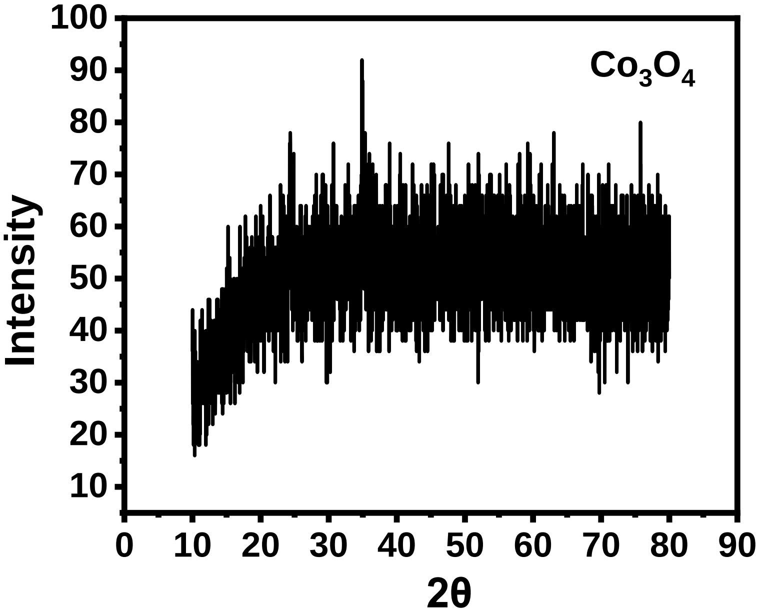

Figure 3.29. XRD patterns of Co_3O_4.

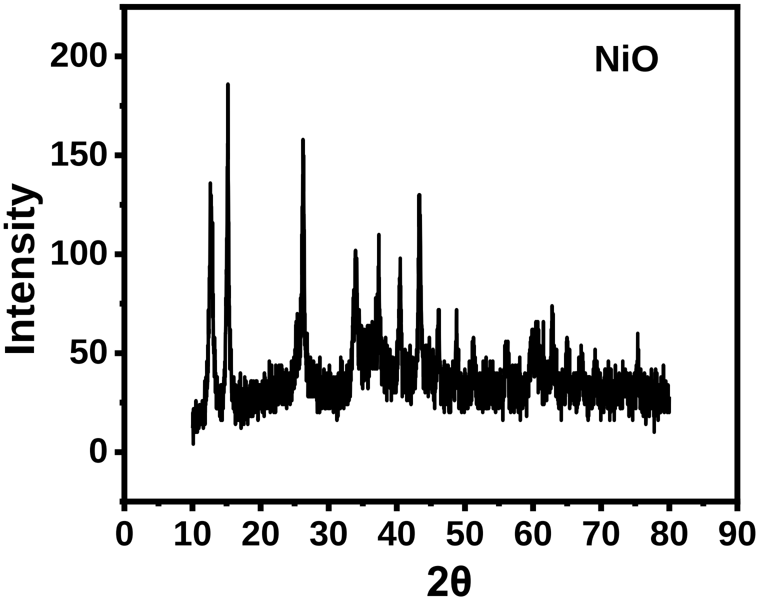

Figure 3.30. XRD patterns of NiO.

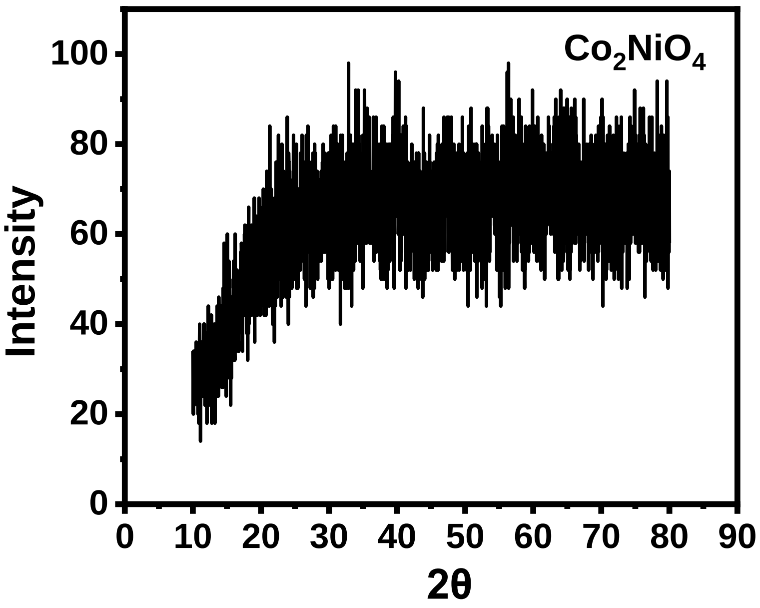

Figure 3.31. XRD patterns of Co_2NiO_4.

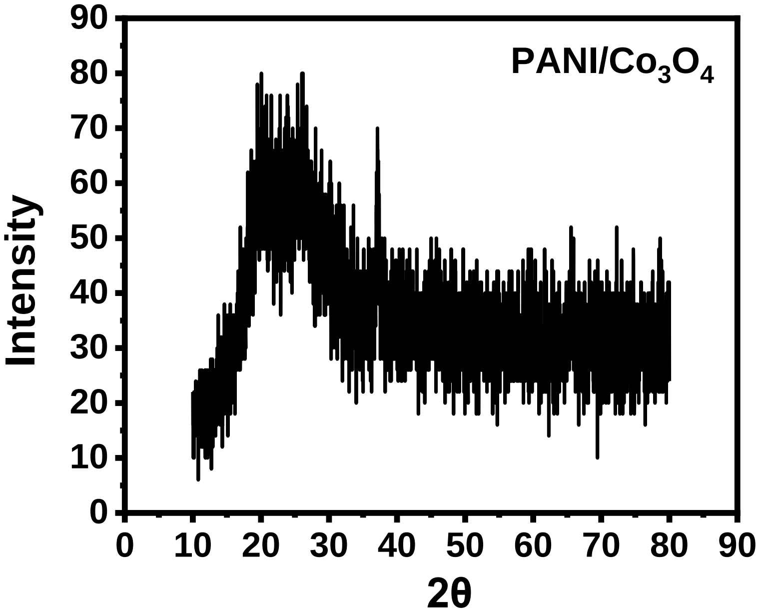

Figure 3.32. XRD patterns of $PANI/Co_3O_4$.

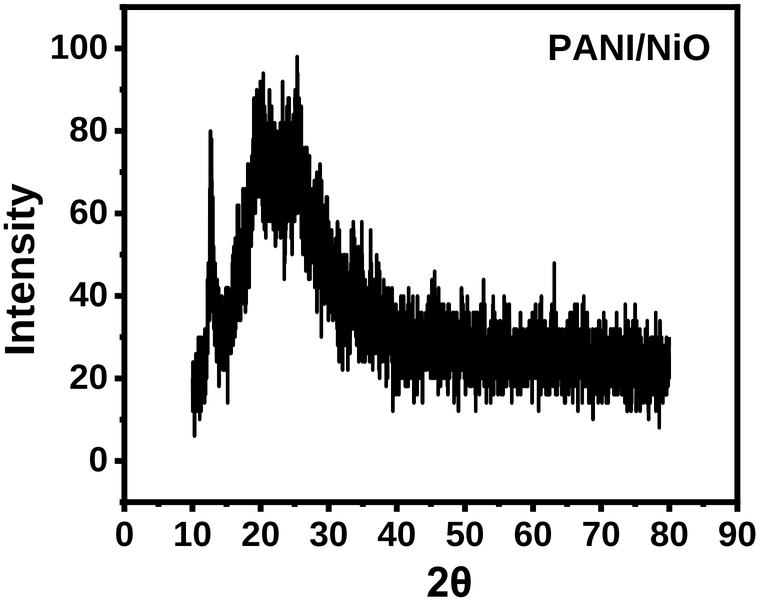

Figure 3.33. XRD patterns of PANI/NiO.

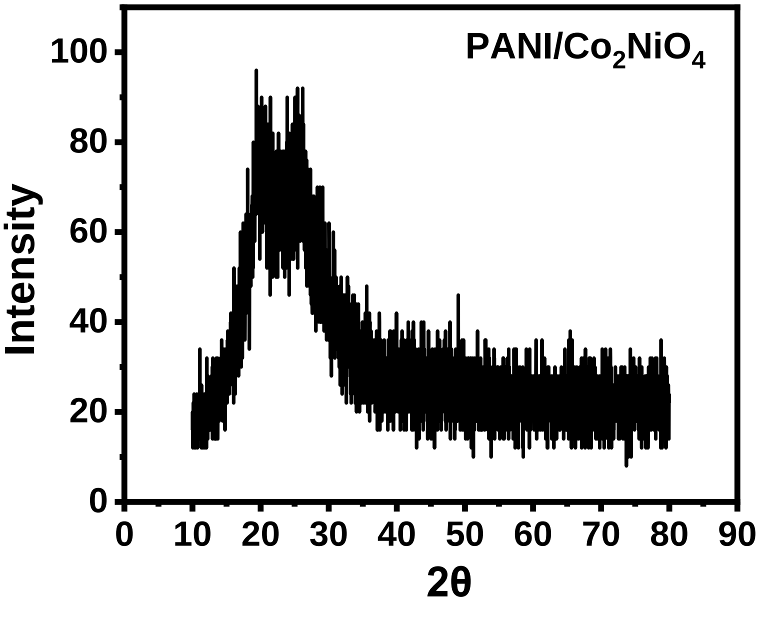

Figure 3.34. XRD patterns of PANI/Co$_2$NiO$_4$.

3.2.3. Hydrogen evolution reaction testing

A three-electrode test system was used to test the HER performance of these active materials. The working electrode was made on clean nickel foam by depository synthetic material, a platinum wire and RHE were used as counter electrode and reference electrode. 1M KOH solution was used as an electrolyte.

In order to understand the catalytic performance of the materials for electrolysis, HER tests were conducted.

Figure 3.35 shows the LSV-CV curves of PANI, Co_3O_4, and PANI/Co_3O_4. To compare the performance differences of each material, a current density of 10 mV/cm^2 was selected as the point for comparison of overpotentials. It can be seen that PANI and Co_3O_4 have the same overpotential of 172 mV to achieve a current density of 10 mV/cm^2. In contrast, the PANI/Co_3O_4 composite material requires a higher overpotential of 202 mV to achieve a current density of 10 mV/cm^2. **Figure 3.36** shows the Tafel slopes, which are used to understand the kinetics at the process. PANI, Co_3O_4, and PANI/Co_3O_4 have relatively close Tafel slopes, which are 151 mV/dec, 157 mV/dec, and 148 mV/dec, respectively. The stability of the catalyst is an important indicator of whether the catalyst has commercial value. **Figure 3.41, Figure 3.42,** and **Figure 3.45** show the comparison diagram of the 1000th cycle LSV-CV curve and the first LSV-CV curve of the material. Polyaniline showed the best stability because its LSV-CV-1 curve closely coincided with the LSV-CV-1K curve, while the LSV-CV-1 curve and LSV-CV-1K curve of Co_3O_4, and PANI/Co_3O_4 all had a shift.

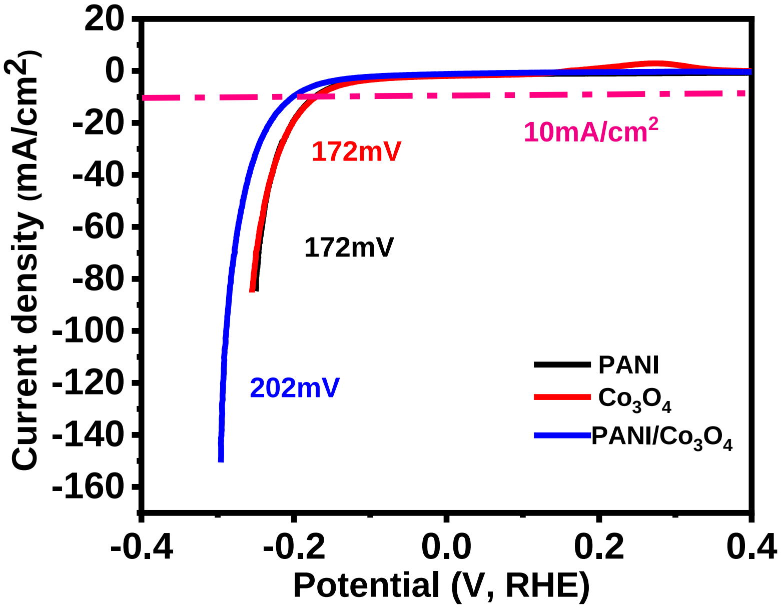

Figure 3.35. LSV-CV curves of PANI, Co_3O_4, and PANI/Co_3O_4 for HER in 1 M KOH.

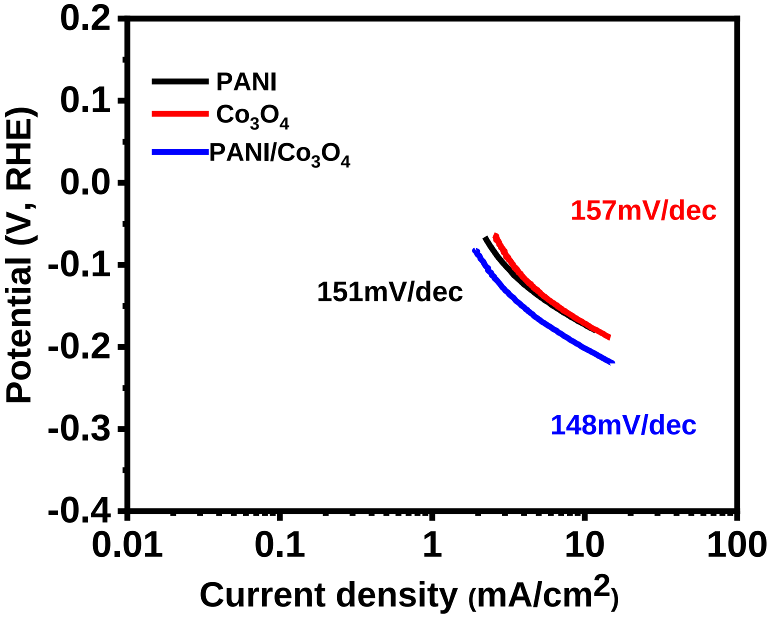

Figure 3.36. Tafel curves for PANI, Co_3O_4, and PANI/Co_3O_4.

Another transition metal oxide, nickel oxide, has also been studied to explore the electrochemical performance of its composite material with polyaniline. **Figure 3.37** shows the LSV-CV curves of PANI, NiO, and PANI/NiO for the returning cycle. The overpotentials of PANI, NiO, and PANI/NiO are 172 mV, 198 mV, and 215 mV, respectively to reach 10 mA/cm^2. **Figure 3.38** shows the Tafel slopes of these three materials. PANI, NiO, and PANI/NiO have relatively close Tafel slopes of 151 mV/dec, 118 mV/dec, and 139 mV/dec, respectively. **Figure 3.41**, **Figure 3.43**, and **Figure 3.46** show the comparison diagram of the 1000th cycle LSV-CV curve and the first LSV-CV curve of the material. Polyaniline showed the best stability because its LSV-CV-1 curve coincided with the LSV-CV-1K curve, while the LSV-CV-1 curve and LSV-CV-1K curve of NiO, and PANI/NiO all had a shift.

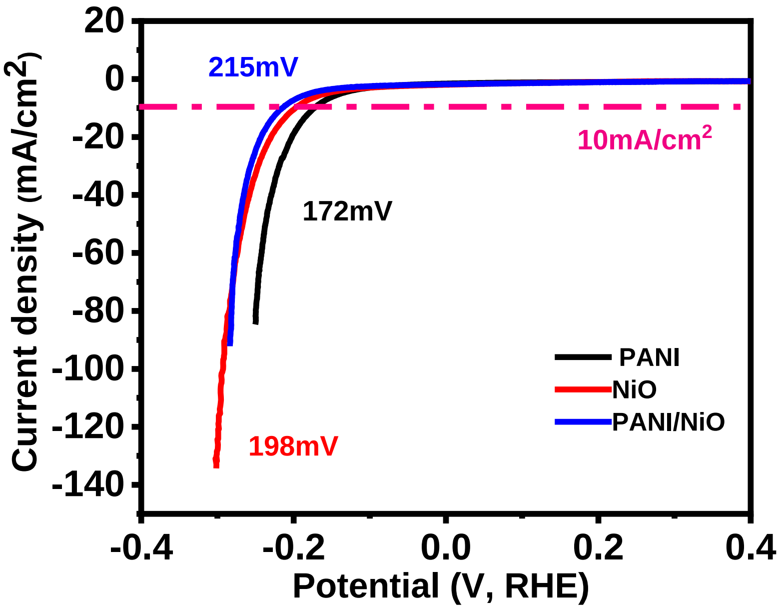

Figure 3.37. LSV-CV curves of PANI, NiO and PANI/NiO for HER in 1 M KOH.

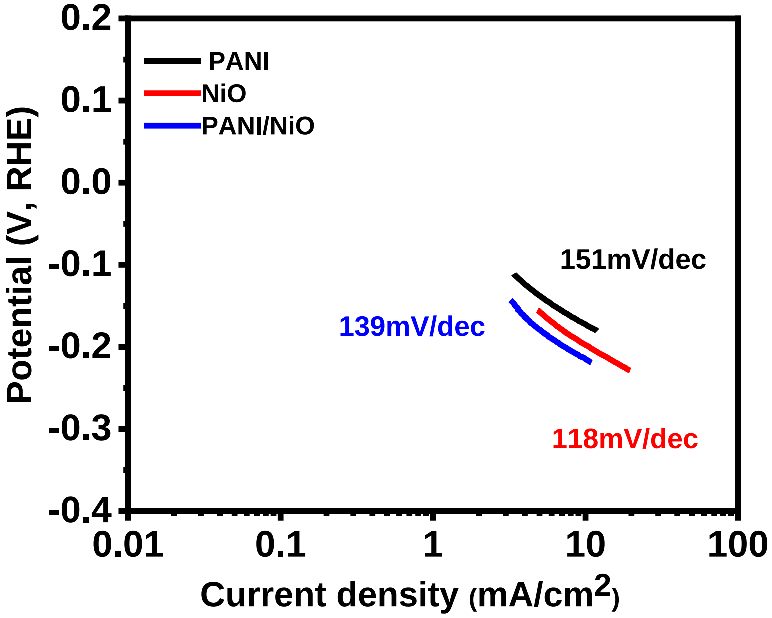

Figure 3.38. Corresponding Tafel curves for PANI, NiO, and PANI/NiO.

Nickel cobalt oxide was also studied to explore the electrochemical performance of its composite material with polyaniline. **Figure 3.39** shows the LSV-CV curves of PANI, Co_2NiO_4, and PANI/Co_2NiO_4. The overpotentials of PANI, Co_2NiO_4, and PANI/Co_2NiO_4 are 172 mV, 175 mV, and 145 mV, respectively to reach 10 mA/cm^2. **Figure 3.40** shows the Tafel slopes of PANI, Co_2NiO_4, and PANI/Co_2NiO_4 were 151 mV/dec, 126 mV/dec, and 214 mV/dec, respectively. **Figure 3.41, Figure 3.44,** and **Figure 3.47** show the comparison diagram of the 1000th cycle LSV-CV curve and the first LSV-CV curve of the material. PANI and Co_2NiO_4 both show better stability because the LSV-CV-1 curve coincided with the LSV-CV-1K curve, while the LSV-CV-1 curve and LSV-CV-1K curve of PANI/Co_2NiO_4 had a significant shift.

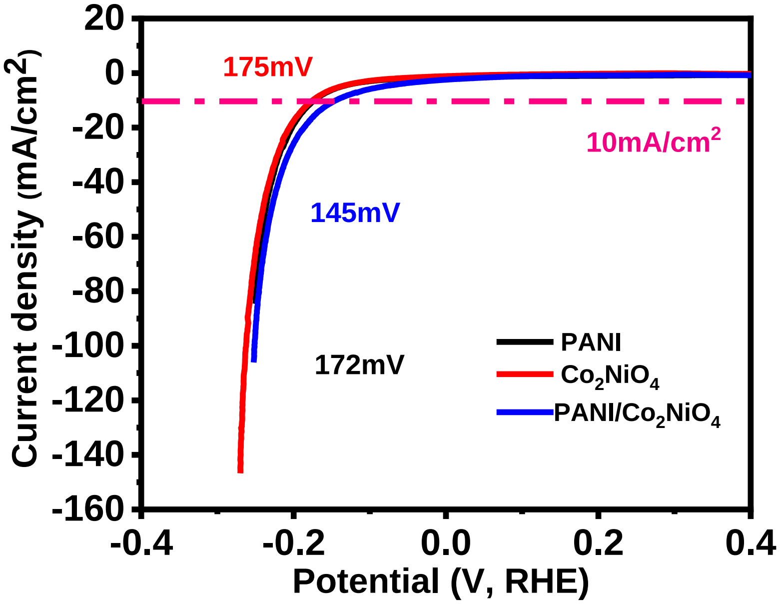

Figure 3.39. LSV-CV curves of PANI, Co_2NiO_4, and PANI/Co_2NiO_4 for HER in 1 M KOH.

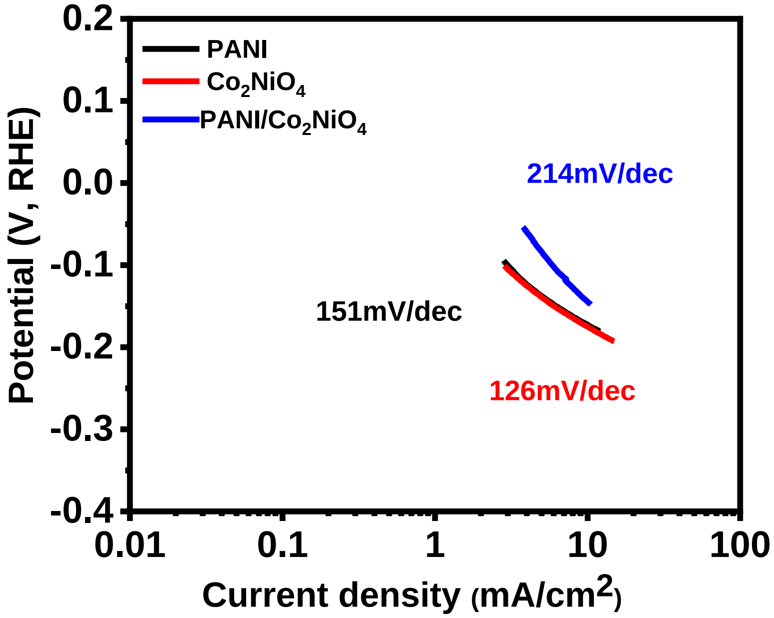

Figure 3.40. Corresponding Tafel curves for PANI, NiO, and PANI/NiO.

Table 3.3. HER characteristics of the samples in 1 M KOH.

Catalyst	$E_{j=10mA/cm^2}$ (V)	Overpotential (mV)	Tafel slope (mV/dec)
PANI	1.402	172	151
Co_3O_4	1.402	172	157
NiO	1.428	198	118
Co_2NiO_4	1.405	175	126
PANI/Co_3O_4	1.432	202	148
PANI/NiO	1.445	215	139
PANI/Co_2NiO_4	1.375	145	214

Table 3.4. Comparison of HER characteristics of various non-noble electrocatalysts.

Catalyst	electrolyte	Overpotential @ j10/mV	Tafel slope	Reference
PANI/CoP@HNWs-CFS	0.5 M H_2SO_4	15	34.5	[46]
PANI/CoNiP-NF	0.5 M H_2SO_4	61	80	[50]
DBC-MoS-PANI2	0.5 M H_2SO_4	196	58	[51]
CoNS-C	0.5 M H_2SO_4	180	66	[52]
Co/Co_3O_4	1 M KOH	90	44	[53]
$NiCo_2S_4$/Ni_3S_2/NF	1 M KOH	105.2	119	[54]
Co_2NiN	1 M KOH	102.6	60.17	[55]
Multishelled NiO	1 M KOH	98	86.4	[56]

To better understand the characteristics of these materials as catalysts for hydrogen evolution reactions, the performance of materials was compared with other similar materials use for water splitting. Compared with PANI and Co_2NiO_4, the electrocatalytic properties of PANI/Co_2NiO_4 were improved, mainly due to the substantial reduction in overpotential. Generally, the hydrogen evolution reaction performs better in acidic electrolytes than in alkaline electrolytes. From the comparison of **Table 3.3** and **Table 3.4**, the performance of PANI/Co_2NiO_4 is acceptable.

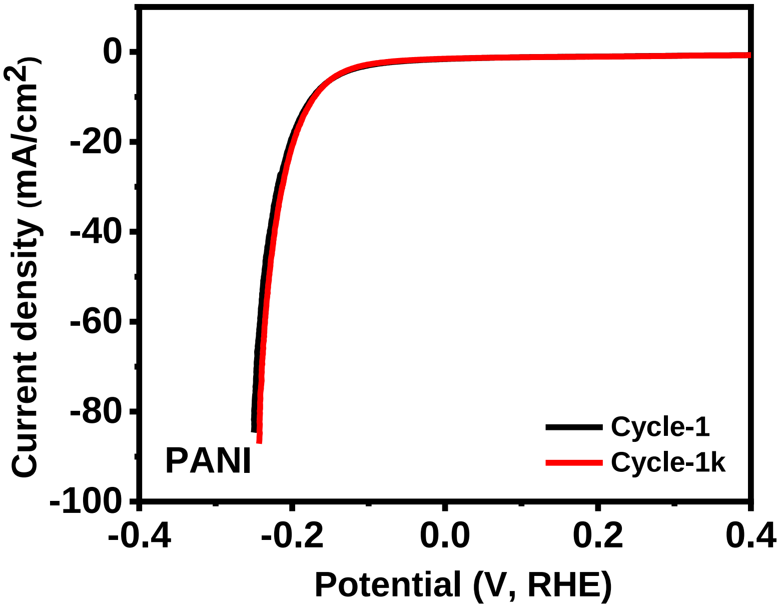

Figure 3.41. LSV & LSV-1K HER stability test of the PANI.

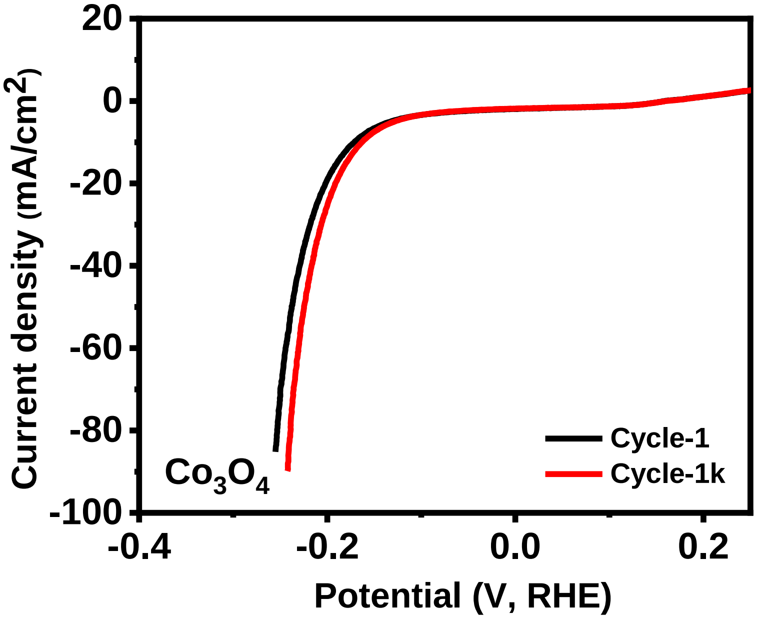

Figure 3.42. LSV & LSV-1K HER stability test of the Co_3O_4.

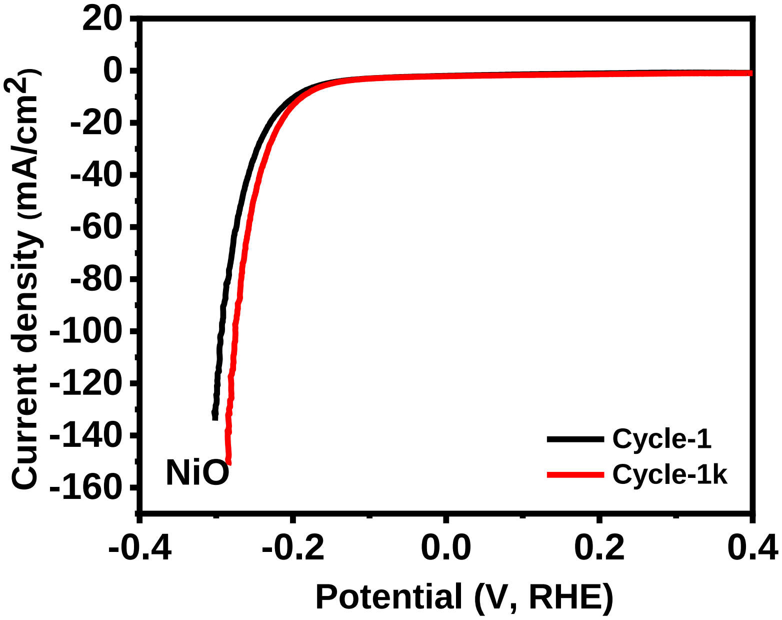

Figure 3.43. LSV & LSV-1K HER stability test of the NiO.

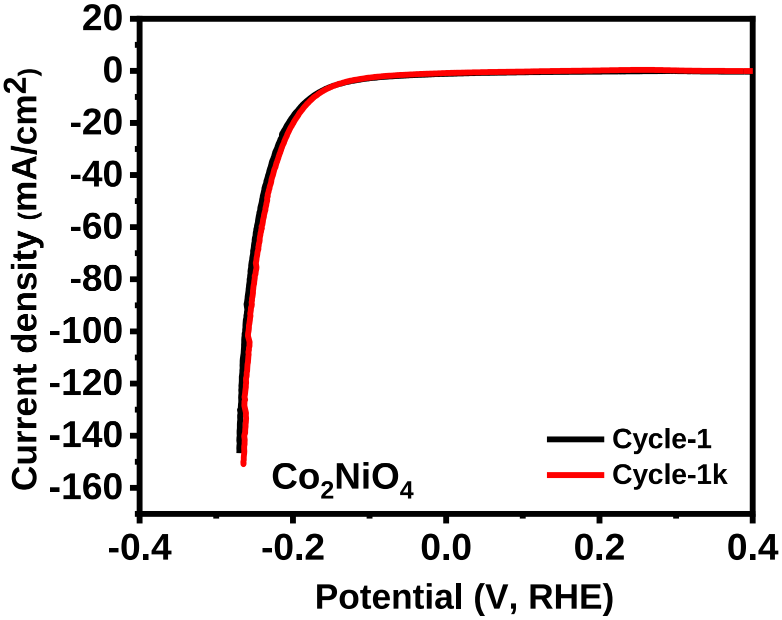

Figure 3.44. LSV & LSV-1K HER stability test of the Co_2NiO_4.

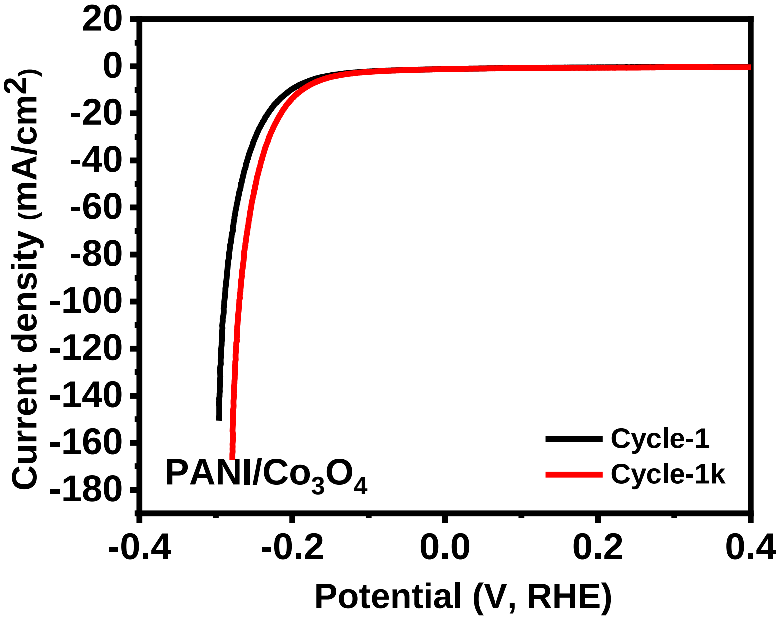

Figure 3.45. LSV & LSV-1K HER stability test of the PANI/Co_3O_4.

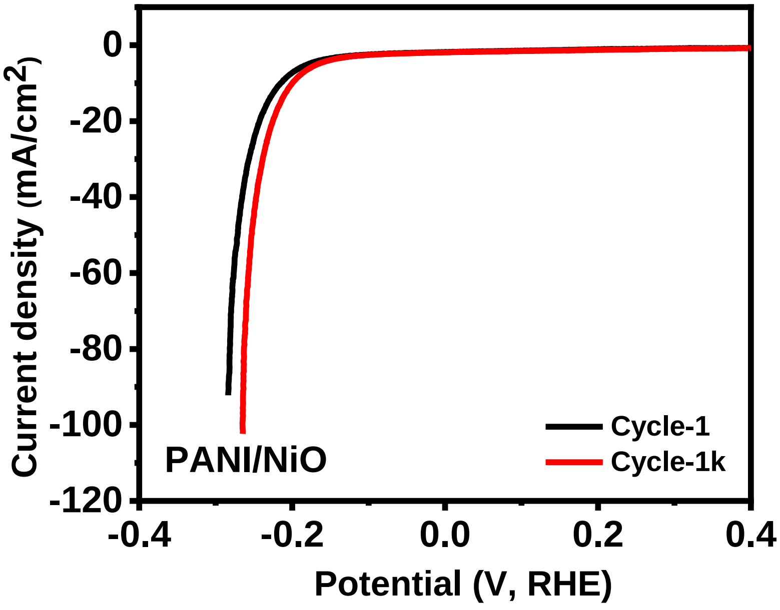

Figure 3.46. LSV & LSV-1K HER stability test of the PANI/NiO.

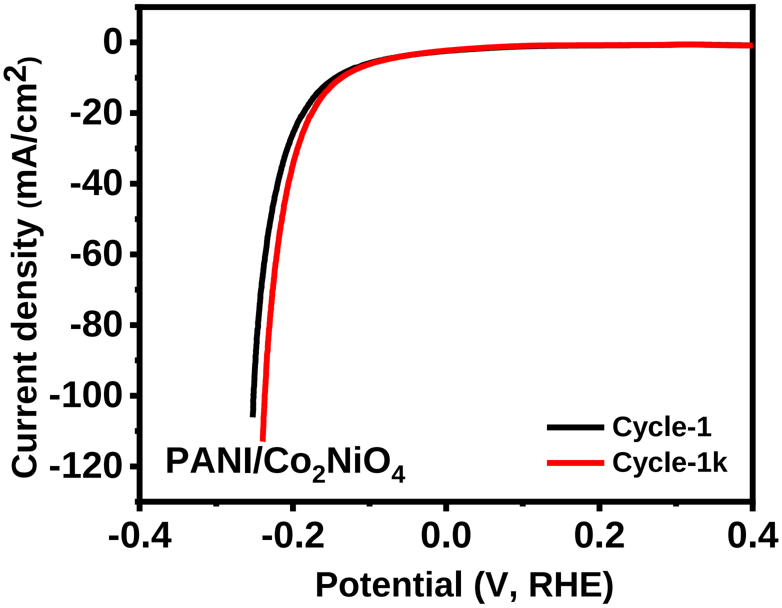

Figure 3.47. LSV & LSV-1K HER stability test of the PANI/Co_2NiO_4.

3.2.4. Oxygen evolution reaction testing

In order to understand the catalytic performance of the material during electrolysis, these materials were also tested under OER conditions. **Figure 3.48** shows the LSV curves of PANI, Co_3O_4, and PANI/ Co_3O_4. In order to compare the performance difference of each material, the current density of 10 mV/cm^2 was selected as the value for the overpotential comparison. From **Figure 3.48,** it can be seen that Co_3O_4 and PANI/Co_3O_4 have the same overpotential of 390 mV to achieve a current density of 10 mV/cm^2. In contrast, PANI composites require a higher overpotential of 420 mV to achieve a current density of 10 mV/cm^2.

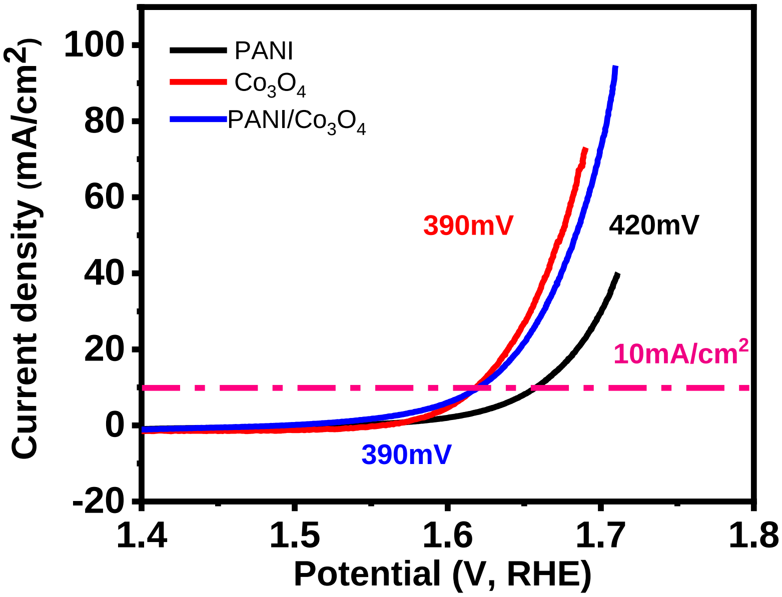

Figure 3.48. LSV-CV curves of PANI, Co_3O_4, and PANI/Co_3O_4.

Tafel slopes of PANI, Co_3O_4 and PANI/Co_3O_4 are 78 mV/dec, 49 mV/dec, and 87 mV/dec, respectively (**Figure 3.49**). The stability of the catalyst is an important indicator to measure whether the catalyst has commercial value. Two different methods were applied to test the stability of the material. **Figure 3.54, Figure 3.55,** and **Figure 3.58** show the comparison chart of the 1000th cycle LSV-CV curve and the first LSV-CV curve of the material. PANI and PANI/ Co_3O_4 have better stability because their LSV-CV-1 curve and LSV-CV-1K curve overlap, while the LSV-CV-1 curve and LSV-CV-1K curve of Co_3O_4 have a deviation.

Another catalyst stability test method is to perform a catalytic reaction on the electrolysis device continuously for 18 hours under a given voltage and then record the current density flowing through the catalyst with time. The chronoamperometry curve of polyaniline (**Figure 3.61**) and cobalt oxide (**Figure 3.62**) did not show a significant change. In contrast, the chronoamperometry curve for the polyaniline-cobalt oxide composite (**Figure 3.65**) attenuated by 40% after 18 hours. This result is consistent when compared with the stability results measured by LSV-CV.

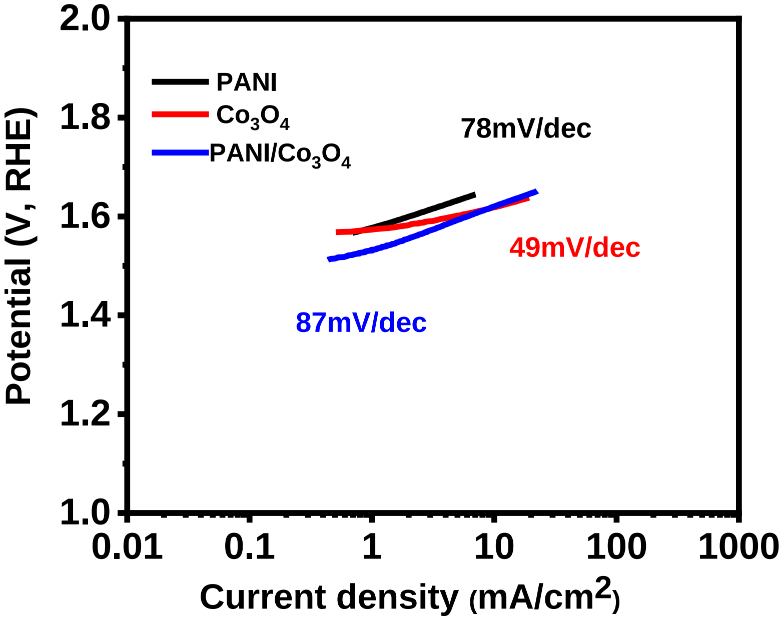

Figure 3.49. Tafel curves for PANI, Co_3O_4, and PANI/Co_3O_4.

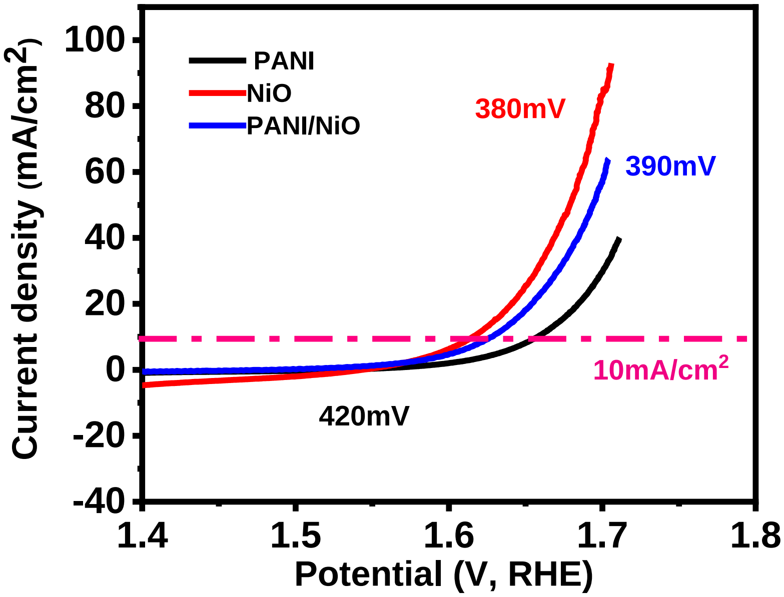

Figure 3.50. LSV-CV curves of PANI, NiO, and PANI/NiO for OER.

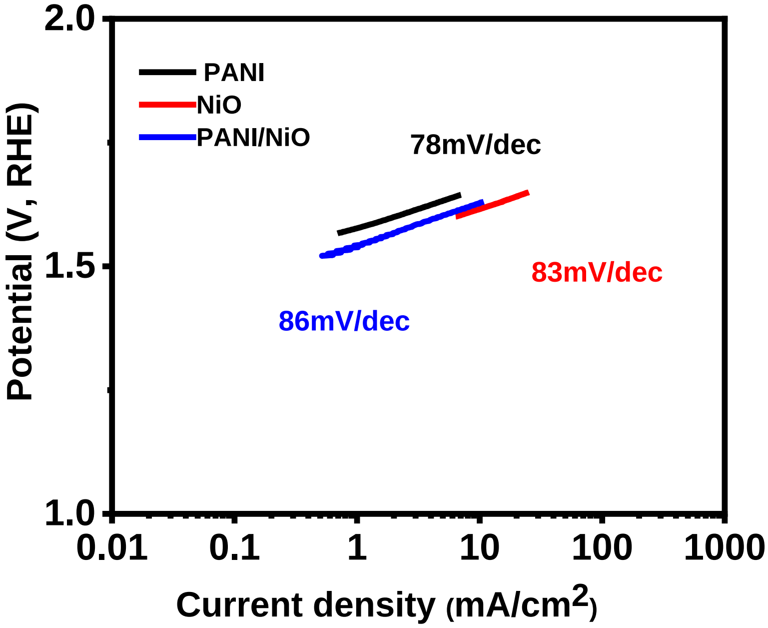

Figure 3.51. Tafel curves for PANI, NiO, and PANI/NiO.

Figure 3.50 shows the LSV curves of PANI, NiO, and PANI/NiO. The overpotentials of PANI, NiO, and PANI/NiO are 420 mV, 380 mV, and 390 mV, respectively, to reach 10 mA/cm^2. **Figure 3.51** shows the Tafel slopes of the PANI, NiO, and PANI/NiO materials, and each has relatively close Tafel slopes of 78 mV/dec, 83 mV/dec and 86 mV/dec, respectively. **Figure 3.54, Figure 3.56,** and **Figure 3.59** show the comparison diagram of the 1000th cycle LSV-CV curve and the first LSV-CV curve of the material. PANI and PANI/NiO show better stability because their LSV-CV-1 curve and LSV-CV-1K curve overlap, while NiO's LSV-CV-1 curve and LSV-CV-1K curve have a significant shift. The result of the chronoamperometry test of polyaniline (**Figure 3.61**) and nickel oxide (**Figure 3.63**) did not show a significant attenuation. In contrast, the chronoamperometry curve of polyaniline-nickel oxide composite (**Figure 3.66**) material attenuated by 25% after 18 hours. This result was consistent with the stability result measured by LSV-CV.

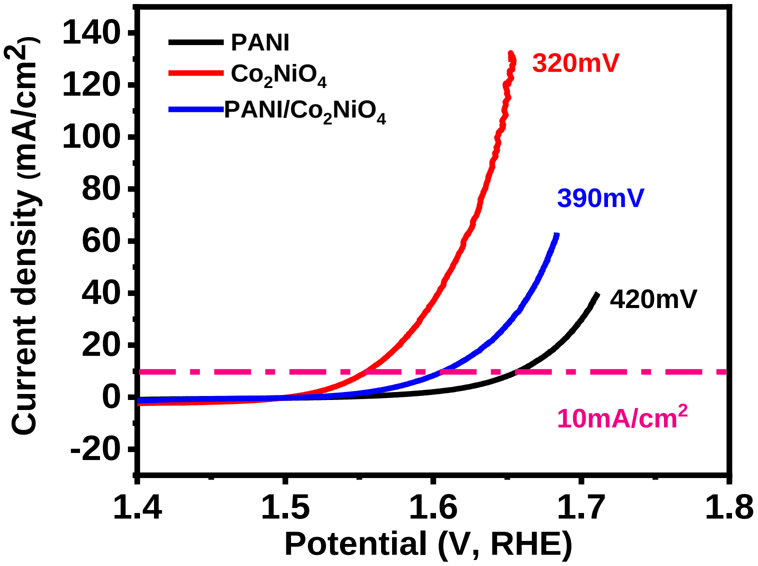

Figure 3.52. LSV-CV curves of PANI, Co_2NiO_4, and PANI/Co_2NiO_4 for OER.

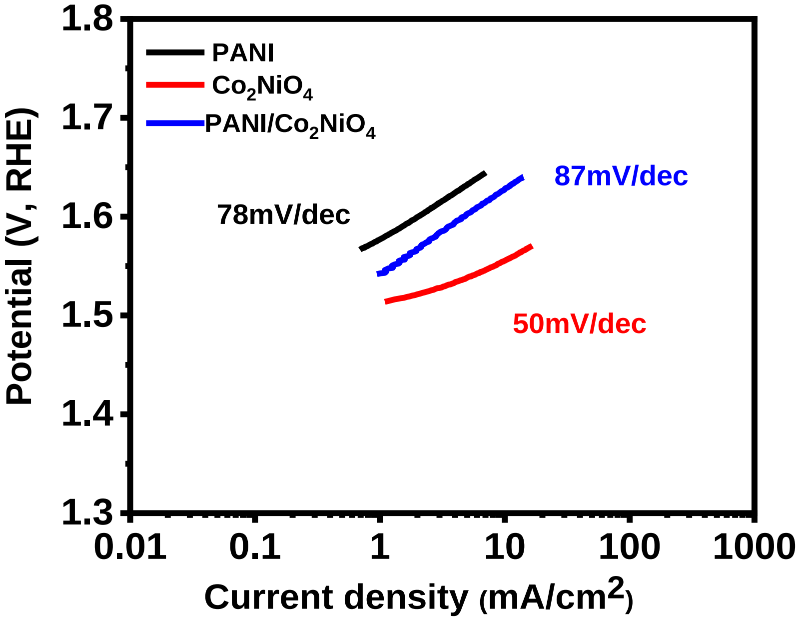

Figure 3.53. Tafel curves for PANI, Co_2NiO_4, and PANI/Co_2NiO_4.

Figure 3.52 shows the LSV curves of PANI, Co_2NiO_4, and PANI/Co_2NiO_4. The overpotentials of PANI, Co_2NiO_4, and PANI/Co_2NiO_4 are 420 mV, 320 mV, and 370 mV, respectively. **Figure 3.53** shows the Tafel slopes of the PANI, Co_2NiO_4, and PANI/Co_2NiO_4 materials, which were 78 mV/dec, 87 mV/dec, and 50 mV/dec, respectively. **Figure 3.54, Figure 3.57,** and **Figure 3.60** show the comparison diagram of the 1000th cycle LSV-CV curve and the first LSV-CV curve of the material. PANI, Co_2NiO_4, and PANI/Co_2NiO_4 all show better stability because their LSV-CV-1 curve coincides with the LSV-CV-1K curve. Chronoamperometry test for polyaniline (**Figure 3.61**) and nickel cobalt oxide (**Figure 3.64**) did not change significantly. On the contrary, the chronoamperometry curve of polyaniline and nickel dicobalt tetroxide composite (**Figure 3.67**) showed a current density increase of nearly 50% after 18 hours.

To study the transfer impedance of charge on the electrode, EIS experiments were performed. As shown in **Table 3.5** and **Figure 3.68** to **Figure 3.74**, the charge transfer resistance value of the PANI (5.1 Ω/cm^2), Co_3O_4 (2.7 Ω/cm^2), NiO (3.3 Ω/cm^2), Co_2NiO_4 (1.4 Ω/cm^2), PANI/Co_3O_4 (2.2 Ω/cm^2), PANI/NiO (3.7 Ω/cm^2), and PANI/Co_2NiO_4 (3.5 Ω/cm^2) at 0.6 V.

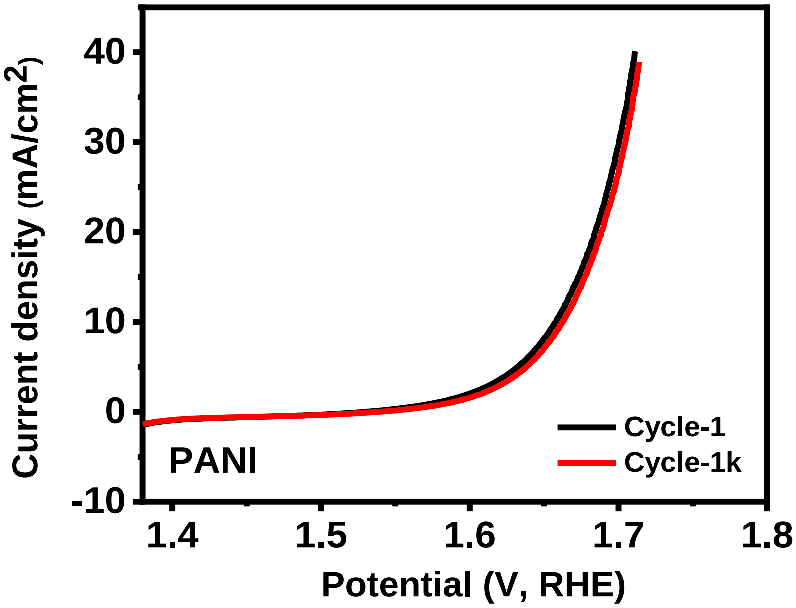

Figure 3.54. LSV & LSV-1K OER stability test of PANI.

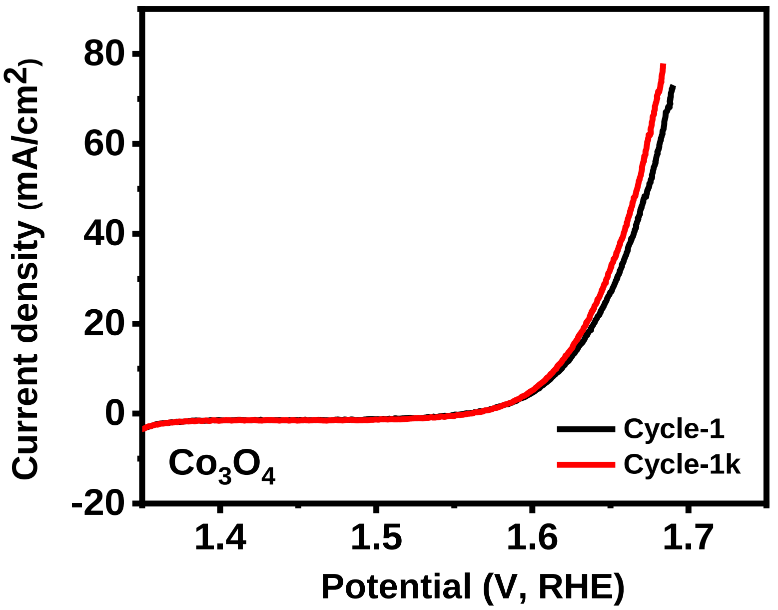

Figure 3.55. LSV & LSV-1K OER stability test of Co_3O_4.

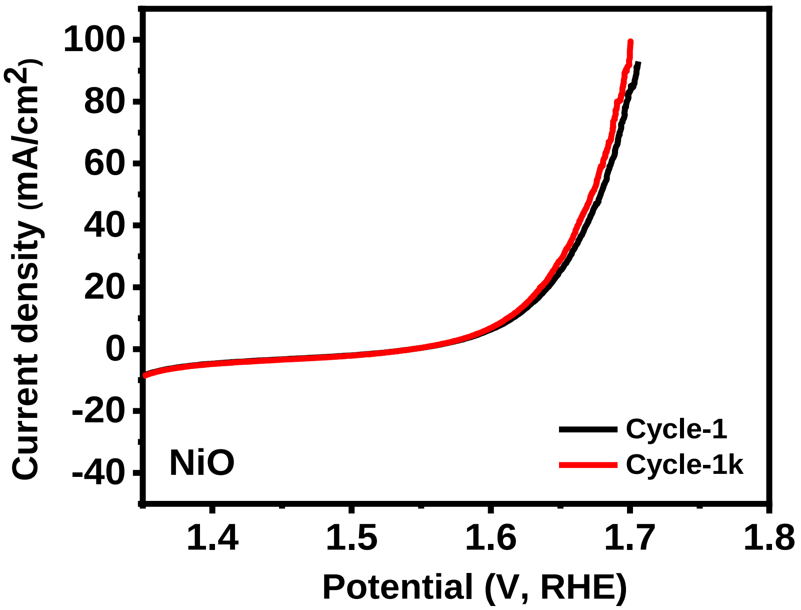

Figure 3.56. LSV & LSV-1K OER stability test of NiO.

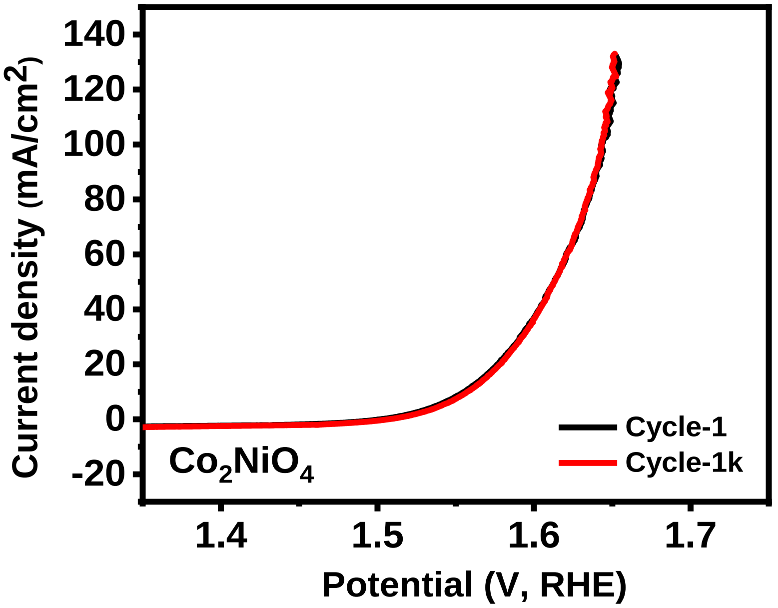

Figure 3.57. LSV & LSV-1K OER stability test of Co_2NiO_4.

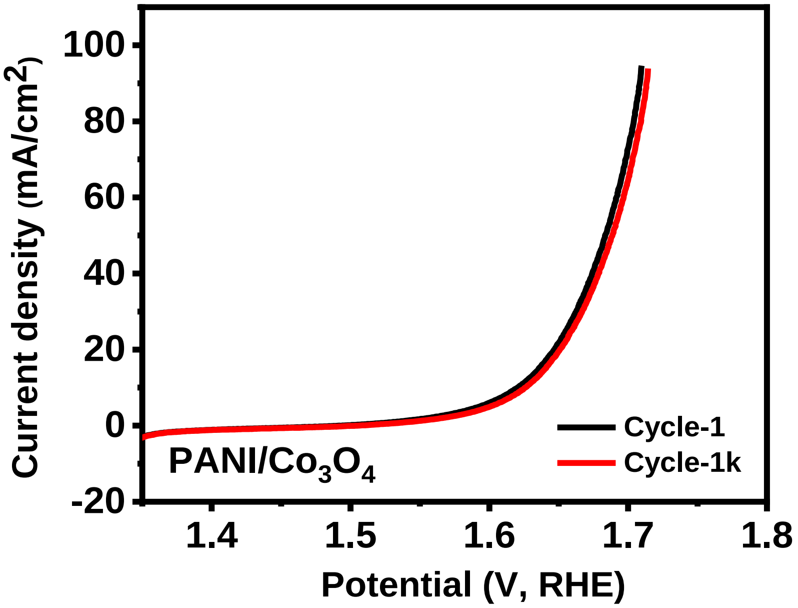

Figure 3.58. LSV & LSV-1K OER stability test of PANI/Co_3O_4.

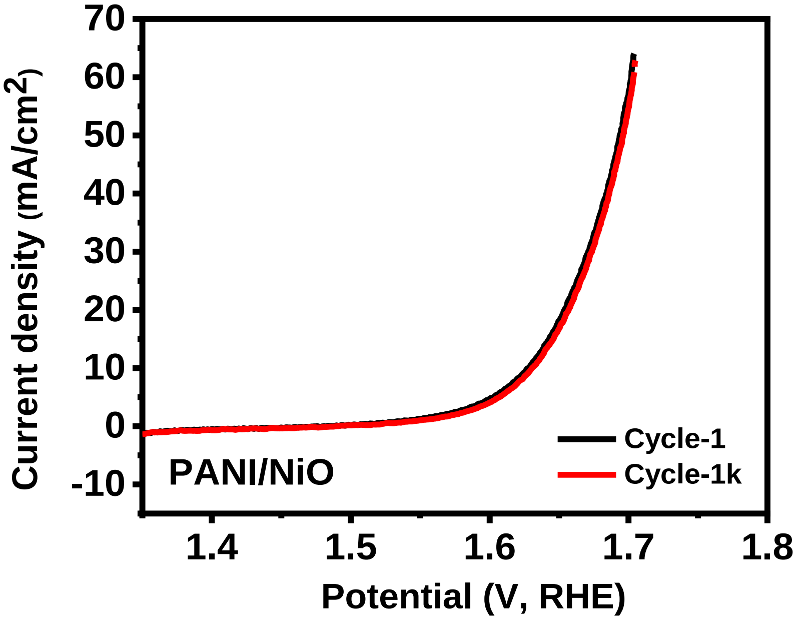

Figure 3.59. LSV & LSV-1K OER stability test of PANI/NiO.

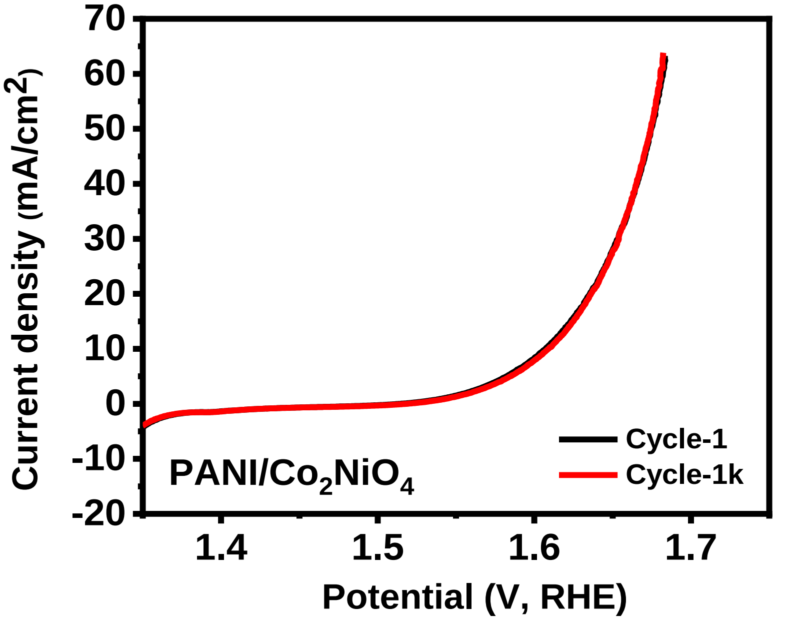

Figure 3.60. LSV & LSV-1K OER stability test of PANI/Co_2NiO_4.

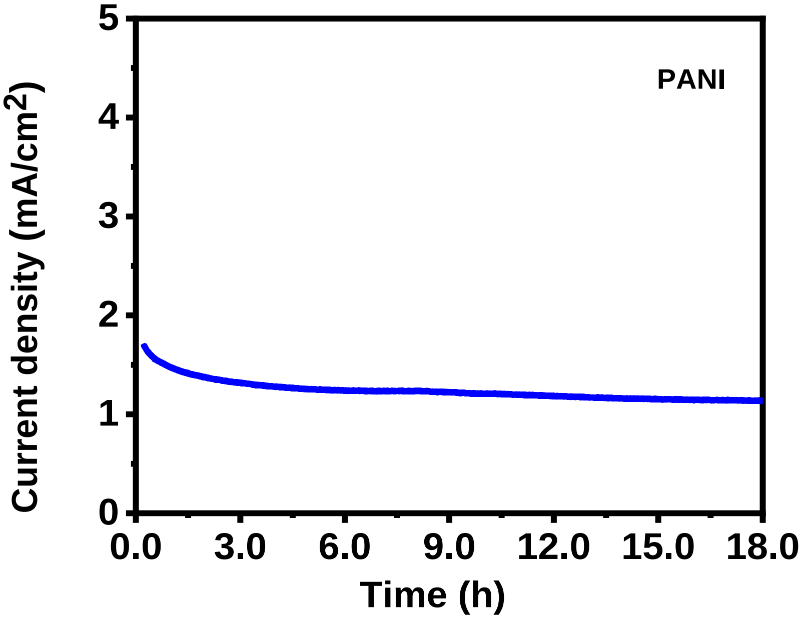

Figure 3.61. Chronoamperometry curve for PANI.

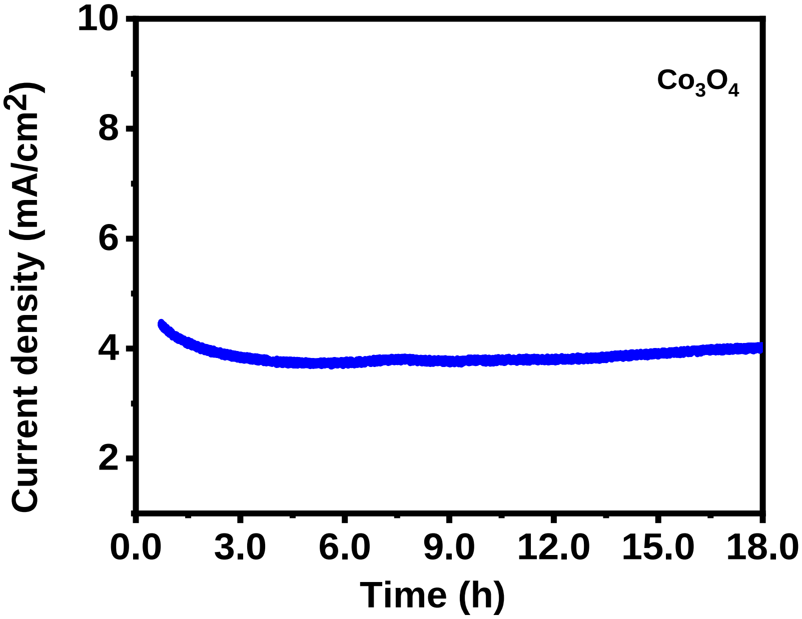

Figure 3.62. Chronoamperometry curve for Co_3O_4.

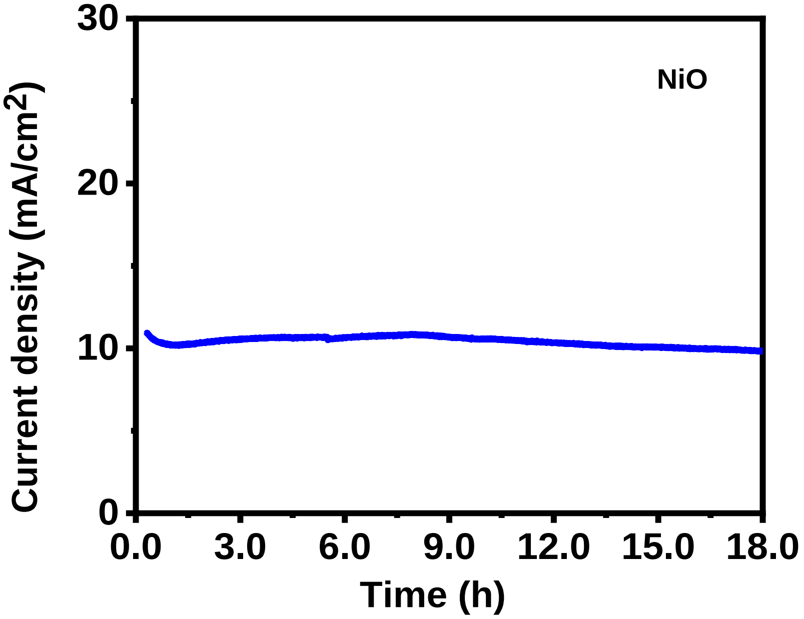

Figure 3.63. Chronoamperometry curve for NiO.

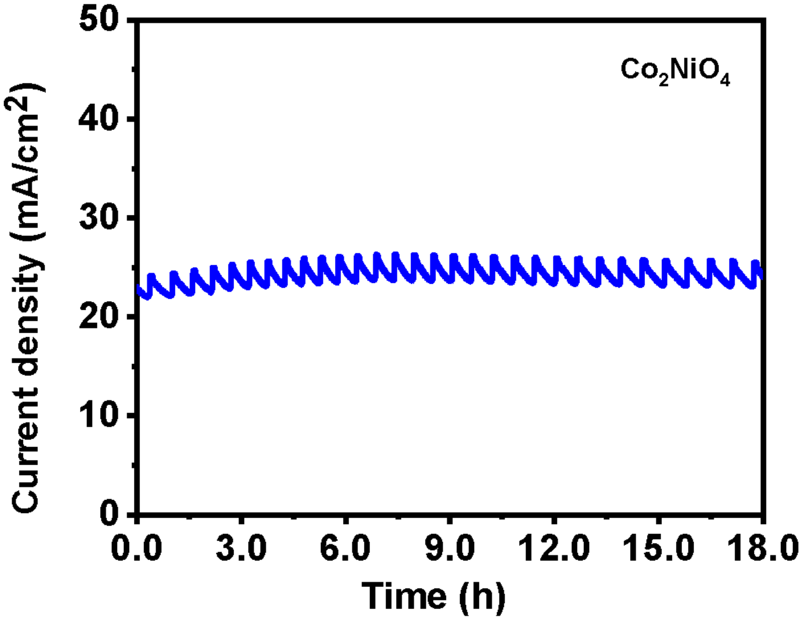

Figure 3.64. Chronoamperometry curve for Co_2NiO_4.

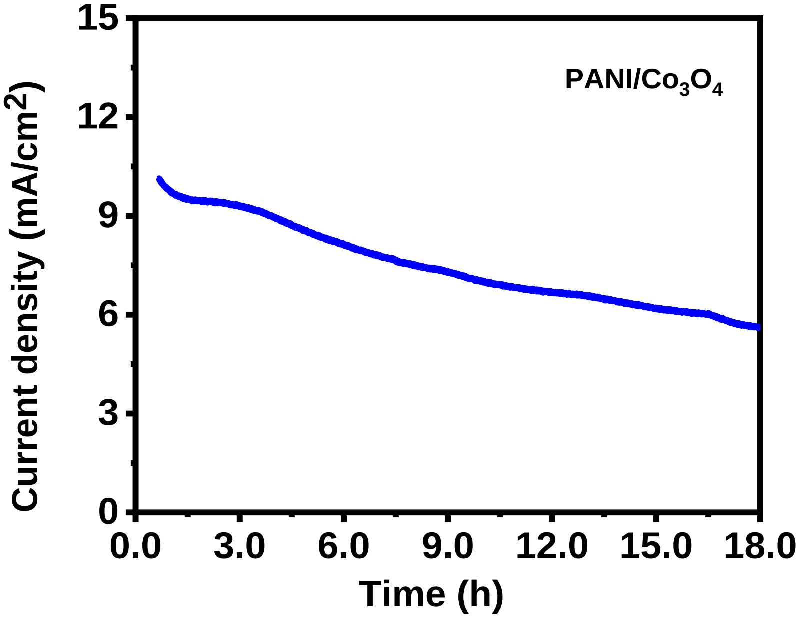

Figure 3.65. Chronoamperometry curve for PANI/Co_3O_4.

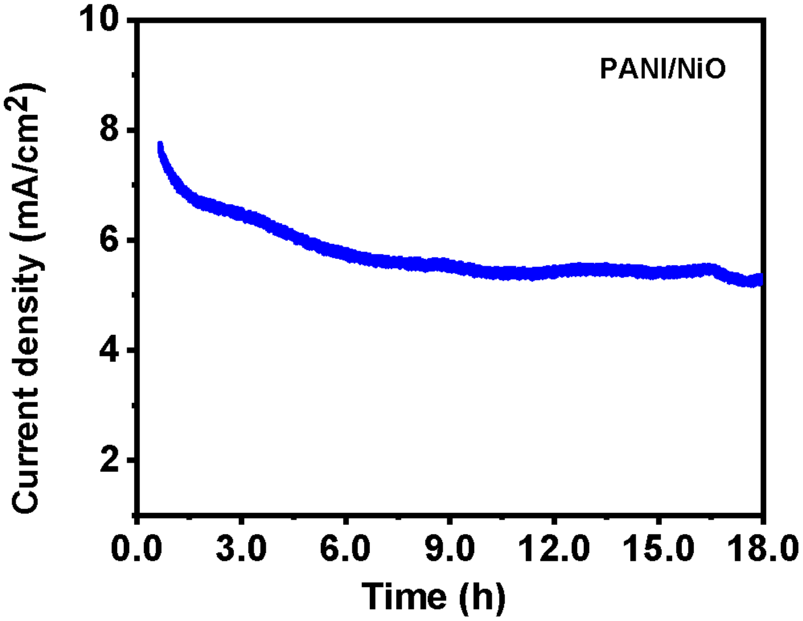

Figure 3.66. Chronoamperometry curve for PANI/NiO.

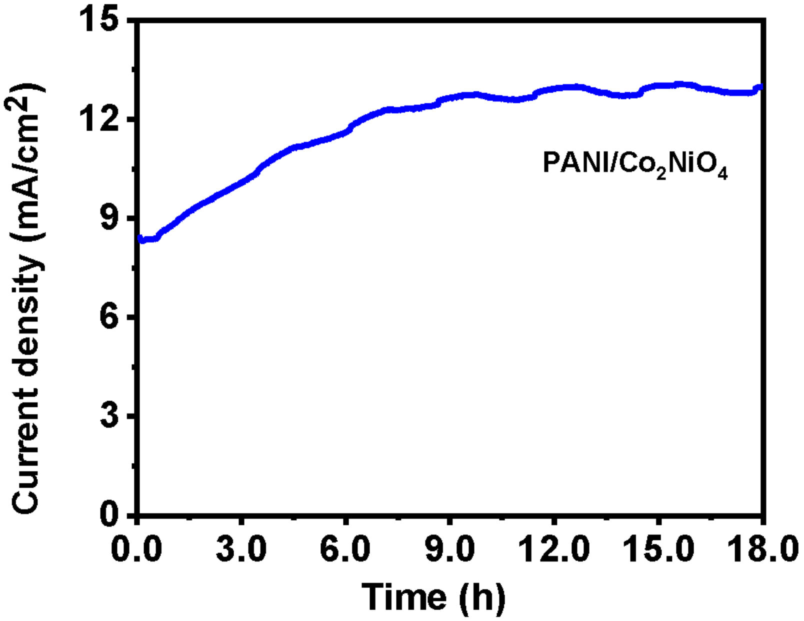

Figure 3.67. Chronoamperometry curve for PANI/Co_2NiO_4.

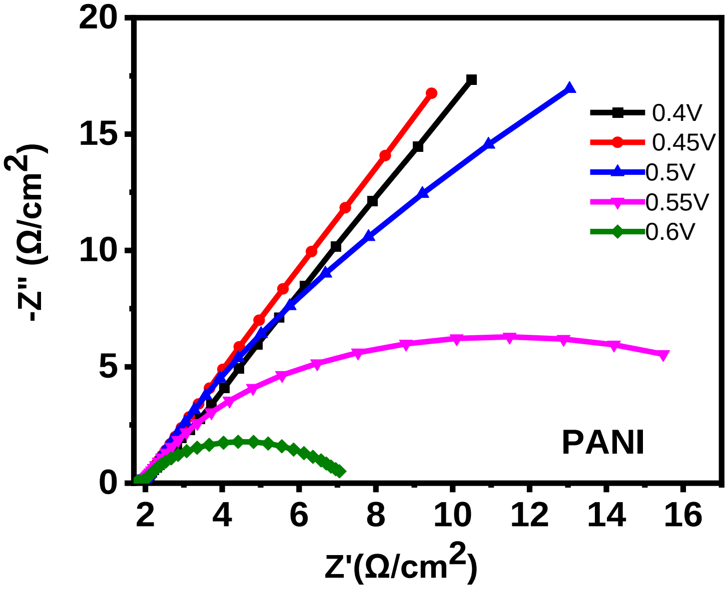

Figure 3.68. Nyquist plots for PANI at various applied potentials.

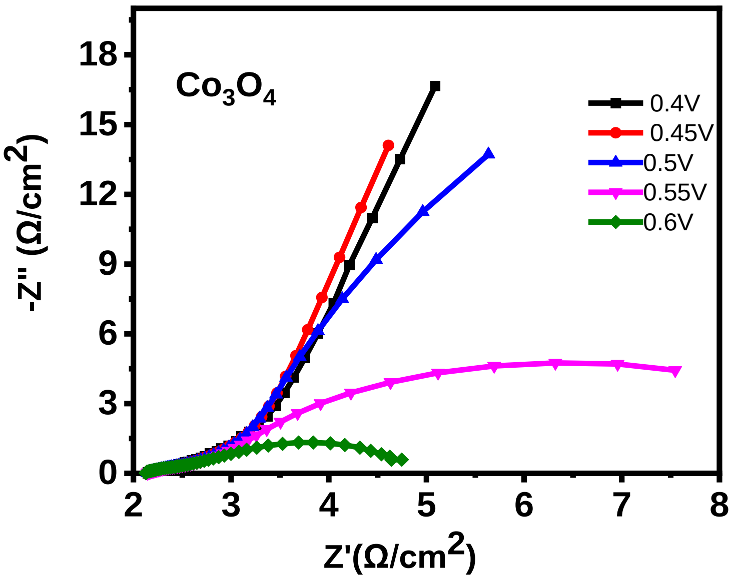

Figure 3.69. Nyquist plots for Co$_3$O$_4$ at various applied potentials.

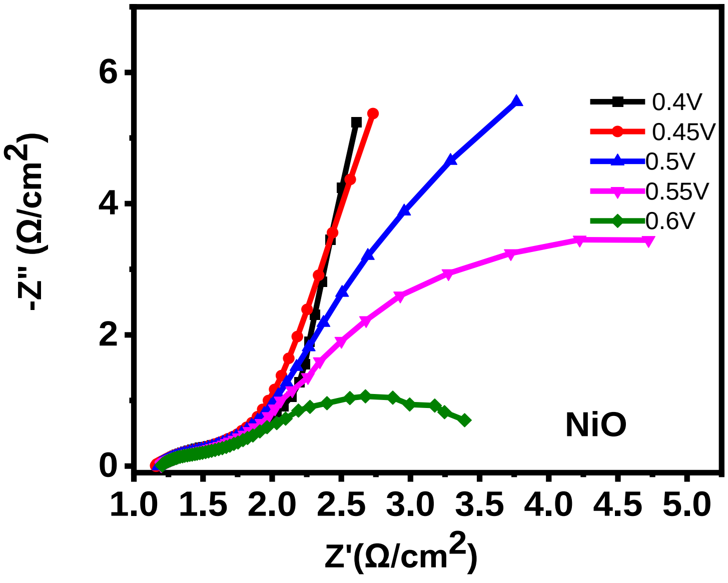

Figure 3.70. Nyquist plots for NiO at various applied potentials.

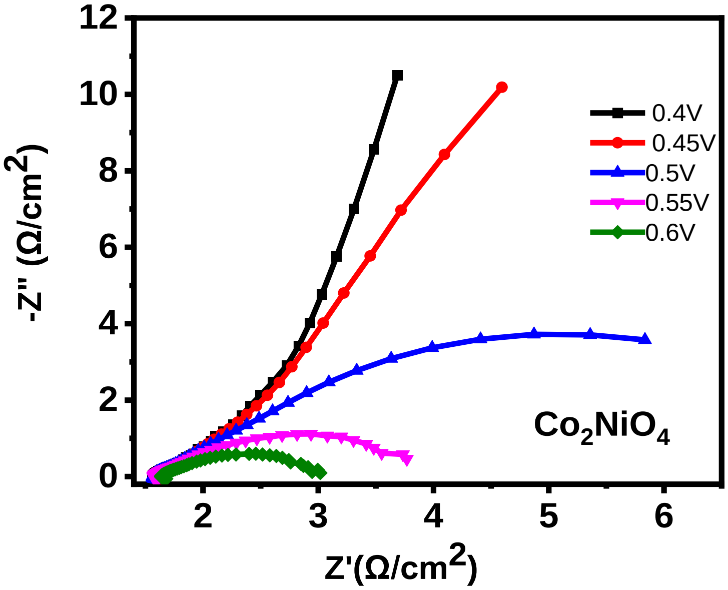

Figure 3.71. Nyquist plots for Co_2NiO_4 at various applied potentials.

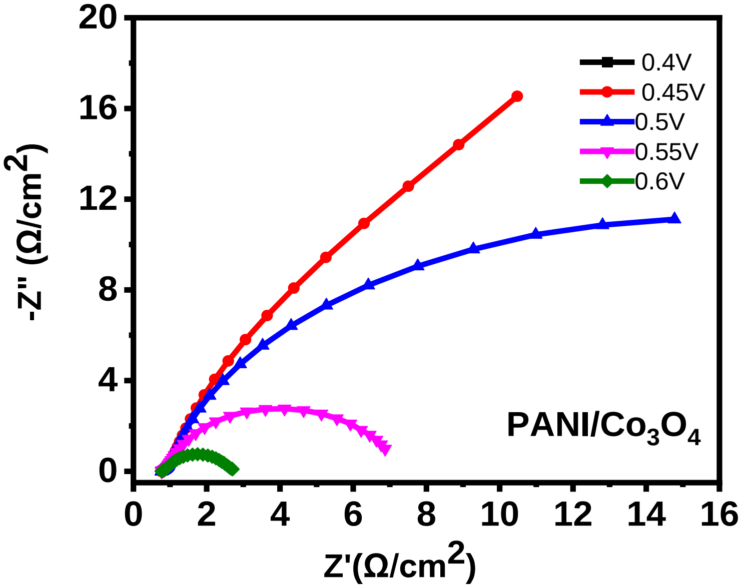

Figure 3.72. Nyquist plots for PANI/Co_3O_4 at various applied potentials.

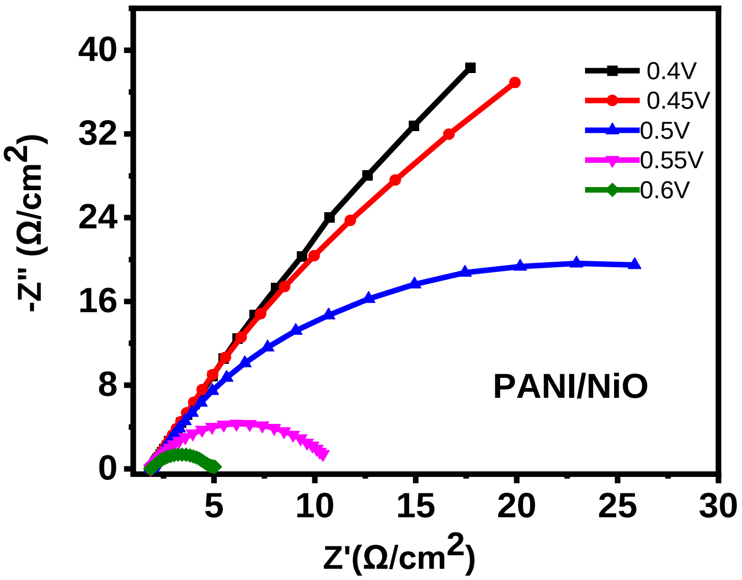

Figure 3.73. Nyquist plots for PANI/NiO at various applied potentials.

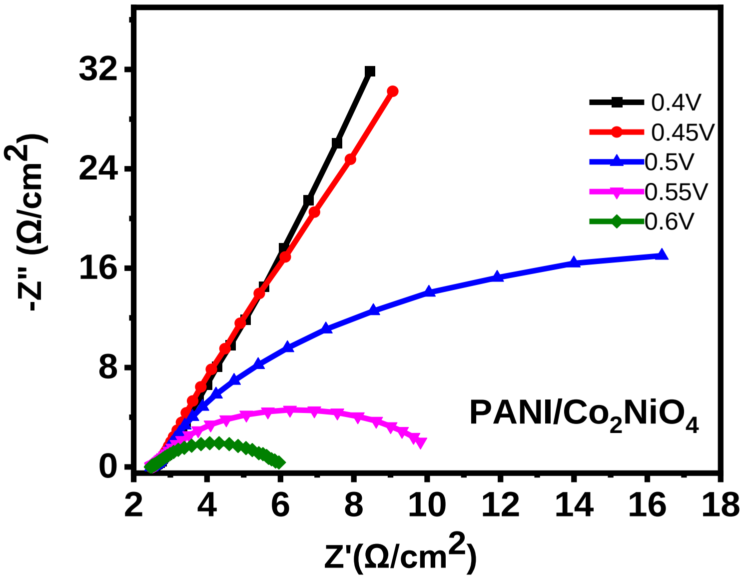

Figure 3.74. Nyquist plots PANI/Co_2NiO_4 at various applied potentials.

Table 3.5. OER characteristics of all samples in 1 M KOH.

Catalyst	$E_{j=10mA/cm^2}$ (V)	Overpotential (mV)	Tafel slope (mV/dec)	R_{ct} (Ω/cm^2)
PANI	1.65	420	151	5.1
Co_3O_4	1.62	390	157	2.7
NiO	1.61	380	118	3.3
Co_2NiO_4	1.55	320	126	1.4
PANI/Co_3O_4	1.62	390	148	2.2
PANI/NiO	1.62	390	139	3.7
PANI/Co_2NiO_4	1.60	370	214	3.5

Table 3.6. Comparison of OER characteristics of various non-noble electrocatalysts.

Catalyst	electrolyte	Overpotential @ j10/mV	Tafel slope	Reference
NiO/MnO_2@PANI	0.1 M KOH	345	42	[45]
M-NiO@Co_3O_4	1 M KOH	290	68	[57]
NiO/Co_3O_4@NC	1 M KOH	240	73	[58]
NiO/Co_3O_4	1 M KOH	262	58	[59]
Co_2NiO_4	1 M KOH	350	124	[59]
$Ni_xCo_yO_4$(x/y=1/4)	1 M KOH	336	36	[60]
Multishelled NiO	1 M KOH	270	57.9	[56]

The composites of polyaniline and transition metal oxide does not show a significant improvement in the oxygen evolution reaction of polyaniline or the transition metal oxide material. Compared with other work, the catalytic performance of these materials are also similar to other reported materials.

3.2.5. Supercapacitor testing

A three-electrode test system was used to test the supercapacitor performance of these active materials.

3.2.5.1. Cyclic voltammetry

When using cyclic voltammetry to investigate the electrochemical properties of materials, the voltage range was 0-0.6 V and different scanning rates were used in the range of 2 mV/s to 300 mV/s. The first thing that should be considered was that the cyclic voltammetry curve of polyaniline was completely different from the cyclic voltammetry curve of polyaniline mentioned earlier (**Figure 3.7)**. The main reason for this phenomenon is that the synthesis conditions of polyaniline, the chemical reagents used, and the potential range of the cyclic voltammetry scan were all different. An oxidation peak and a reduction peak can be seen in **Figure 3.75**. The peak potential of the redox peak did not change significantly with the scan rate, which means that the material was more reversible. During the cyclic voltammetry scanning process, the current flowing through the polyaniline material was significantly higher than that of the previous material suggesting high specific capacitance.

Figure 3.76 shows the CV scan curve of cobalt oxide. Three oxidation peaks were observed in the low-frequency scan. The reason for this phenomenon was that Co_3O_4 was in a typical spinel structure, so there were divalent and trivalent cobalt ions in the crystal. When the scanning potential was lower these ions have sufficient response time and this response was directly manifested as a clear oxidation peak. When scanning at a high potential these ions do not have enough time to respond and the result was that their oxidation peaks merge.

Figure 3.77 reveals the electrochemical characteristics of nickel oxide at different scan rate. Nickel oxide has only one valence state, so only one oxidation peak and one reduction peak appear in the CV curve. It can be seen that the redox peak potential of nickel oxide shifts with the change of scan rate. In addition, it can be seen that the current density flowing through the material was higher, which means that the specific capacitance of the material was higher.

Figure 3.78 was the CV curve of cobalt nickel oxide at different scanning frequencies. Two oxidation peaks are clearly shown on the CV curve at low scan rate, which represent the oxidation peaks of nickel and cobalt. During high scan rate, the separate oxidation peaks merge into one peak. In addition, the peak potential of the oxidation peak has a shift with the change of the scan rate.

Figure 3.79 shows the CV curve of the composite material of polyaniline and cobalt oxide at different scan rate. Of special note, two clear redox peaks appear on the CV curve even at high scan rate. The combination of PANI and Co_3O_4 did not improve the electrochemical performance of the material.

Figure 3.80 shows the CV curve of the composite material of polyaniline and nickel oxide at different scan rate. Redox peaks were observed even at high scan rate. Compared with pure nickel oxide the current density flowing through the composite material was similar to the current density flowing through the polyaniline material. The introduction of nickel oxide did not significantly change the electrochemical properties of polyaniline.

Figure 3.81 shows the CV curve of the composite material of polyaniline and nickel cobalt oxide. Compared with pure polyaniline and pure nickel cobalt oxide the current density flowing through the material had a increase, which means that the capacitance of the composite material had been improved. In addition, the redox peak potential did not shift too much with the scan rate. This means that the reversibility of the material has also been improved.

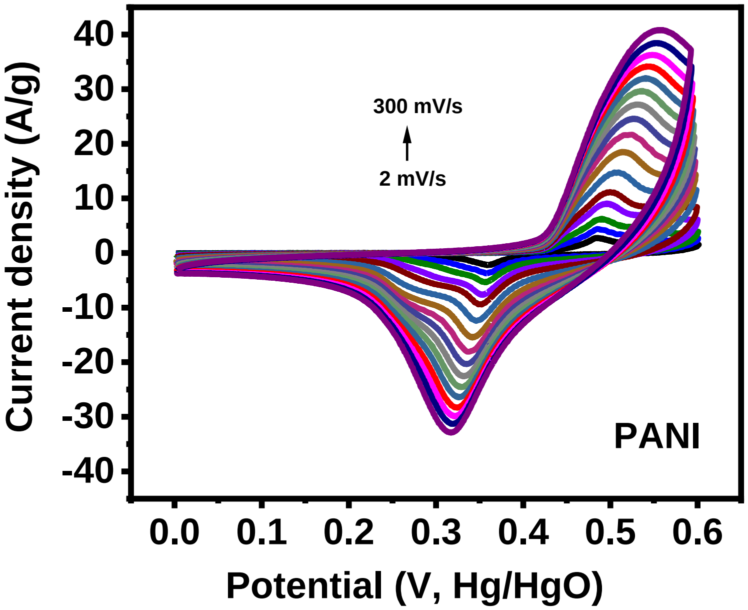

Figure 3.75. CV curves of PANI at different scan rates.

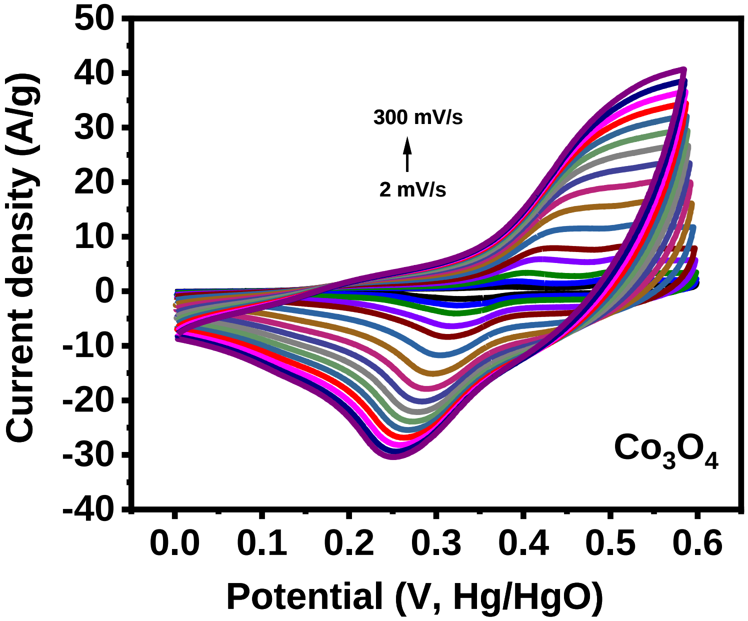

Figure 3.76. CV curves of Co_3O_4 at different scan rates.

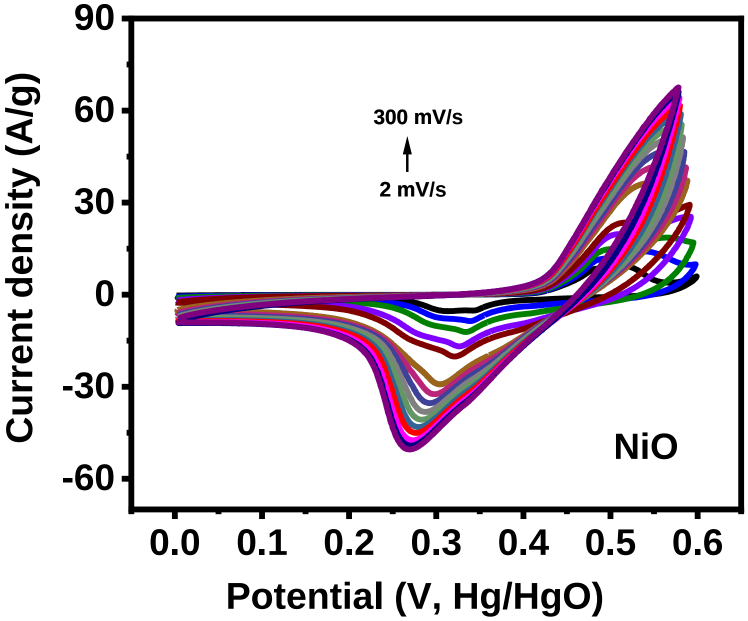

Figure 3.77. CV curves of NiO at different scan rates.

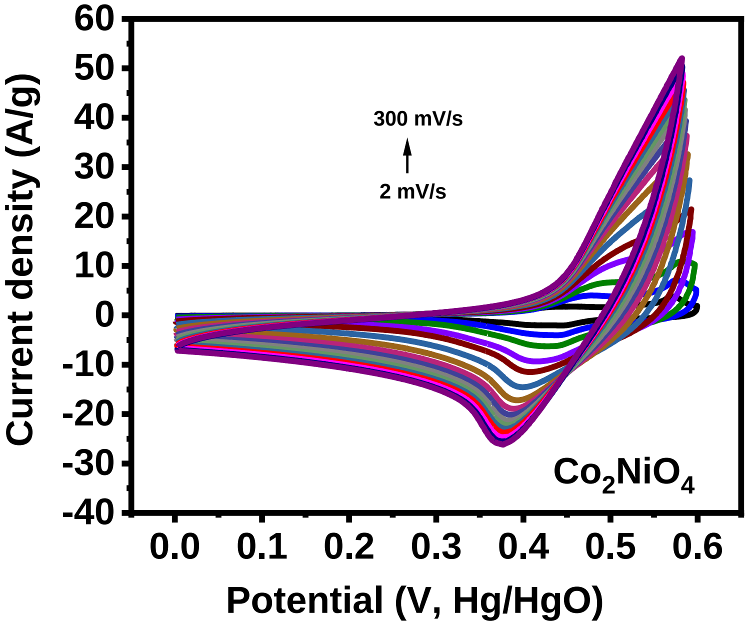

Figure 3.78. CV curves of Co_2NiO_4 at different scan rates.

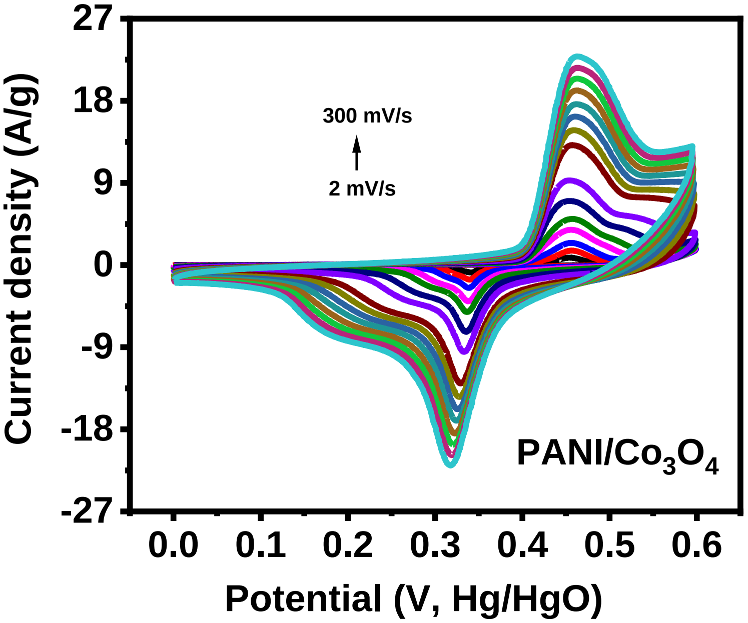

Figure 3.79. CV curves of PANI/Co_3O_4 at different scan rates.

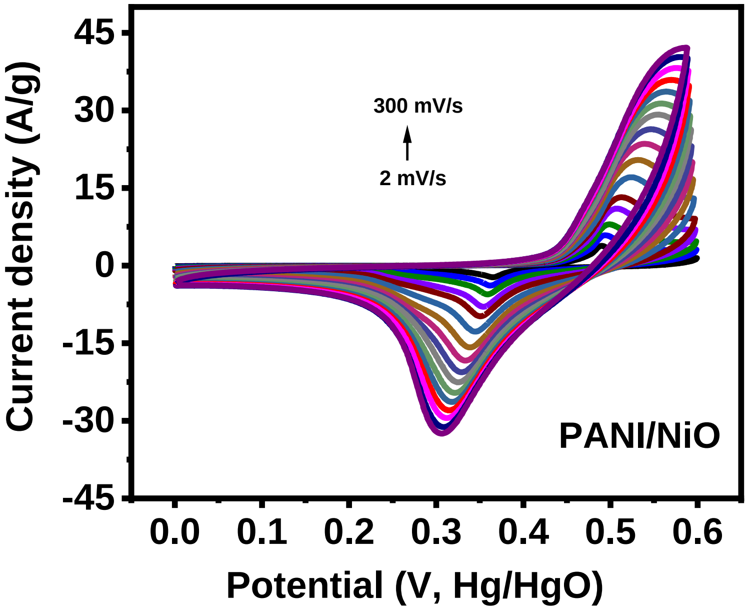

Figure 3.80. CV curves of PANI/NiO at different scan rates.

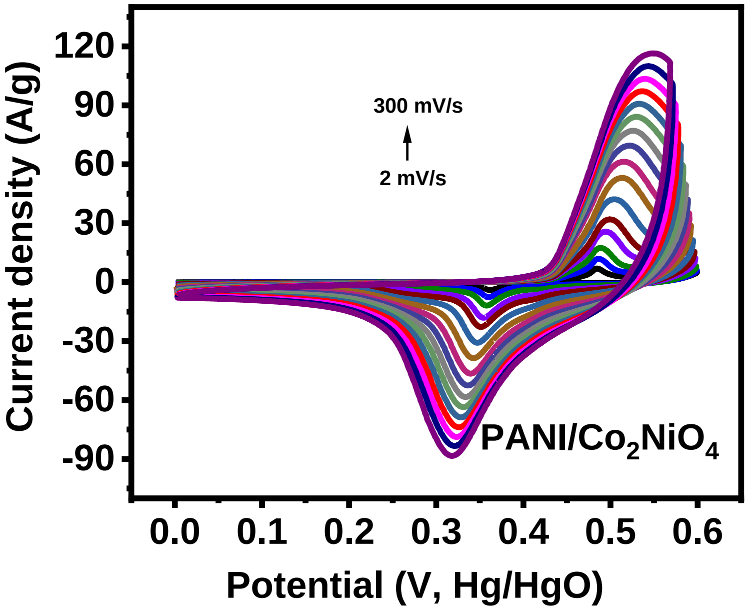

Figure 3.81. CV curves of PANI/Co_2NiO_4 at different scan rates.

In order to compare the electrochemical performance of polyaniline and metal oxide composites more intuitively, the scan rate and specific capacitance relationship diagrams of related materials were compared. All materials showed the same trend of change in specific capacitance with increasing scan rate. From **Figure 3.82**, it can be seen that the simple combination of polyaniline and cobalt oxide did not improve the electrochemical performance of the material. When the scan rate was 2 mV/s the specific capacitance of cobalt oxide was as high as 819 F/g, compared to polyaniline that had a specific capacitance of 438 F/g, while the composites of polyaniline and cobalt oxide exhibited a much lower specific capacitance of 222 F/g at the same scan rate.

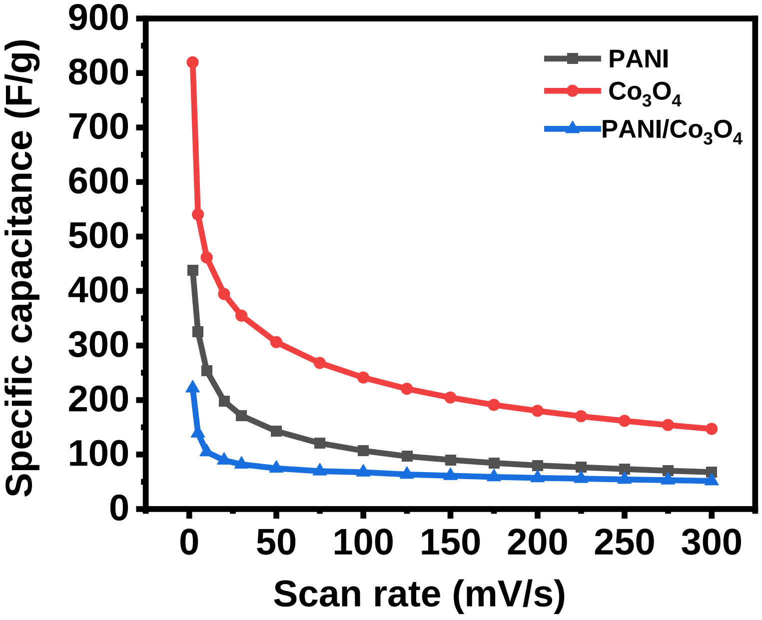

Figure 3.82. Specific capacitance versus scan rates for PANI, Co_3O_4, and PANI/Co_3O_4.

Figure 3.83 shows the comparison of electrochemical performance before and after polyaniline nickel oxide composites. It can be seen that the composites of polyaniline and nickel oxide exhibits electrochemical characteristics very similar to the polyaniline material itself. It can also be seen that the CV scan rate and specific capacitance curve of the composite material of polyaniline and polyaniline nickel oxide coincide closely. The capacitance characteristics of nickel oxide were much better than composite materials although its stability was poor. When the scan rate was 2 mV/s nickel oxide shows a high specific capacitance of up to 1202 F/g, while the specific capacitance of polyaniline nickel oxide composite material was only 488 F/g, and the specific capacitance of polyaniline was 438 F/g. It was worth noting that the electrochemical performance of polyaniline nickel cobalt oxide (**Figure 3.84**) had been expected to improve both in terms of specific capacitance and stability. When the scan rate was 2 mV/s the specific capacitances of polyaniline and nickel cobalt oxide were 438 F/g and 640 F/g, respectively. However, at the same scanning rate the specific capacitance of the corresponding materials of polyaniline and nickel cobalt oxide was 706 F/g.

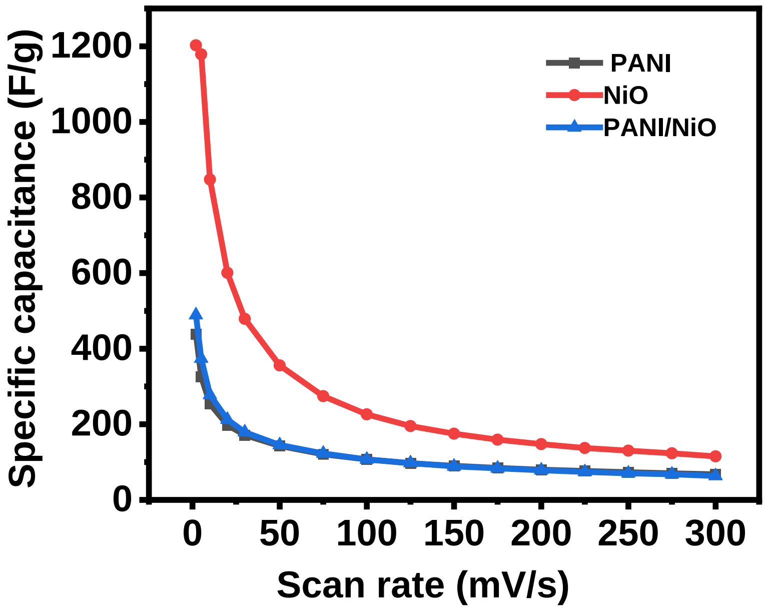

Figure 3.83. Specific capacitance versus scan rates for PANI, NiO, and PANI/NiO.

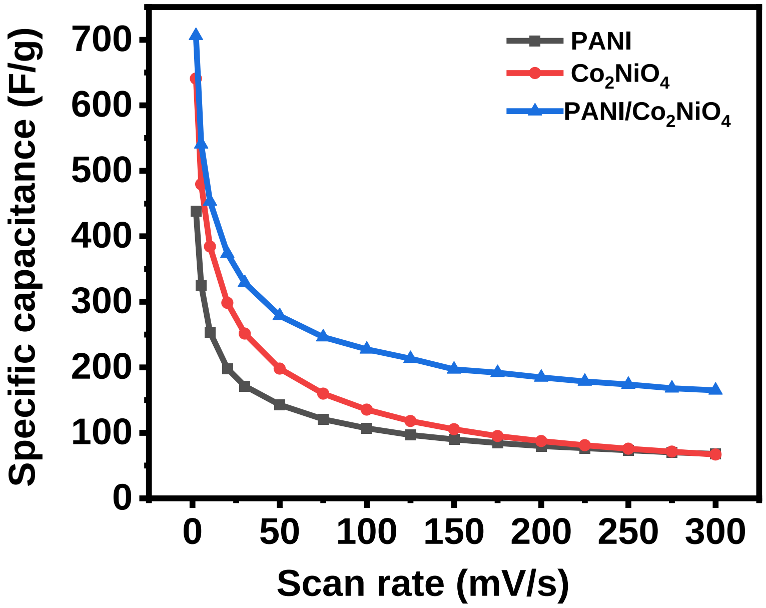

Figure 3.84. Specific capacitance versus scan rates for PANI, Co_2NiO_4, and PANI/Co_2NiO_4.

3.2.5.2. Galvanostatic charge-discharge test

In order to further understand the capacitance characteristics of these materials they have also been tested with constant current charging and discharging. The constant current charging and discharging were performed in the current density range from 30 A/g to 0.5 A/g, and the test voltage range was 0-0.6 V. Constant current charging and discharging can help understand the specific capacitance and the rate performance of the material under different current densities.

Figures 3.85 - 3.91 show the galvanostatic charge-discharge curves of different materials at different current densities. From these constant current charge and discharge curves at different current densities, the capacitance characteristics of the materials can be directly seen. The charge and discharge time of a material are directly related to their specific capacitance. From the perspective of capacitance characteristics alone, nickel oxide exhibited the best capacitance characteristics. Taking the CD curve with a charge-discharge current density of 0.5 A/g as an example, it takes about 3300 s for NiO to complete a charge-discharge cycle, while it takes only 130 s for PANI/Co_3O_4 to complete a cycle under the same current density.

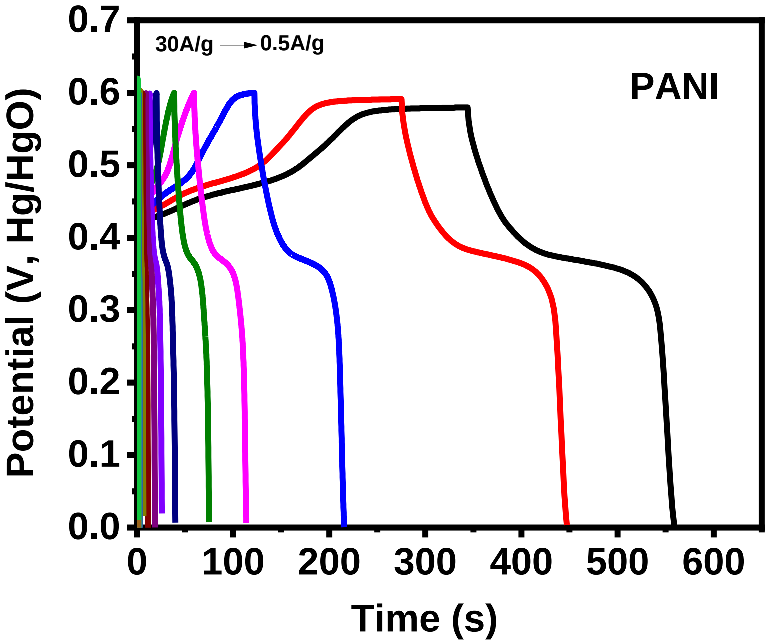

Figure 3.85. Potential versus time at different current density for PANI.

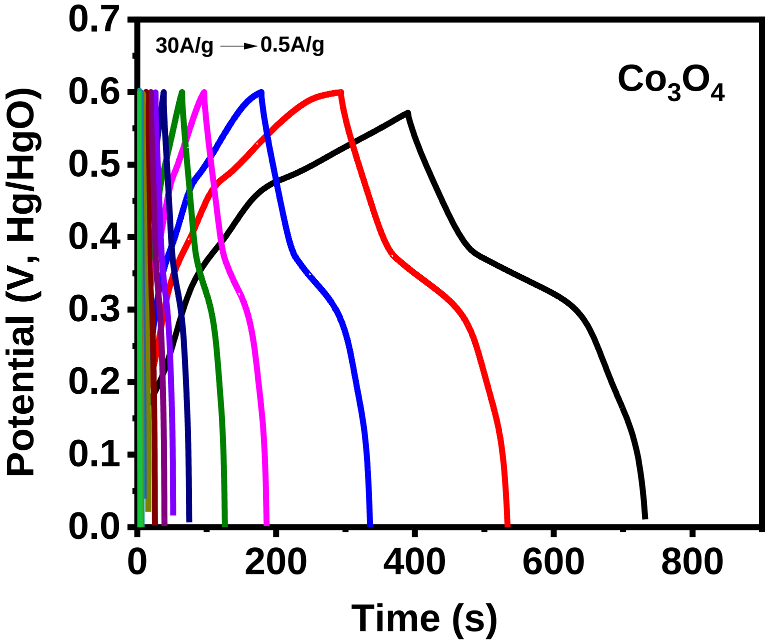

Figure 3.86. Potential versus time at different current density for Co_3O_4.

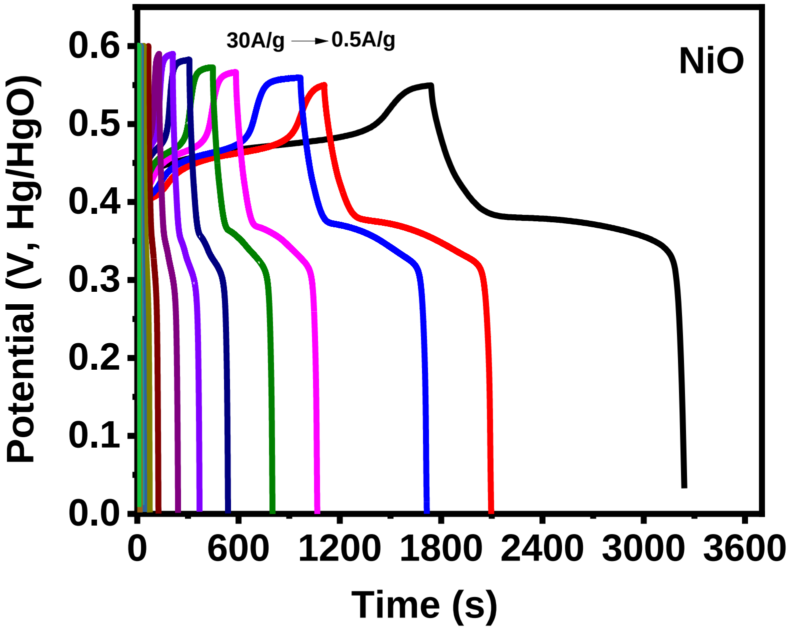

Figure 3.87. Potential versus time at different current density for NiO.

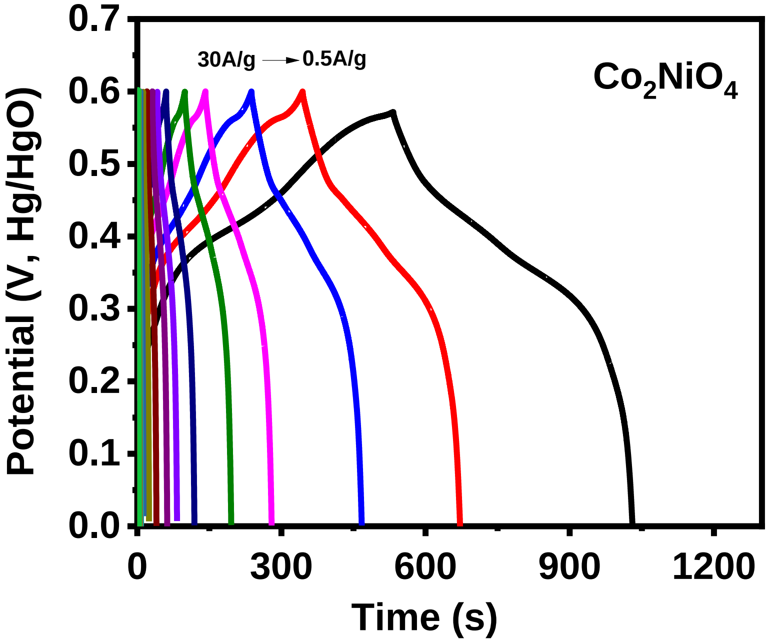

Figure 3.88. Potential versus time at different current density for Co_2NiO_4.

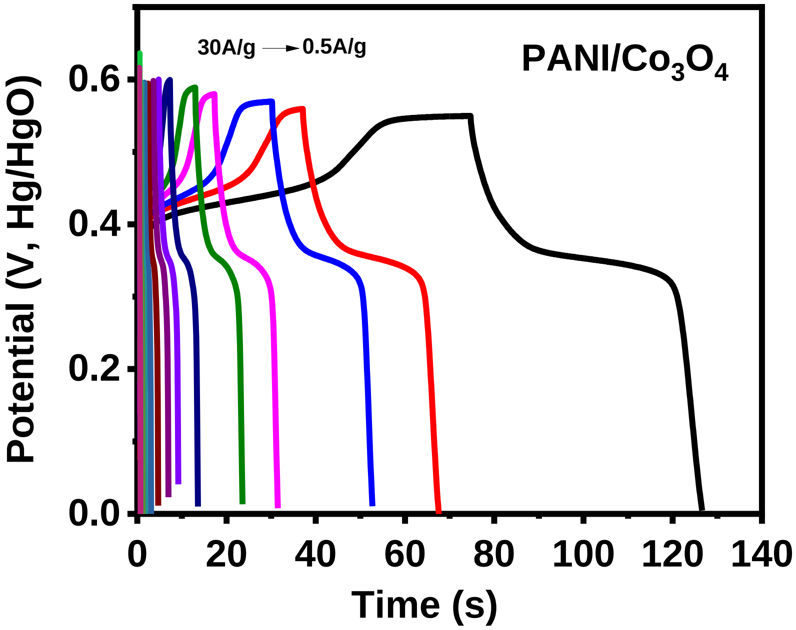

Figure 3.89. Potential versus time at different current density for PANI/Co_3O_4.

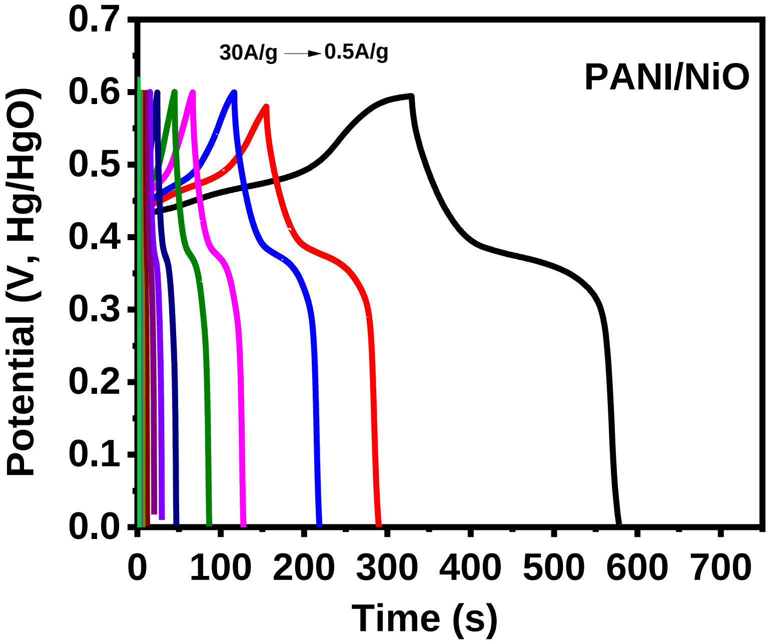

Figure 3.90. Potential versus time at different current density for PANI/NiO.

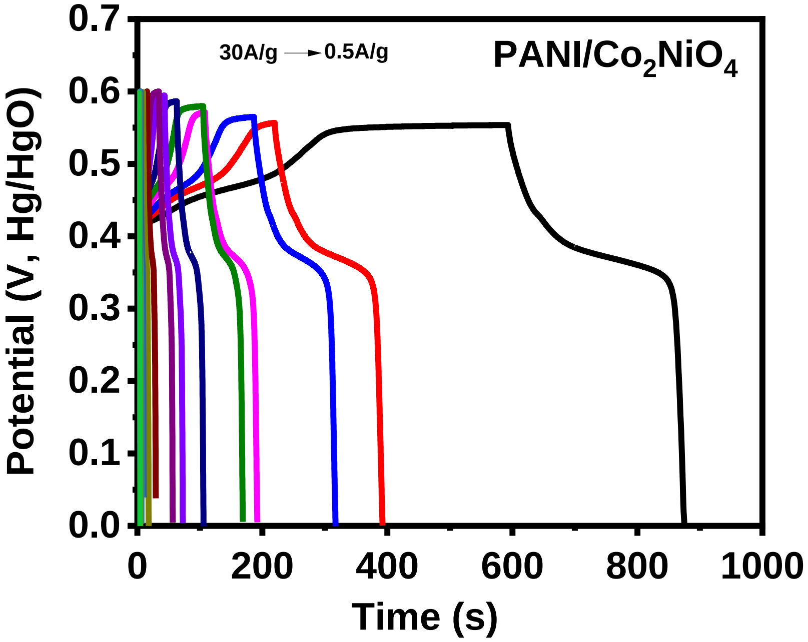

Figure 3.91. Potential versus time at different current density for PANI/Co_2NiO_4.

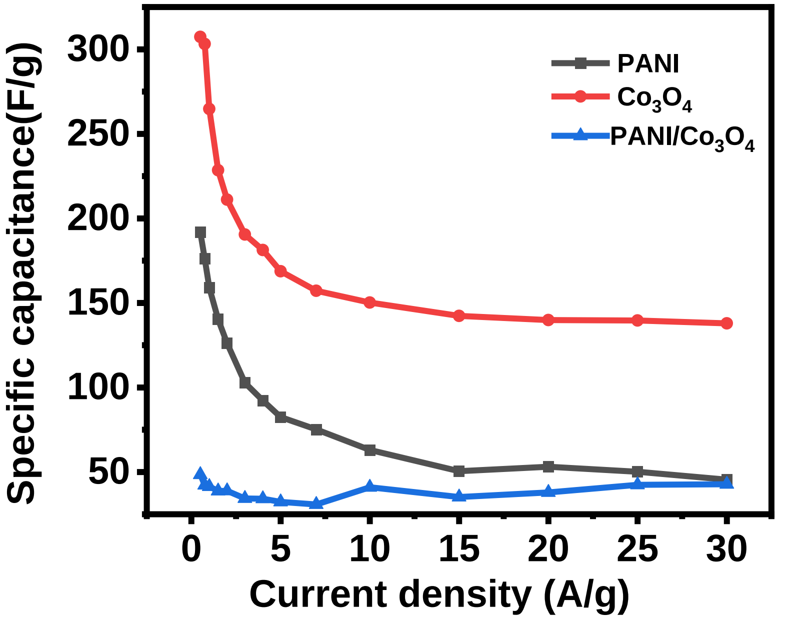

Figure 3.92. Specific capacitance versus current density for PANI, Co_3O_4, and PANI/Co_3O_4.

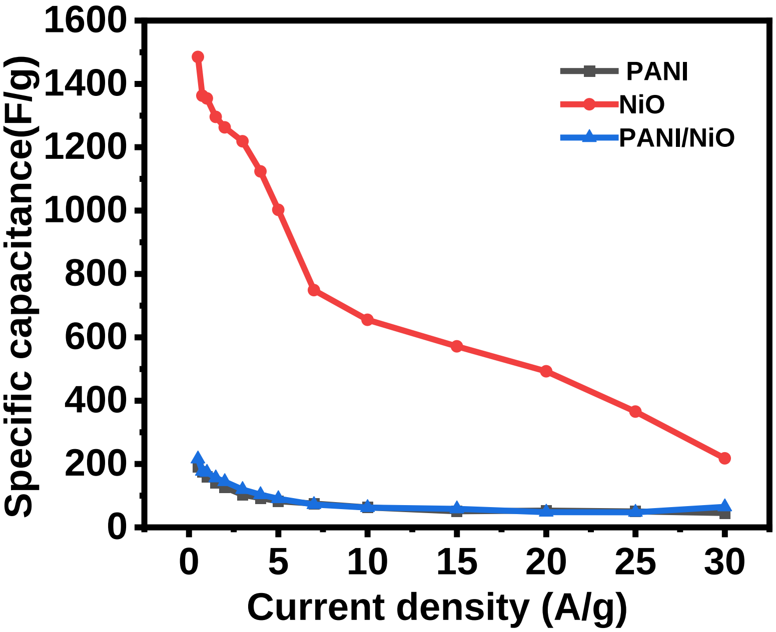

Figure 3.93. Specific capacitance versus current density for PANI, NiO, and PANI/NiO.

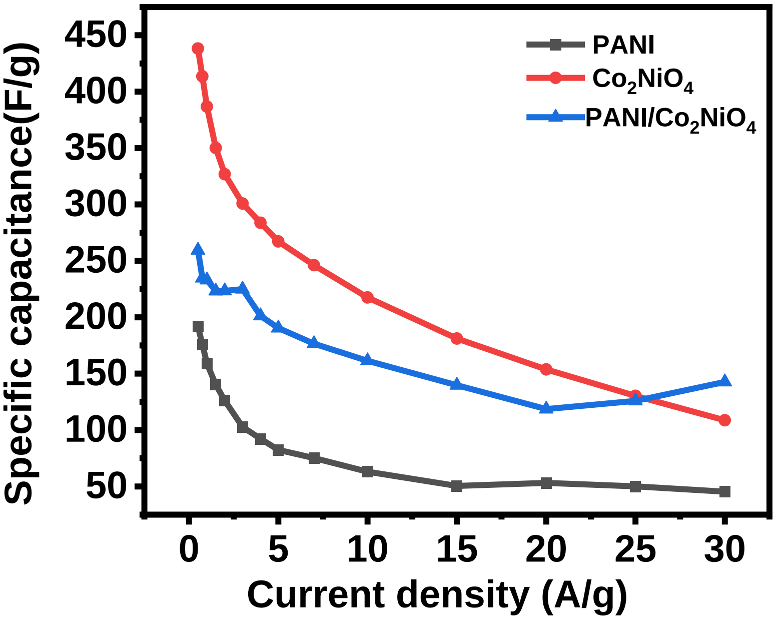

Figure 3.94. Specific capacitance versus current density for PANI, Co_2NiO_4, and $PANI/Co_2NiO_4$.

Figure 3.92 shows that the electrochemical performance of the composite polyaniline and cobalt oxide has not improved. This result was consistent with the result measured by cyclic voltammetry. **Figure 3.93** shows that the electrochemical properties of the composite of polyaniline and nickel oxide are similar to that of pure polyaniline. This means that simple compounding cannot improve the electrochemical performance of polyaniline or metal oxides. From the feedback information shown in **Figure 3.94**, the composite material of polyaniline and nickel cobalt oxide has improved specific capacitance compared with polyaniline. What was more noteworthy was that the stability of the material itself has been greatly improved. When the charge and discharge current density was 0.5 A/g, PANI, Co_3O_4, NiO, Co_2NiO_4, PANI/Co_3O_4, PANI/NiO, and PANI/Co_2NiO_4 show 192 F/g, 307 F/g, 1485 F/g, 497F/g, 221 F/g, 271 F/g and 541 F/g specific capacitances, respectively.

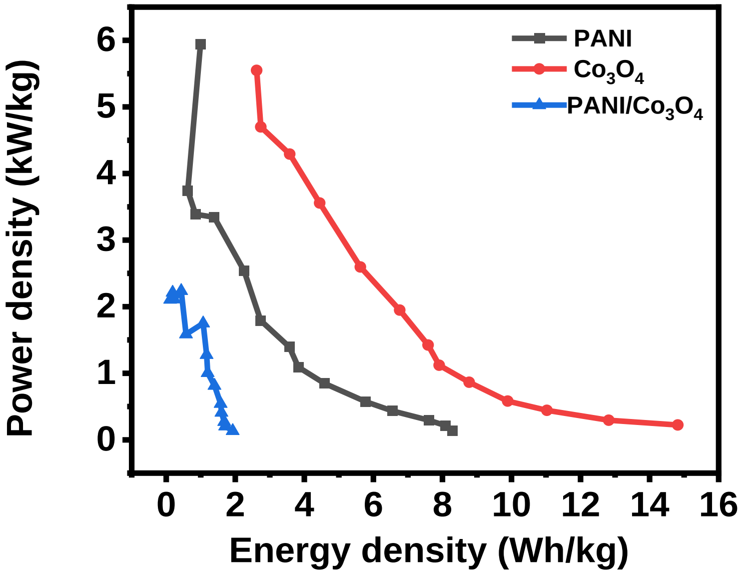

Figure 3.95. Power density versus energy density for PANI, Co_3O_4, and PANI/Co_3O_4.

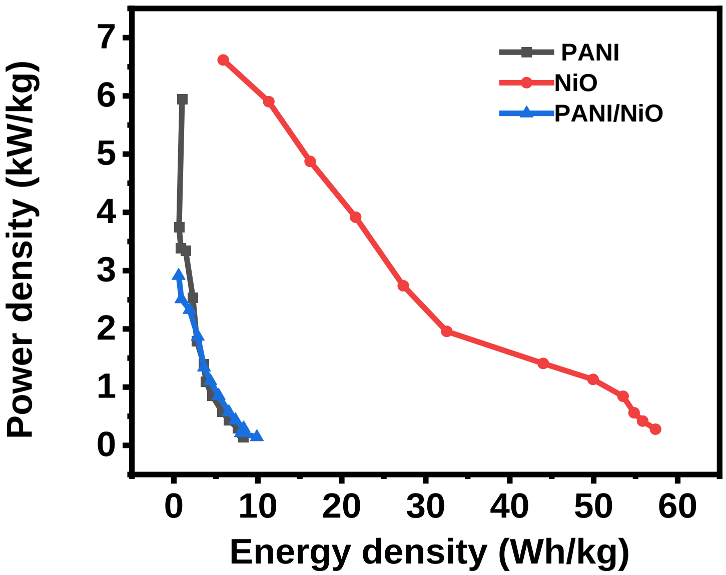

Figure 3.96. Power density versus energy density for all the samples PANI, NiO, and PANI/NiO.

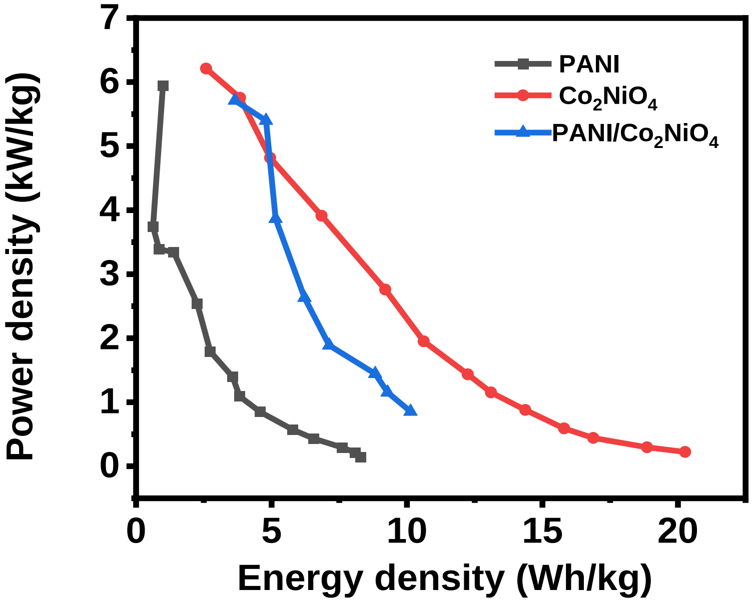

Figure 3.97. Power density versus energy density for PANI, Co_2NiO_4, and PANI/Co_2NiO.

Figure 3.95-3.97 show the Ragone plot of the PANI, Co_3O_4, NiO, Co_2NiO_4, PANI/Co_3O_4, PANI/NiO, and PANI/Co_2NiO_4. Combined with the data in **Table 3.7**, metal oxide materials with pseudocapacitance characteristics have a better energy density than carbon materials, and NiO exhibited a high energy density as high as 57 Wh/kg.

Table 3.7. Energy and power density of all the samples.

Material	Energy density (Wh/kg)	Power density (W/kg)
PANI	8	5944
Co_3O_4	15	5548
NiO	57	6615
Co_2NiO_4	20	6210
PANI/Co_3O_4	2	2107
PANI/NiO	10	2089
PANI/Co_2NiO_4	11	5364

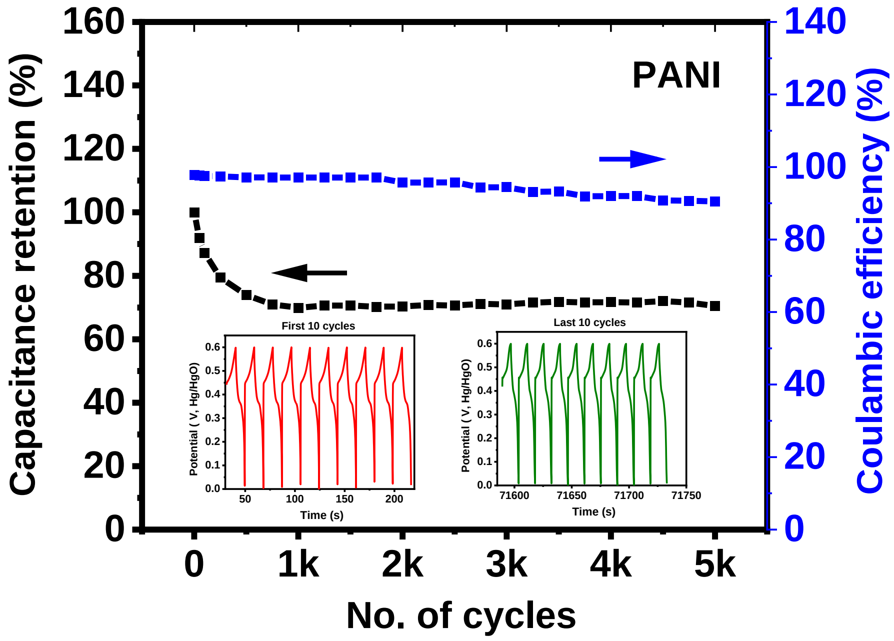

Figure 3.98. Stability curves for PANI.

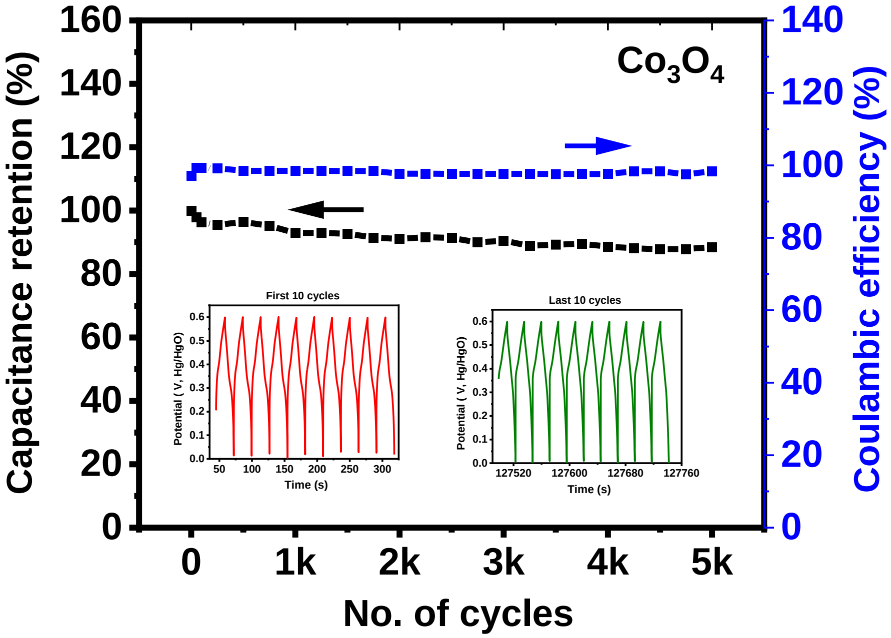

Figure 3.99. Stability curves for Co_3O_4.

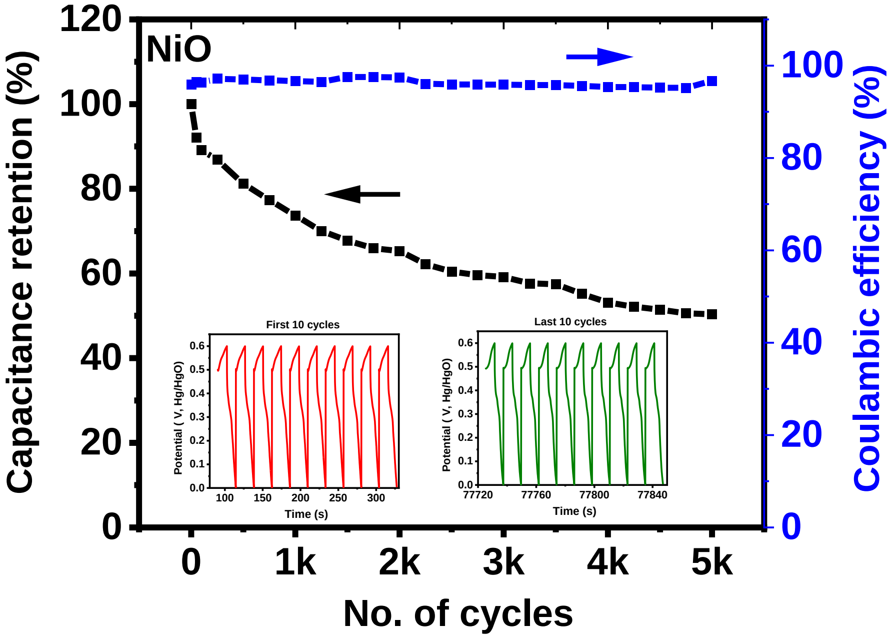

Figure 3.100. Stability curves for NiO.

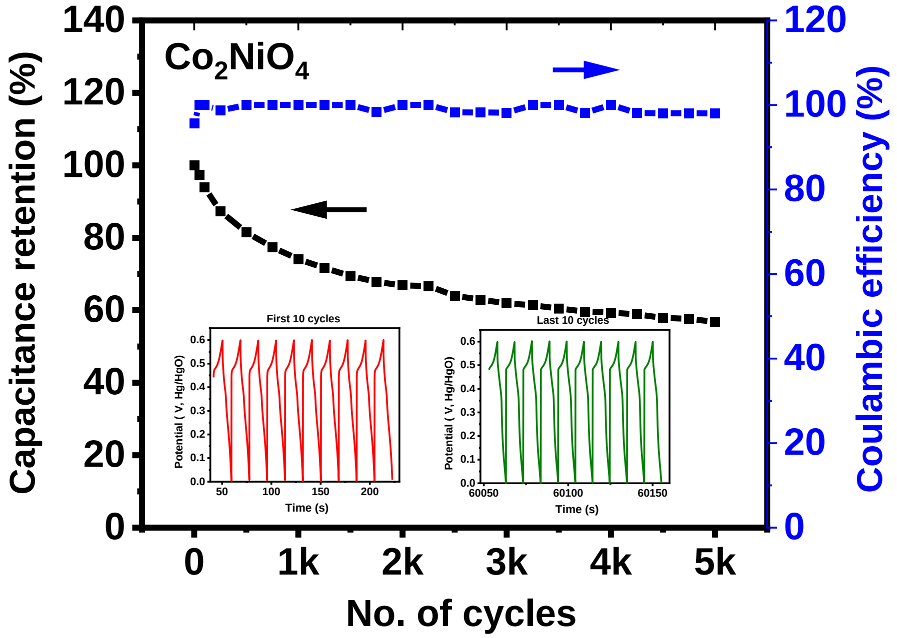

Figure 3.101. Stability curves for Co$_2$NiO$_4$.

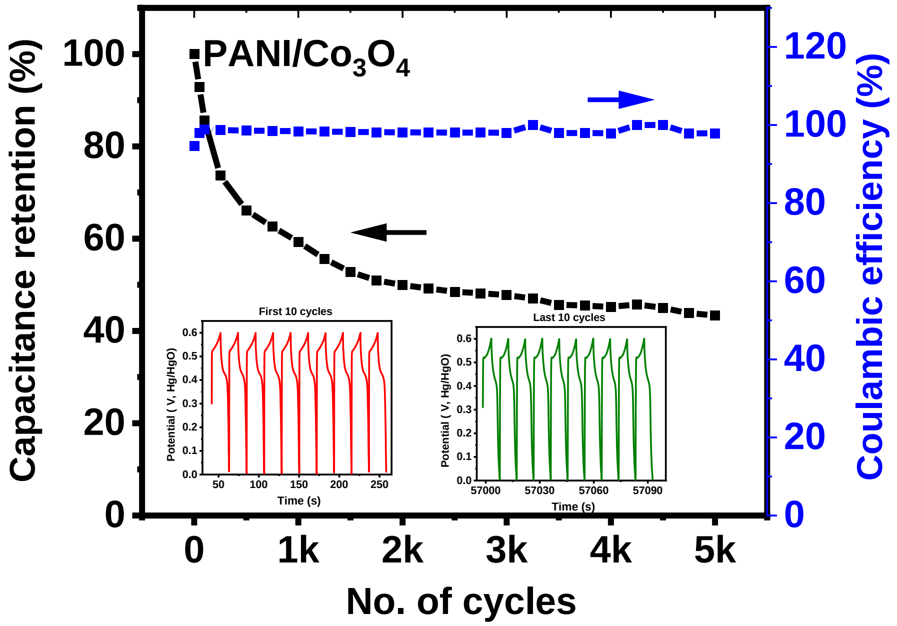

Figure 3.102. Stability curves for PANI/Co$_3$O$_4$.

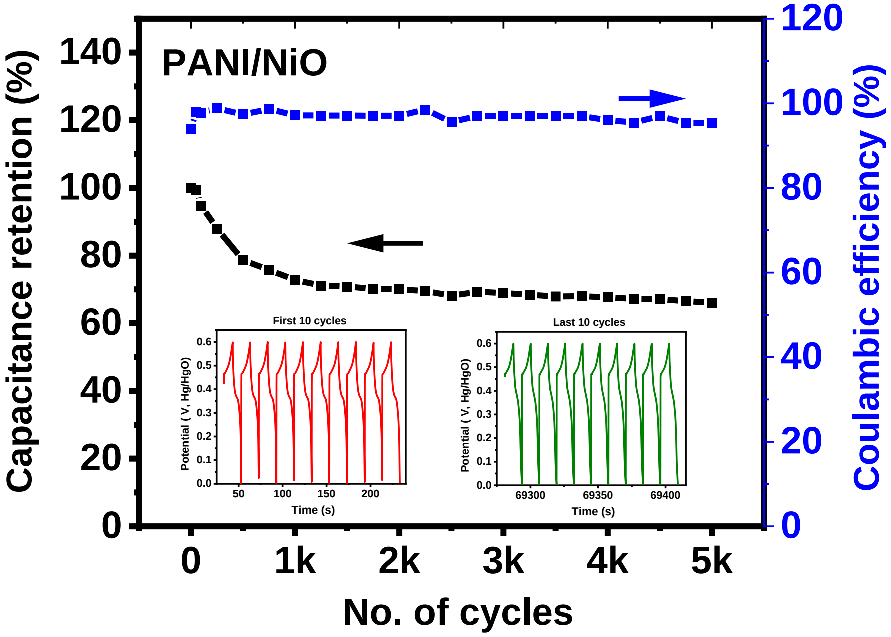

Figure 3.103. Stability curves for PANI/NiO.

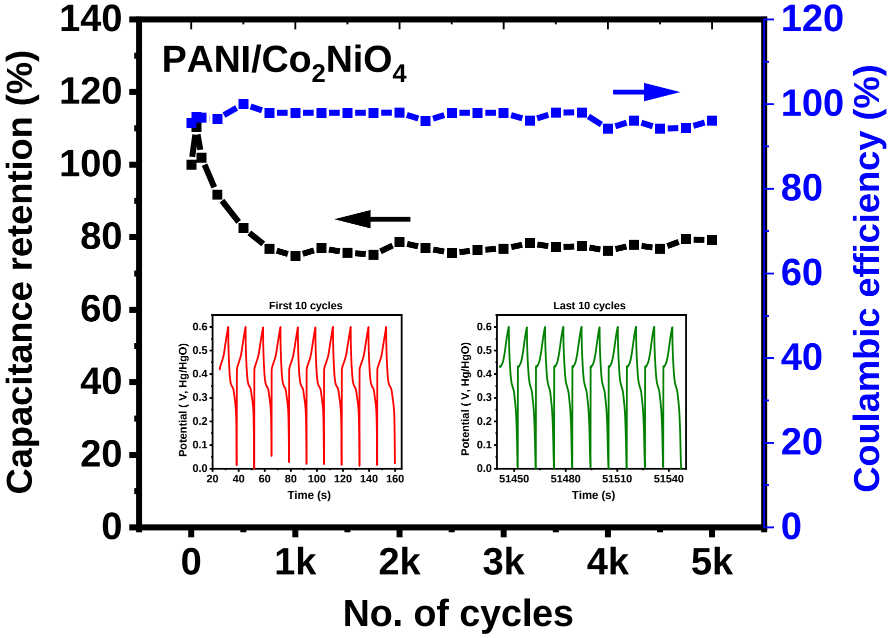

Figure 3.104. Stability curves for PANI/Co_2NiO_4.

In order to understand the electrochemical stability of these materials, 5000 cycles of charge and discharge tests were performed. Two pieces of information can be directly obtained from these charge and discharge curves, capacitance retention and Coulombic efficiency. From **Figures 3.98 - 3.104**, it can be seen that except for the polyaniline material the coulombic efficiency for other samples has not changed much with the increase of the number of charge and discharge cycles, maintaining a coulombic efficiency of 100%. Only the coulombic efficiency of polyaniline (**Figure 3.98**) decreases slightly with the increase of the number of charge and discharge cycles of the material, and it still maintained a coulombic efficiency of 90% after 5000 charge and discharge cycles. The cycle stability of polyaniline decreased to 70%. Cobalt oxide (**Figure 3.99**) was relatively stable and about 90% of the capacitance remains after 5000 charge-discharge cycles. However, the composite material of polyaniline and cobalt oxide (**Figure 3.102**) showed poor capacitance retention of 43%. Although NiO (**Figure 3.100**) had a high specific capacitance, its stability was poor. After 5000 charge and discharge cycles, only 42% of the capacitance remained. The stability of polyaniline nickel oxide composite (**Figure 3.103**) was higher than that of cobalt oxide. After 5000 charge and discharge cycles its capacitance retention value was 70%. Nickel cobalt oxide (**Figure 3.101**) did not show good stability. After 5000 charge-discharge cycles, the retention of its capacitance was only 50%, while the composite material of polyaniline and nickel cobalt oxide was stable in the material in terms of performance, 70% of the capacitance remained after 5000 charge-discharge cycles.

CHAPTER IV

CONCLUSION

Developing energy conversion and storage devices is an effective method to provide for efficient and economical use of green energy. Hydrogen gas with high energy density, a wide range of applications, and green environmental protection, can be directly produced by the electrolysis of water. At present, the focus of the research on electrolyzed water is to find a catalyst with high activity, good stability, and low cost to reduce energy consumption.

As a new type of energy storage device with unique characteristics, supercapacitors play an important role. The current focus of supercapacitor research is to seek electrode materials with high stability, specific capacitance, and energy density. As a conductive polymer with excellent electrochemical performance, polyaniline has been widely studied in the fields of supercapacitor energy storage materials and electrolytic water catalysts. It is worth noting that different shapes of polyaniline, such as nanowire tubes, nanospheres, nanofibers, etc. can be achieved by controlling the synthesis conditions. In this work, cheap and easily available polyaniline was used as the precursor and carbon nanomaterials with the abundant hollow structure were obtained via a high-temperature reaction with potassium hydroxide. In addition, polyaniline transition metal oxides with polyaniline nanotubes as carriers were also synthesized to investigate the performance of supercapacitor energy storage materials and the performance of water-splitting catalysts.

1. As a conductive polymer with rich microscopic shapes and rich in carbon elements, polyaniline can be used as a precursor for supercapacitor carbon materials. In this work, potassium hydroxide was used as an activator to etch polyaniline nanotubes to obtain nanotubes with rich pore structures. Different mass ratios of polyaniline potassium hydroxide are used to obtain carbon materials.

2. The hydrothermally synthesized Co_3O_4, NiO, and Co_2NiO_4 were separately dissolved in the polyaniline synthesis reactor and the composites of polyaniline and these transition metal oxides was obtained.

REFERENCES

1. Walker, Richard P. "The Wind Energy Development Process." Edited by Richard P. Walker, and Andrew Swift. John Wiley & Sons, Inc, Hoboken, NJ, 2015.
2. Breeze PA, Books24x7 I. Power Generation Technologies, Second Edition. 2nd ed. Waltham, MA;Kidlington, Oxford, UK;: Newnes; 2014
3. Abu-Rub H, Malinowski M, Al-Haddad K. Power Electronics for Renewable Energy Systems, Transportation and Industrial Applications. 1st ed. John Wiley & Sons, Incorporated; 2014.
4. Hoffmann P, 1935, ProQuest (Firm). Tomorrow's Energy: Hydrogen, Fuel Cells, and the Prospects for a Cleaner Planet. Rev. and expand ed. Cambridge, Mass: MIT Press; 2012.
5. Miranda PE. Science and Engineering of Hydrogen-Based Energy Technologies: Hydrogen Production and Practical Applications in Energy Generation. First ed. Cambridge, MA: Elsevier; 2019.
6. Giddey S, Badwal SPS, Munnings C, Dolan M. Ammonia as a Renewable Energy Transportation Media. ACS sustainable chemistry & engineering. 2017; 5:10231-10239.
7. Martin KE, Kopasz JP, McMurphy KW. Status of fuel cells and the challenges facing fuel cell technology today. In: ACS Symposium Series. Vol 1040. American Chemical Society; 2010:1-13. doi:10.1021/bk-2010-1040.ch001
8. Mendell BN, Brunwick LP, ProQuest (Firm). Modular Electricity Storage: Benefits

and Costs. Hauppauge, N.Y: Nova Science Publishers; 2012.

9. Lu M, Beguin F, Frackowiak E, ProQuest (Firm). Supercapacitors: Materials, Systems, and Applications. Weinheim: Wiley-VCH; 2013.

10. Yu A, Chabot V, Zhang J, ProQuest (Firm). Electrochemical Supercapacitors for Energy Storage and Delivery: Fundamentals and Applications. 1st ed. Boca Raton, FL: CRC Press; 2017.

11. Winter M, Brodd RJ. What are batteries, fuel cells, and supercapacitors? Chemical Reviews. 2004;104(10):4245-4269. doi:10.1021/cr020730k

12. Largeot C, Portet C, Chmiola J, Taberna PL, Gogotsi Y, Simon P. Relation between the ion size and pore size for an electric double-layer capacitor. Journal of the American Chemical Society. 2008;130(9):2730-2731. doi:10.1021/ja7106178

13. Witomska S, Liu Z, Czepa Wå, et al. Graphene Oxide Hybrid with Sulfur-Nitrogen Polymer for High-Performance Pseudocapacitors. Journal of the American Chemical Society. 2019;141(1):482-487. doi:10.1021/jacs.8b11181

14. Volkov A v., Sun H, Kroon R, et al. Asymmetric Aqueous Supercapacitor Based on p- And n-Type Conducting Polymers. ACS Applied Energy Materials. 2019;2(8):5350-5355. doi:10.1021/acsaem.9b00853

15. Moussa M, El-Kady MF, Dubal D, et al. Self-Assembly and Cross-Linking of Conducting Polymers into 3D Hydrogel Electrodes for Supercapacitor Applications. ACS Applied Energy Materials. 2020;3(1):923-932. doi:10.1021/acsaem.9b02007

16. Wang Y, Guo J, Wang T, Shao J, Wang D, Yang Y-W. Mesoporous Transition Metal Oxides for Supercapacitors. Nanomaterials. 2015;5:1667-1689. doi:10.3390/nano5041667

17. Wang L, Duan G, Zhu J, Chen S-M, Liu X-H, Palanisamy S. Mesoporous transition metal oxides quasi-nanospheres with enhanced electrochemical properties for supercapacitor applications. Journal of colloid and interface science. 2016;483:73-107.

18. Gasteiger H, Krischer K, Scrosati B. Electrochemical cells: Basics. In: Scrosati B, Abraham KM, Van Schalkwijk W, Hassoun J, eds. Hoboken, NJ, USA: John Wiley & Sons, Inc; 2013:1-19.

19. Tang X, Qi Z. Study on an actively controlled battery ultracapacitor hybrid in stand-alone PV system. Advanced Technology of Electrical Engineering and Energy. 2006;25:37-41.

20. Tie SF, Tan CW. A review of energy sources and energy management system in electric vehicles. Renewable and Sustainable Energy Reviews. 2013;20:82-102. doi:10.1016/j.rser.2012.11.077

21. Suryanarayanan S, Mancilla-David F, Mitra J, Li Y. Achieving the smart grid through customer-driven microgrids supported by energy storage. In: Proceedings of the IEEE International Conference on Industrial Technology. ; 2010:884-890. doi:10.1109/ICIT.2010.5472581

22. Idriss H, Scott M, Subramani V. Compendium of Hydrogen Energy: Hydrogen

Production and Purification. In: Compendium of Hydrogen Energy. Elsevier; 2015:1-522. doi:10.1016/b978-1-78242-361-4.00001-7

23. Wang S, Lu A, Zhong C-J. Hydrogen production from water electrolysis: role of catalysts. Nano Convergence. 2021;8:4. doi:10.1186/s40580-021-00254-x

24. Godula-Jopek A, Stolten D, Bourasseau C. Hydrogen Production: By Electrolysis. Weinheim, Germany: WILEY-VCH Verlag GmbH & Co. KGaA; 2015.

25. Peng L, Zheng X, Li L, et al. Chimney effect of the interface in metal oxide/metal composite catalysts on the hydrogen evolution reaction. Applied Catalysis B: Environmental. 2019;245:122-129. doi:10.1016/j.apcatb.2018.12.035

26. Watzele S, Fichtner J, Garlyyev B, Schwä JN, Bandarenka AS. On the Dominating Mechanism of the Hydrogen Evolution Reaction at Polycrystalline Pt Electrodes in Acidic Media. Published online 2018. doi:10.1021/acscatal.8b03365

27. Li Y, Wu Z-S, Lu P, et al. Chimney effect of the interface in metal oxide/metal composite catalysts on the hydrogen evolution reaction. Adv Sci. 2020;2020:1903089. doi:10.1002/advs.201903089

28. Zhu K, Shi F, Zhu X, Yang W. The roles of oxygen vacancies in electrocatalytic oxygen evolution reaction. Nano Energy. 2020;73:104761. doi:10.1016/j.nanoen.2020.104761

29. Dai L, Xue Y, Qu L, Choi HJ, Baek JB. Metal-Free Catalysts for Oxygen Reduction Reaction. Chemical Reviews. 2015;115(11):4823-4892. doi:10.1021/cr5003563

30. Zhang B, Zhu C, Wu Z, et al. Integrating Rh Species with NiFe-Layered Double

Hydroxide for Overall Water Splitting. Nano Letters. 2020;20(1):136-144. doi:10.1021/acs.nanolett.9b03460

31. Esquius JR, Algara-Siller G, Spanos I, Freakley SJ, Schlögl R, Hutchings GJ. Preparation of solid solution and layered Irox−Ni(OH)2 oxygen evolution catalysts: Toward optimizing iridium efficiency for OER. ACS Catalysis. 2020;10(24):14640-14648. doi:10.1021/acscatal.0c03866

32. Tsuji R, Koshino Y, Masutani H, et al. Water Electrolysis Using Thin Pt and RuOx Catalysts Deposited by a Flame-Annealing Method on Pencil-Lead Graphite-Rod Electrodes. ACS Omega. 2020;5(11):6090-6099. doi:10.1021/acsomega.0c00074

33. Han N, Luo S, Deng C, Zhu S, Xu Q, Min Y. Defect-Rich FeN0.023/Mo2C Heterostructure as a Highly Efficient Bifunctional Catalyst for Overall Water-Splitting. ACS Applied Materials and Interfaces. doi:10.1021/acsami.0c19839

34. Hou X, Zhou H, Zhao M, Cai Y, Wei Q. MoS2 Nanoplates Embedded in Co-N-Doped Carbon Nanocages as Efficient Catalyst for HER and OER. ACS Sustainable Chemistry and Engineering. 2020;8(14):5724-5733. doi:10.1021/acssuschemeng.0c00810

35. Syed AA, Dinesan MK. Review: Polyaniline-A novel polymeric material. Talanta. 1991;38(8):815-837. doi:10.1016/0039-9140(91)80261-W

36. Ameen S, Shaheer Akhtar M, Husain M. A review on synthesis processing, chemical and conduction properties of polyaniline and its nanocomposites. Science of Advanced Materials. 2010;2(4):441-462. doi:10.1166/sam.2010.1126

37. Plesu N, Ilia G, Pascariu A, Vlase G. Preparation, degradation of polyaniline doped with organic phosphorus acids and corrosion essays of polyaniline-acrylic blends. Synthetic Metals. 2006;156(2-4):230-238. doi:10.1016/j.synthmet.2005.11.006

38. Wang Y, Jing X. Intrinsically conducting polymers for electromagnetic interference shielding. Polymers for Advanced Technologies. 2005;16(4):344-351. doi:10.1002/pat.589

39. Diggikar RS, Deshmukh SP, Thopate TS, Kshirsagar SR. Performance of Polyaniline Nanofibers (PANI NFs) as PANI NFs-Silver (Ag) Nanocomposites (NCs) for Energy Storage and Antibacterial Applications. ACS Omega. 2019;4(3):5741-5749. doi:10.1021/acsomega.8b02834

40. Chen N, Ni L, Zhou J, et al. Sandwich-Like Holey Graphene/PANI/Graphene Nanohybrid for Ultrahigh-Rate Supercapacitor. Published online 2018. doi:10.1021/acsaem.8b00725

41. Diggikar RS, Deshmukh SP, Thopate TS, Kshirsagar SR. Performance of Polyaniline Nanofibers (PANI NFs) as PANI NFs-Silver (Ag) Nanocomposites (NCs) for Energy Storage and Antibacterial Applications. ACS Omega. 2019;4(3):5741-5749. doi:10.1021/acsomega.8b02834

42. Ghosh K, Yue CY, Sk MM, Jena RK. Development of 3D Urchin-Shaped Coaxial Manganese Dioxide@Polyaniline (MnO2@PANI) Composite and Self-Assembled 3D Pillared Graphene Foam for Asymmetric All-Solid-State Flexible Supercapacitor Application. ACS Applied Materials and Interfaces. 2017;9(18):15350-15363.

doi:10.1021/acsami.6b16406

43. Liu X, Wang J, Yang G. In Situ Growth of the Ni3V2O8@PANI Composite Electrode for Flexible and Transparent Symmetric Supercapacitors. ACS Applied Materials and Interfaces. 2018;10(24):20688-20695. doi:10.1021/acsami.8b04609

44. Ren L, Zhang G, Yan Z, et al. Three-Dimensional Tubular MoS2/PANI Hybrid Electrode for High Rate Performance Supercapacitor. ACS Applied Materials and Interfaces. 2015;7(51):28294-28302. doi:10.1021/acsami.5b08474

45. He J, Wang M, Wang W, et al. Hierarchical Mesoporous NiO/MnO2@PANI Core-Shell Microspheres, Highly Efficient and Stable Bifunctional Electrocatalysts for Oxygen Evolution and Reduction Reactions. ACS Applied Materials and Interfaces. 2017;9(49):42676-42687. doi:10.1021/acsami.7b07383

46. Feng JX, Tong SY, Tong YX, Li GR. Pt-like hydrogen evolution electrocatalysis on PANI/CoP hybrid nanowires by weakening the shackles of hydrogen ions on the surfaces of catalysts. Journal of the American Chemical Society. 2018;140(15):5118-5126. doi:10.1021/jacs.7b12968

47. Huang M, Zhang H, Yin S, Zhang X, Wang J. PtAg Alloy Nanoparticles Embedded in Polyaniline as Electrocatalysts for Formate Oxidation and Hydrogen Evolution. ACS Applied Nano Materials. 2020;3(4):3760-3766. doi:10.1021/acsanm.0c00442

48. Zhu T, Zhou J, Li Z, Li S, Si W, Zhuo S. Hierarchical porous and N-doped carbon nanotubes derived from polyaniline for electrode materials in supercapacitors. Journal of Materials Chemistry A. 2014;2(31):12545-12551.

doi:10.1039/c4ta01465k

49. Arsalani N, Tabrizi AG, Ghadimi LS. Novel PANI/MnFe2O4 nanocomposite for low-cost supercapacitors with high rate capability. Journal of Materials Science: Materials in Electronics. 2018;29(7):6077-6085. doi:10.1007/s10854-018-8582-6

50. Meng F, Yu Y, Sun D, et al. Three-Dimensional Needle Branch-like PANI/CoNiP Hybrid Electrocatalysts for Hydrogen Evolution Reaction in Acid Media. ACS Applied Energy Materials. Published online 2021. doi:10.1021/acsaem.0c03033

51. Das S, Ghosh R, Routh P, et al. Conductive MoS_2 Quantum Dot/Polyaniline Aerogel for Enhanced Electrocatalytic Hydrogen Evolution and Photoresponse Properties. 2018;23:26. doi:10.1021/acsanm.8b00373

52. Deng W, Jiang H, Chen C, et al. Co-, N-, and S-Tridoped Carbon Derived from Nitrogen- and Sulfur-Enriched Polymer and Cobalt Salt for Hydrogen Evolution Reaction. ACS Applied Materials and Interfaces. 2016;8(21):13341-13347. doi:10.1021/acsami.5b12666

53. Yan X, Tian L, He M, Chen X. Three-Dimensional Crystalline/Amorphous Co/Co_3O_4 Core/Shell Nanosheets as Efficient Electrocatalysts for the Hydrogen Evolution Reaction. Nano Letters. 2015;15(9):6015-6021. doi:10.1021/acs.nanolett.5b02205

54. Liu H, Ma X, Rao Y, et al. Heteromorphic NiCo2S4/Ni3S2/Ni Foam as a Self-Standing Electrode for Hydrogen Evolution Reaction in Alkaline Solution. ACS Applied Materials and Interfaces. 2018;10(13):10890-10897. doi:10.1021/acsami.8b00296

55. Feng X, Wang H, Bo X, Guo L. Bimetal-Organic Framework-Derived Porous Rodlike Cobalt/Nickel Nitride for All-pH Value Electrochemical Hydrogen Evolution. ACS Applied Materials and Interfaces. 2019;11(8):8018-8024. doi:10.1021/acsami.8b21369

56. Sun H, Xu X, Yan Z, et al. Porous multishelled Ni2P hollow microspheres as an active electrocatalyst for hydrogen and oxygen evolution. Chemistry of Materials. 2017;29(19):8539-8547. doi:10.1021/acs.chemmater.7b03627

57. Cheng F, Fan X, Chen X, et al. Surface-Restructured Core/Shell NiO@Co3O4 Nanocomposites as Efficient Catalysts for the Oxygen Evolution Reaction. Industrial and Engineering Chemistry Research. 2019;58(36):16581-16587. doi:10.1021/acs.iecr.9b02626

58. Tahir M, Pan L, Zhang R, et al. High-Valence-State NiO/Co3O4 Nanoparticles on Nitrogen-Doped Carbon for Oxygen Evolution at Low Overpotential. ACS Energy Letters. 2017;2(9):2177-2182. doi:10.1021/acsenergylett.7b00691

59. Zhang J, Qian J, Ran J, Xi P, Yang L, Gao D. Engineering Lower Coordination Atoms onto NiO/Co3O4Heterointerfaces for Boosting Oxygen Evolution Reactions. ACS Catalysis. 2020;10(21):12376-12384. doi:10.1021/acscatal.0c03756

60. Deng X, Öztürk S, Weidenthaler C, Tüysüz H. Iron-Induced Activation of Ordered Mesoporous Nickel Cobalt Oxide Electrocatalyst for the Oxygen Evolution Reaction. ACS Applied Materials and Interfaces. 2017;9(25):21225-21233. doi:10.1021/acsami.7b02571